HDR qualification. Different spin current sources: from interfaces to bulk materials

J.-C. Rojas-Sánchez

Habilitation à Diriger des Recherches de l'Université de Lorraine

Présenté par :

Juan-Carlos ROJAS-SANCHEZ

Institut Jean Lamour UMR 7198 CNRS - Université de Lorraine

Different spin current sources: from interfaces to bulk materials

---

Soutenue publiquement le 16 Septembre 2020 à Nancy devant le jury suivant:

Mme Julie GROLLIER	UMPhy CNRS/Thales	Referee
M. Andrew KENT	New York University	Referee
M. Sergio VALENZUELA	ICN2, Univ. Aut. de Barcelona	Referee
Mme. Ingrid MERTIG	Martin-Luther-Universität Halle-Wittenberg	
M. Albert FERT	UMPhy CNRS/Thales	
M. Olivier FRUCHART	SPINTEC (Univ. Grenoble Alpes, CNRS, CEA)	
M. Pietro GAMBARDELLA	ETH Zurich	
M. François MONTAIGNE	Université de Lorraine (UL)	

Invited:

M. Stéphane ANDRIEU (UL)

M. Stéphane MANGIN (UL)

M. Sébastien PETIT-WATELOT (UL)

Abstract

During the last years, my research activities have been focused on the conversion of spin current into charge current and vice versa. The study of this conversion based on the spin orbit interactions in 3D and 2D materials are topics of great interest in the scientific and technological community. I intend to continue some lines of research (spintronics), expand others (spin-orbitronics) and embrace other very new ones for me (spin caloritronics). This is summarized in the points described below. To achieve these objectives, I have the support of colleagues from my team and Institute of great scientific and human quality. I have access to different experimental platforms, some that I have developed over the last few years and others that I will develop in order to move forward with my new lines of research. I also count on the support and collaboration of colleagues outside the IJL, in France and abroad. Finally, in order to move forward with this scientific project, it is important to have young masters, doctorate and post-doctorate students. I have already achieved some important results with two PhD students (Pierre Vallobra and Thai Ha Pham), currently I have started to supervise a post-doc thanks to a French ANR project of which I am the local PI. I have submitted and will continue to submit scientific projects with the healthy ambition of advancing these projects and having the human resources (students) to guide them, transmit knowledge and advance together towards a development of this field of science. And why not, not only fundamental researches but also towards a technology transfer. An important step to obtain the funding that will allow me to achieve all of this is precisely to obtain my HDR.

Therefore, this manuscript is to get that French diploma. I have organized the manuscript by an introduction to "classical" or "conventional" spintronics where we have seen concepts like giant magnetoresistance, tunnel magnetoresistance and spin-transfer torque.

I will then describe the relative new concepts for understanding phenomena based on spin-orbit coupling. Concepts such as spin current, spin Hall effect (*relatively new* since it was theoretically brought to light in 1971 without the current name), Edelstein effect (also known as inverse spin Galvanic effect) and spin-orbit torque, among others.

In chapter II, I will go on to describe the conversion of spin current into charge current in bulk materials. The technique of ferromagnetic resonance and spin pumping as the method of choice will be developed. I will present the results taking into account the effect of spin memory loss on the interfaces so one should not expect the same conversion efficiency on a bilayer FM1/HM (ferromagnetic/heavy metal) as on another bilayer FM2/HM.

In chapter III, I will continue with the conversion of spin current into charge current but this time at the interfaces. I will present my results obtained during my last years of research. Mainly the quite known results now in Ag/Bi Rashba interface, Rashba interface between $SrTiO_3/LaAlO_3$ oxides and α-Sn topological insulator.

Chapter IV is devoted to the direct effects. Charge to spin currents conversion in mainly by spin-torque ferromagnetic resonance. The first part is shown some results in bulk and in the second part, some prospects to have results exploiting charge to spin conversion at interfaces.

Chapter V is also dedicated to direct effect. In this case, the study of the spin-orbit torques to be able to switch the magnetization. I will show mainly some results based in

$Pt/Co/Ni)_3/AlOx$ and W/CoTb/AlOx. In the last chapter, I discuss three ongoing projects. (i) One related to new concepts including the spin Anomalous Hall effect and the Rashba effect on bulk due to inversion symmetry breaking even in amorphous material, the research for SOT self-torques to be able to switch the magnetization without any external field, and without the use of heavy materials. (ii) Another one related to the exploration of a magnetoelectric oxide, $Ga_{2-x}Fe_xOx$, for its exploitation in spin-orbitronics. (iii) A third one related to the exploration and research of new 2D systems such as topological insulators materials, based on or in combination with Heusler compounds. This is for the research and exploitation of these heterostructures in spin-orbitronics and spin-caloritronics.

Dedication

TO MY FAMILY

Acknowledgements

It is a long list to whom I owe a lot and to whom I am forever grateful for their support. Eternal gratitude to my *alma mater* in Peru (Universidad Nacional de Ingeniería where I studied Physics) and in Argentina (Instituto Balseiro where I did my master and doctorate in Physics).
Let me now start from my arrival in France, that July 11, 2011, with my wife and our two children of 11 years and 26 months, respectively. Huge thanks to Laurent Vila who hired me for a postdoctoral position. To all the nano-structures and magnetism team of INAC CEA-Grenoble, now part of Spintec. To my former bosses there and to my fellows. Thanks to Mathieu, Jean-Phillipe, Piotr, William, Dai, Murat, Céline, Alain and all the team. As well as our colleagues at Spintec, in particular Nahuel, Mair, Mihail, Olivier and Gilles, and at the Instiuto Luis Neel, in particular Nora, Stefania, Jan, etc.
UMPhi CNRS/Thales hired me as a post-doc in 2013 after some inconveniences with the administration because of my visa status as a scientist but "without a job or contract". Here again I found a pleasant working environment. Thanks to all at UMPhi: Jean-Marie, Henri, Nicolas, Agnés, Manu, Vincent, ...
In 2015, I landed in Nancy as a permanent CNRS researcher at the Jean Lamour Institute even though at first I thought Lamour was "L'amour" (the love). I am equally happy here and grateful to the entire SPIN team as well as the entire laboratory. Thanks to Daniel, Michel, Stéphane A, Stéphane M, Sébastien, Olivier and everyone else. Thanks to Julius for his quick and efficient review of my HDR manuscript.
Thanks to the distinguished members of the jury for agreeing to be part of my HDR evaluation and qualification. As well as the three invited, and Olivier Copie who helped me with the rehearsals for an optimal oral presentation.
Thanks to all my colleagues and to our students who made possible the progress we have made. A special thanks to Professor Albert Fert with whom we have collaborated almost since I arrived in France. A huge thanks to him and to France who have allowed me to grow as a scientist by letting me develop the research we have carried out.
Finally, thanks again to my family, for their effort and constant support. Yohana, César and Fabián: I know that it is not always easy, but I want you know that I am infinitely grateful to you.

Table of contents

I. Introduction

I.1 Spintronics

In the late 1980s two papers reported the experimental discovery of giant magnetoresistance (GMR) [1,2]. They reported very large electrical resistance changes in response to an applied magnetic field. Changes of 50% in superlattices of Fe/Cr [1] and 6% in tri-layers of Fe/Cr/Fe [2] at low temperature. In the case of superlattices, the authors noted that the magnetoresistive effect at room temperature is still significant [1]. Although there was much work, especially theoretical, since the late 1960s to arrive at these results, in the 1980s the scientific community still did not widely believe that such effects were physically possible. These works are thus considered to be the birth of spintronics and led to the 2007 Nobel Prize for Albert Fert and Peter Grunberg. A few years later, the GMR effect was also tested on multilayers deposited by sputtering [3], and the effect was equally important at room temperature [4]. But what is spintronics? It is a science or field of research, not only a technology, that study the role not only of electron charge but also the one of electron spin in a number of physics phenomena in condensed matter. In the beginning of spintronics, manipulation and creation of spin polarized current was a key new concept developed. Thus, the production of spin polarized current by magnetic materials was used in "classical" spintronics. That is in the first decade after GMR discovery. Other events that boosted the activity of research in spintronics were the discovery of Tunnel Magnetoresistance (TMR) and spin transfer torque (STT). In **Figure I.1** are shown the concept and schematic of the GMR as well as the mainstream application in technology, the read/writer HDD. The industrial applications of these discoveries, such as Hard Disk Drive (HDD) write/read head by IBM in 1997, heightened even more the spintronics activities not only for fundamental research but now also for the potential applications.

Beyond applications in read/writer HDD, both GMR and TMR are widely used in magnetic sensors.

Prior to introduce the spin current concept, let's remember the spin polarized current which has been used in the beginning of spintronics. In these beginnings of the spintronics the spin-polarized currents were produced by using the influence of the orientation of the spin on the transport properties of the electrons in ferromagnetic conductors as suggested first by Mott [5], and had been experimentally demonstrated and theoretically described in the sixties [6] and seventies [7,8].

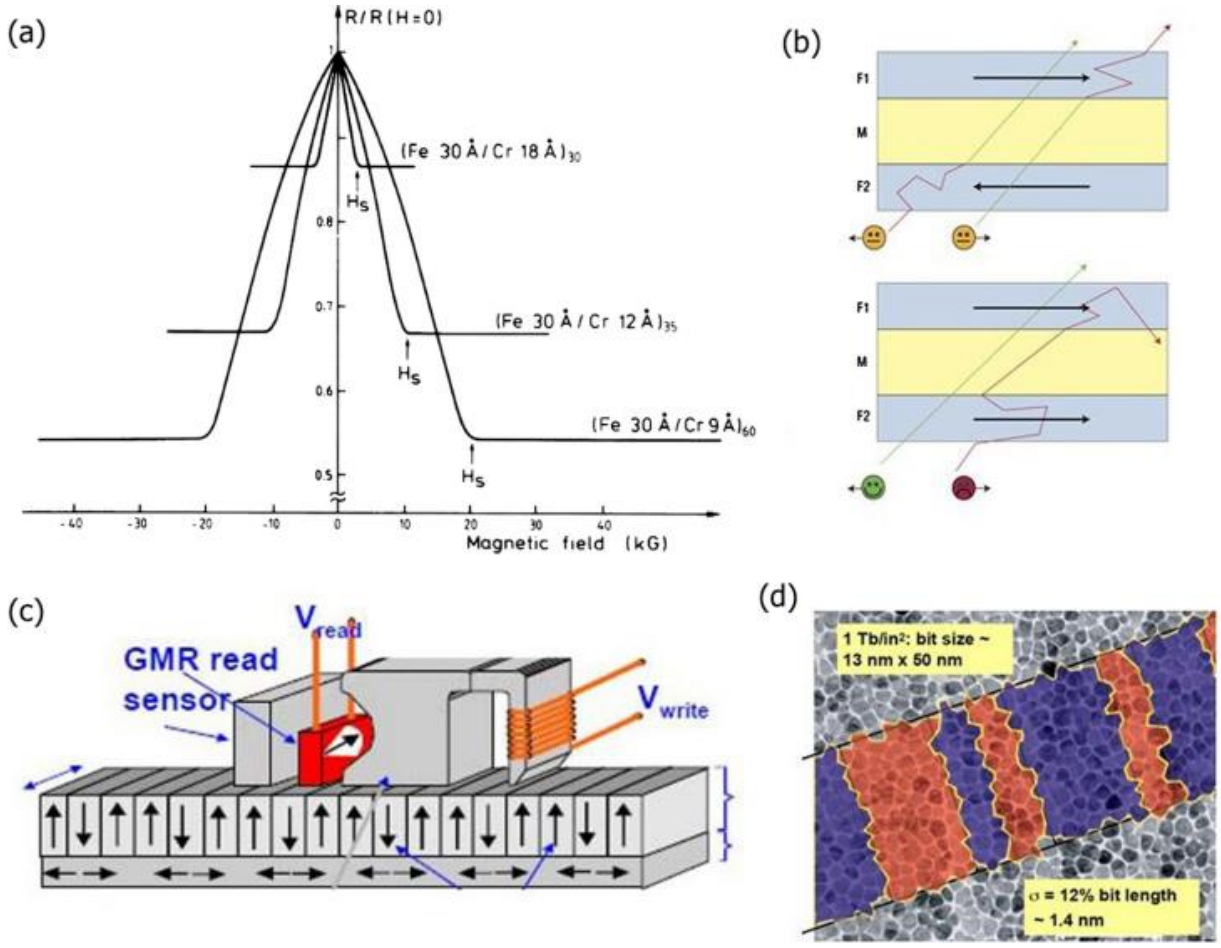

Figure I.1 Discovery of GMR. (a) GMR in Fe/Cr(001) multilayers [1]. With the current definition of the magnetoresistance ratio, MR=100×[$R_{AP} - R_P/R_p$], MR= 85% for the Fe 3 nm/Cr 0.9 nm multilayers. GMR effects were observed at about the same time with Fe/Cr/Fe trilayers by the team of Peter Grünberg at Jülich [2]. (b) Schematic of the mechanism of the GMR. In the parallel magnetic configuration (bottom), the electrons of one of the spin directions can go easily through all the magnetic layers and the short-circuit through this channel leads to a small resistance. In the antiparallel configuration (top), the electrons of each channel are slowed down every second magnetic layer and the resistance is high. (c) Schematic of a GMR write/read head in HDD. (d) Example of magnetic bits on the HDDs of today. Taken from ref. [9].

Larger magnetoresistance than in metallic trilayer structure was found in a magnetic tunnel junction (MTJ) where the metallic spacer in GMR structure was replaced but an insulator. This tunnel barrier was made of aluminum oxide at first, but single-crystalline MgO holds ones of the current TMR records at room temperature - 600% [10]. The first works on MTJ and TMR were reported in 1975 [11] and 1982 [12]. The physical origin of this large TMR having a single-crystal barrier has been attributed to symmetry selection at a FM/I interface [13–16]. In such interfaces, an evanescent wave function of a given symmetry is connected to the Bloch functions of the same symmetry and spin direction at the Fermi level

of the electrodes. In (001)MgO barriers, one of the symmetries corresponding to highly spin-polarized bands has a much slower decay, which results in a higher TMR. Other symmetry rules have been observed in barriers made of different materials, leading to different properties such as negative effective spin polarization in $SrTiO_3$-based MTJ [17]. This is, one sign of TMR in Co/MgO/Co MTJ and the opposite in Co/$SrTiO_3$/Co one.

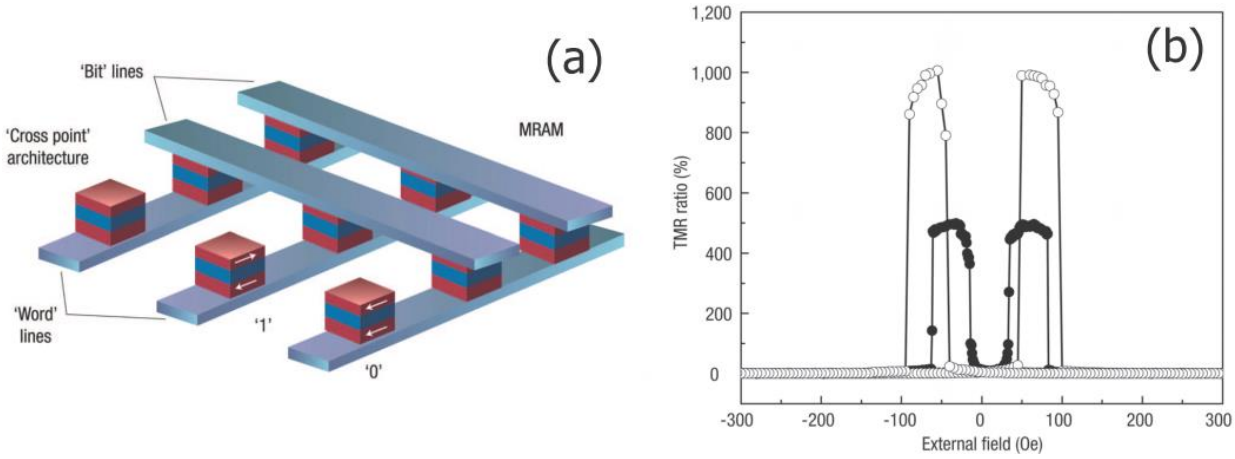

Figure I.2 a) Principle of the magnetic random access memory (MRAM) in the basic "cross point" architecture. The binary information "0" and "1" is recorded on the two opposite orientations of the magnetization of the free layer of magnetic tunnel junctions (MTJs), which are connected to the crossing points of two perpendicular arrays of parallel conducting lines. For writing, current pulses are sent through one line of each array, and only at the crossing point of these lines the resulting magnetic field is high enough to orient the magnetization of the free layer. For reading, one measures the resistance between the two lines connecting the addressed cell [18]. b) High magnetoresistance, TMR=(R_{max}−R_{min})/R_{min}, measured by for the magnetic stack [19]: $(Co_{25}Fe_{75})_{80}B_{20}$(4 nm)/MgO(2.1 nm)/ $(Co_{25}Fe_{75})_{80}B_{20}$(4.3 nm) annealed at 475 °C after growth, measured at room temperature (closed circles) and low temperature (open circles). Taken from ref. [20]. A transistor is not shown at each crossing point in (a) that prevents current from flowing at each crossing when voltage is applied between the bit and word lines.

In a suitable FM/I/FM MTJ heterostructure two resistance sates, high and low, correspond to either parallel (usually low resistance) or antiparallel (usually high resistance) orientation of the magnetization in the ferromagnetic layers. Therefore those states are associated to 1 or 0 in order to store information. Hence, new applications can be found to storage information using a MTJ as a magnetic bit element or in a logic circuit exploiting the 1 and 0 states. To change from one state to another or "write" the information an external magnetic field is used. This is possible using "word" and "bit" lines as displayed in the **Figure I.2**. This so called magnetic random access memory (MRAM) doesn't need power to keep stored the information, thus reducing the energy needed to operate these MRAM. Consequently, this new MRAM, which is a non-volatile memory, allows reducing energy consumption. MRAMs are in the market since 2006.

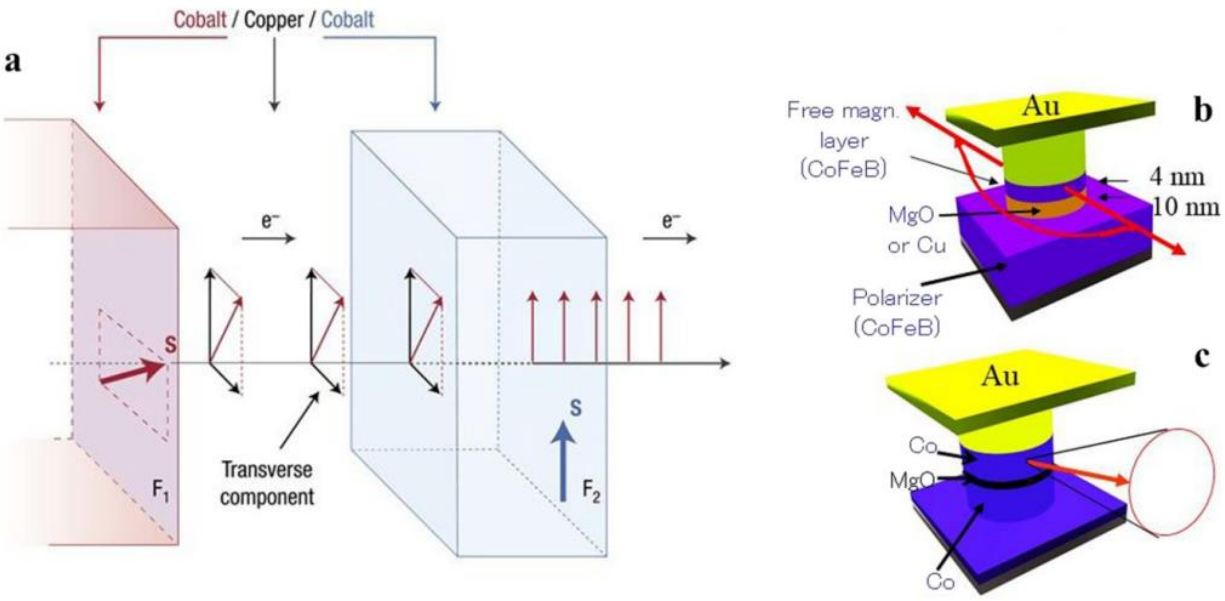

Figure I.3 (a) Illustration of the spin transfer concept introduced by John Slonczewski [21] and Berger [22]. A spin-polarized current is prepared by a first magnetic layer F with an obliquely oriented spin polarization with respect to the magnetization axis of a second layer F2. When it goes through F2, the exchange interaction aligns its spin polarization along the magnetization axis. The exchange interaction being spin conserving, the transverse spin polarization lost by the current is transferred to the total spin of F2, which can also be described by a spin-transfer torque acting on F2 [18]. (b) MTJ nano-pillar (as well, schematic of STT-RAM) for experiments of magnetic switching by STT: the magnetization of the free magnetic layer is reversed by the STT due to injection of a spin-polarized current created by the CoFeB layer. (c) Same as (b), but with the creation of a steady-state gyration of the magnetization of the free layer (STT oscillator). Taken from [9].

Still it is possible to reduce even more the energy consumption in the magnetic memory if we are able to replace the external magnetic field for the write operation. Thus was possible using the spin transfer torque (STT) concept introduced by Slonczewski [21] and Berger [22] in 1996. In this spin-transfer idea, one manipulates the magnetic moment of a ferromagnetic layer without applying any magnetic field but only by transfer of spin angular momentum from a spin-polarized current. The spin-polarized current is generated by the first magnetic element: the current coming out from the first magnetic layer is spin-polarized due to exchange interaction with the magnetization. The injection of a spin-polarized current into a second magnetic element leads to the transfer of the transverse component of the spin-polarized current, which creates torque acting on the magnetization of the second magnetic element. This spin-transfer torque can be used to either switch the magnetization or to create a steady-state gyration regime. In the latter case, GMR or TMR can be used to translate this

magnetization gyration into an oscillating voltage in the microwave frequency range, leading to the concept of spin-transfer oscillator as depicted in **Figure I.3**.
The new kind of memory based on STT, namely STT-MRAM, was developed in 2005 [23]. The first product in the market was in 2012 by EverSpin [24] and several companies, including Samsung and Intel, have announced mass production during the last two years.

I.2 Spin-orbit coupling (SOC) and Spin-orbitronics

New concepts and discoveries are rapidly emerging in the field of spintronics and in cross-disciplinary areas. This gives rise to different effects that are named here and there. All these effects can be encompassed in two basic concepts, although they can be understood - if desired - phenomenological. Namely: i) the spin current, and ii) the interconversion of spin current and charge current. Most of these new effects involving detection, manipulation or generation at some point of a spin current are based on spin-orbit coupling (SOC). We speak then of spintronics 2.0 or spin-orbitronics.

Spin current

A pure spin current in metals is simply defined as electrons with opposite spins moving in opposite directions. So, there is not net flow of electrons charges but only electrons spins [25,26]. Thus a spin current will not generate a measurable electrical voltage but a spin accumulation. Such conveyance of angular moment is realized through spin waves in insulator ferromagnetic. It should be noted that a typical electrical current in a non-magnetic metal is called "charge current".
There are different ways to generate spin currents depending on the physical origin of the excitation such as heat [27,28], light [29], ferromagnetic resonance spin pumping [30], acoustic wave [31–33], and spin-orbit coupling phenomena [25,34–36].

Spin-charge current interconversion

Once the concept of spin current is understood, one then wishes to create, manipulate and detect a spin current either to develop new devices for practical applications or to investigate new phenomena for fundamental research. This comes down to two key operations: conversion of a charge current into a spin current, and its reciprocal: conversion of a spin current into a charge current.
Today, the conversions of spin current into charge current and vice versa are essential operations in spintronics devices.

Spin Hall effect (SHE)

The spin Hall effect can be understood as the electron spin dependent asymmetric scattering [37–39] due to spin-orbit coupling. In the direct SHE, an electrical current flowing through a material with a relativistic spin-orbit coupling will generate a transversal spin current (direct SHE). The reciprocal effect also exists and is called inverse SHE (ISHE). It happens when a pure spin current, injected through a material with spin-orbit coupling properties, generates a transverse charge current. This asymmetric scattering was first

proposed in 1971 by Dyakonov and Perel [34]. However the interest was triggered with the fast development of the spintronics and a new theoretical work with similar predictions by Hirsch [25] who gave the name to the phenomena. SHE and ISHE were predicted and detected in semiconductors [40–43] like GaAs [42], pSi [43], pGe [44] and nGe [45–47]; in metals such as Al [48], Pt [49–57], Pd [53,58], Ta [59–61] and W [62–66], and in alloys [67–69] such as CuIr [70], CuBi [71], CuPb [72], AuW [73–75], CuPt and AuTa [75]. The spin Hall effect is a bulk manifestation of the charge-spin current conversion due to spin-orbit coupling. Thus the charge-spin current conversion happens in the bulk of the material but its detection should be performed at the edge of the sample. A schematic representation of the SHE and ISHE is showed in **Figure I.4**.

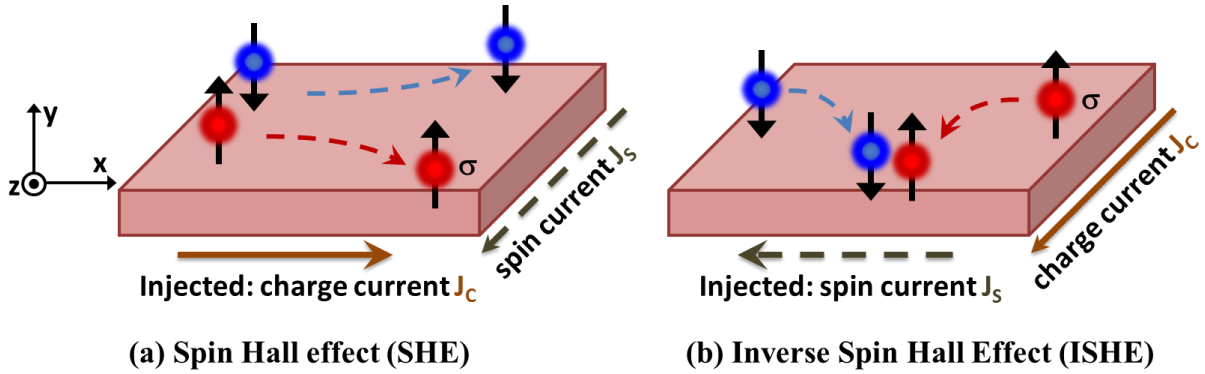

(a) Spin Hall effect (SHE) **(b) Inverse Spin Hall Effect (ISHE)**

Figure I.4 Schematic of SHE and ISHE. In (a) a charge current Jc is injected along +x and due to spin-orbit coupling a transversal spin current JS is generated along +z with a spin polarization σ along +y. In (b) a spin current Js with a spin polarization σ along +y is injected along –x. Thanks to SOC this spin current is converted in a transversal charge current along +z. Note that in SHE a spin accumulation is generated in the z-edge of the sample with opposite spin polarization for each edge but not electrical signal can be measured. In contrast, in the reciprocal effect, ISHE, a charge accumulation is generated thus an electrical signal along z can be measured.

Mechanism of the SHE

As for the Anomalous Hall effect (AHE), we have intrinsic and extrinsic [76] contributions to the SHE, all due to SOC. The intrinsic mechanism is related to the interband coherence induced by an external electric field, i.e an injection of charge current. There is two kind of extrinsic mechanism where electrons are deflected after scattering in an impurity due to effective SOC: the skew scattering and side jump. These contributions are illustrated in **Figure I.5**.

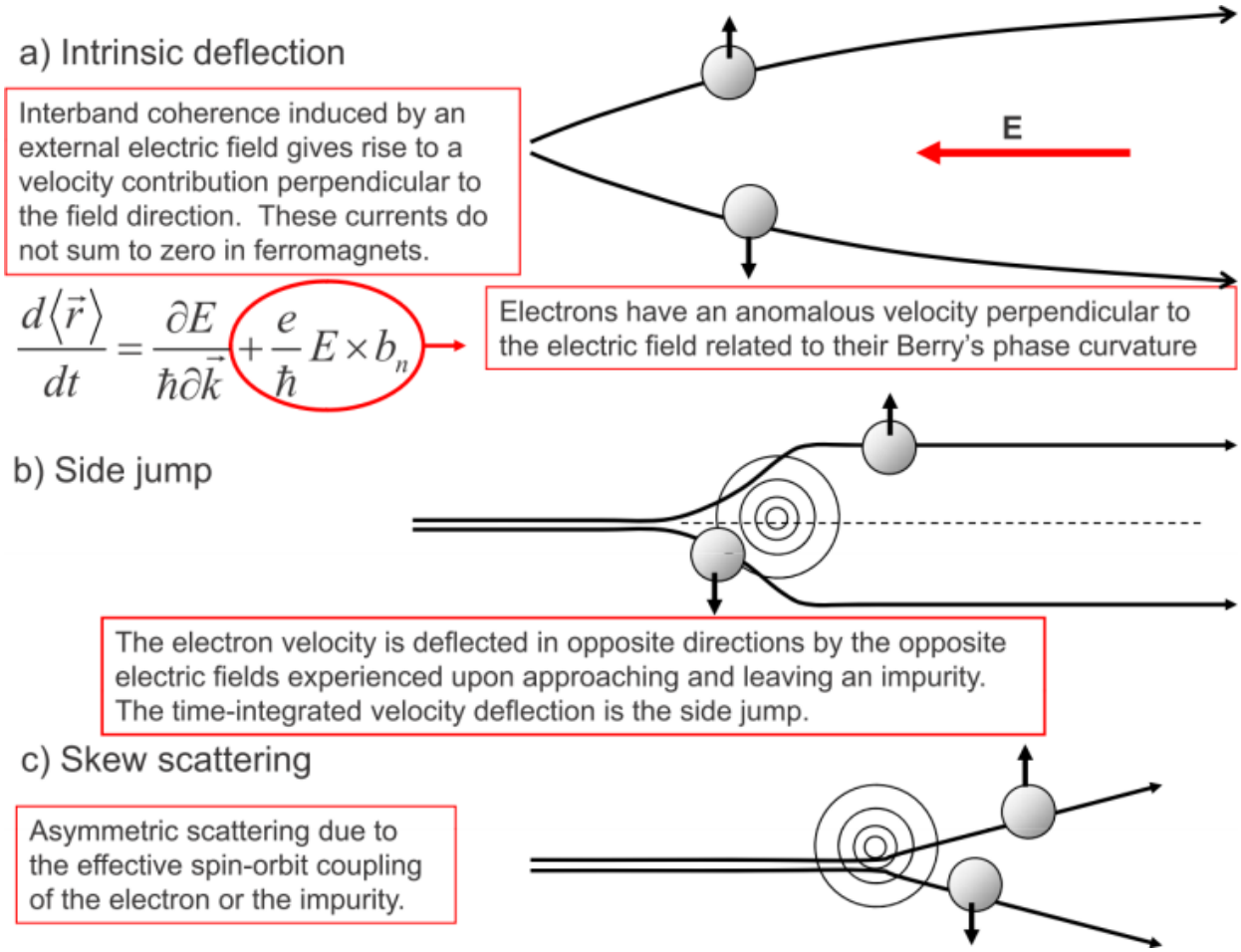

Figure I.5 Illustration of the three main mechanisms that can give rise to an AHE as well as SHE. Taken from [77].

For sake of comparison **Figure I.6** shows three effects: Hall effect, AHE and SHE. In the Hall effect (discovery by Sir Edwin Hall in 1879) a conductor develops a transverse voltage due to the Lorentz force acting on the charge current in the presence of an external magnetic field. The AHE happens in FM materials. In FM materials the transverse voltage is not simply proportional to the magnetic field, but there is an additional contribution related to the magnetization. Thus, the electrons flowing in a ferromagnetic conductor acquire a transverse velocity with opposite directions for different spin orientations. Therefore, spin dependent transverse velocity results in a net transverse voltage. As mentioned, in the SHE upon an injection of a charge current and without any external magnetic field is created no net voltage but a transverse spin accumulation is generated.

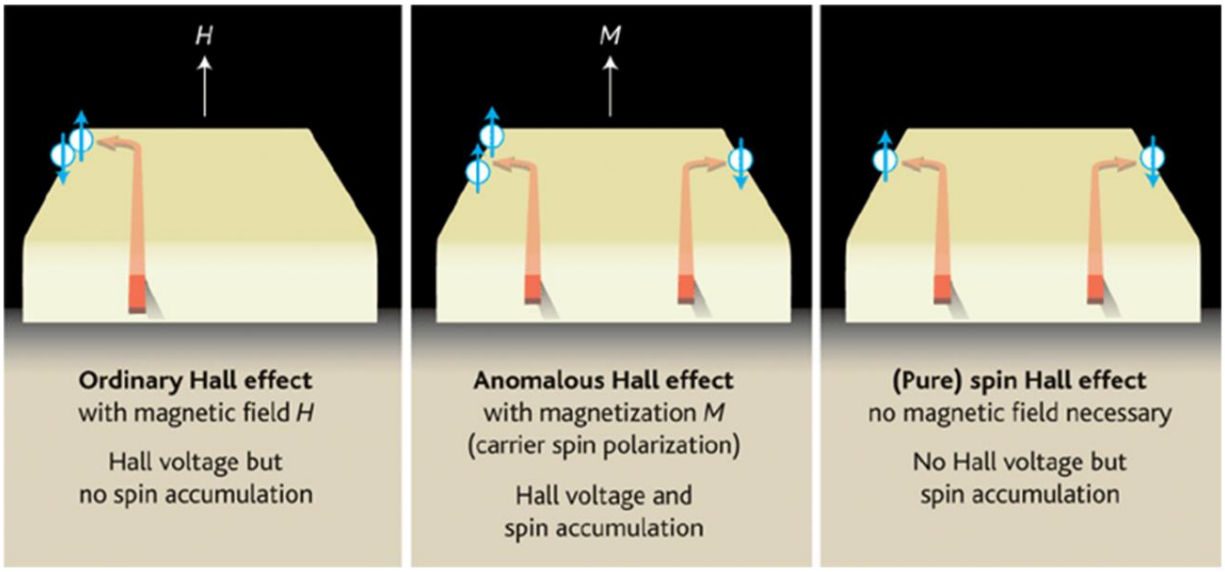

Figure I.6 Illustration of three phenomena due to SOC: Ordinary Hall effect in normal metals, AHE in magnetic metals, and SHE in normal metals with strong SOC. Taken from [78].

Efficiency of SHE

The conversion ratio between the charge current and spin current is called the spin Hall angle (θ_{SHE}) which is a dimensionless parameter. The same parameter quantifies the efficiency of the reciprocal effect, ISHE. The spin Hall angle is subsequently a key parameter to qualify a material for the integration in new experiments, and new spintronics-based devices. Large spin Hall angles can be found in 5*d* or 4*d* transition metals such as Pt, Ta, and W. Additionally in metal alloys such as CuBi, CuIr, and AuW, it will be possible to tune the magnitude of the spin Hall angle varying the composition of the alloy. Here there is a path to explore new alloys of Cu or Au host doped with impurities such as C, Bi or Os, in order to enlarge the SHE efficiency due to resonant asymmetric scattering by impurities [68,69] as proposed already in 1981 [67]. Indeed, the spin Hall resistivity, ρ_{SHE}, is proportional to the longitudinal resistivity ρ for an intrinsic and skew scattering contributions but is proportional to the square of such longitudinal resistivity for a side-jump contribution. The spin Hall angle being also the ratio of spin Hall resistivity over the charge or longitudinal resistivity, i.e. $\theta_{SHE} = \rho_{SHE} / \rho$. Thus, by looking new alloys materials with strong spin-orbit coupling where we can change the longitudinal resistivity therefore the spin Hall angle can be modulated. If side-jump contribution or intrinsic mechanism are dominant, then $\theta_{SHE} \propto \rho$, otherwise if skew scattering mechanism is predominant, then θ_{SHE} is independent of ρ. An experimental demonstration of side-jump mechanism contribution was achieved in the AuTa alloy [75].

Independently of the value of the spin Hall angle, interfaces play also an important role in the injection of pure spin current from one layer to another due to the spin-flip scattering at the interfaces and spin resistance at the interfaces. Thus, we talk about an interfacial spin memory loss (SML) [57,79–81]. The relevance of such SML effect in the correct qualification of spin

Hall angle in materials was recently pointed out [57,80]. One can optimize the spin Hall angle in a material, however its contribution to the spin injection could be strongly decrease by the interface. For example, in metallic-ferromagnetic/normal-metal (FM/NM) systems with large SML or poor transmission coefficient, part of the spin current injected from one layer to the other one will be lost at the interface.

Edelstein Effect and Inverse Edelstein effect

aka Rashba-Edelstein effect, Inverse spin galvanic effect and its reciprocals.

More efficiency spin-charge current interconversion due to SOC can be harnessed in two-dimensional (2D) electron gas (2DGES) at the surfaces of new kind of materials so-called 3D topological insulators (TIs) and at Rashba interfaces due to its spin texture or spin momentum locking (momentum and spin electrons are locked to be orthogonal, suppressing back-scattering). These systems are characterized by their dispersion relationship in the reciprocal space $E(k)$. **Figure I.7** displays a schematic of a Rashba interface (a) and a TI (b) in equilibrium. We can observe in the Rashba interface a splitting of the sub-bands depending on the spin. Thus at a given energy level there is two contours with opposite spin texture.

A 3D topological insulator can ideally be considered as an insulator in its volume but having gapless metallic states on its surfaces. In the topological insulator, due to arguments of symmetry and spin-orbit coupling, these surface states, so-called topological states, exhibit a linear dispersion relation $E(k)$, as for massless Dirac Fermions. An example of this linear relationship of the topological surfaces states is shown in **Figure I.7b** which is so called Dirac dispersion cone or Dirac cone and which is usually detected by Angular Resolution Photoelectron spectroscopy (ARPES). At the Fermi level, in the simplest case of circular contours, there are two contours for the Rashba interface and one for the topological states [82–85].

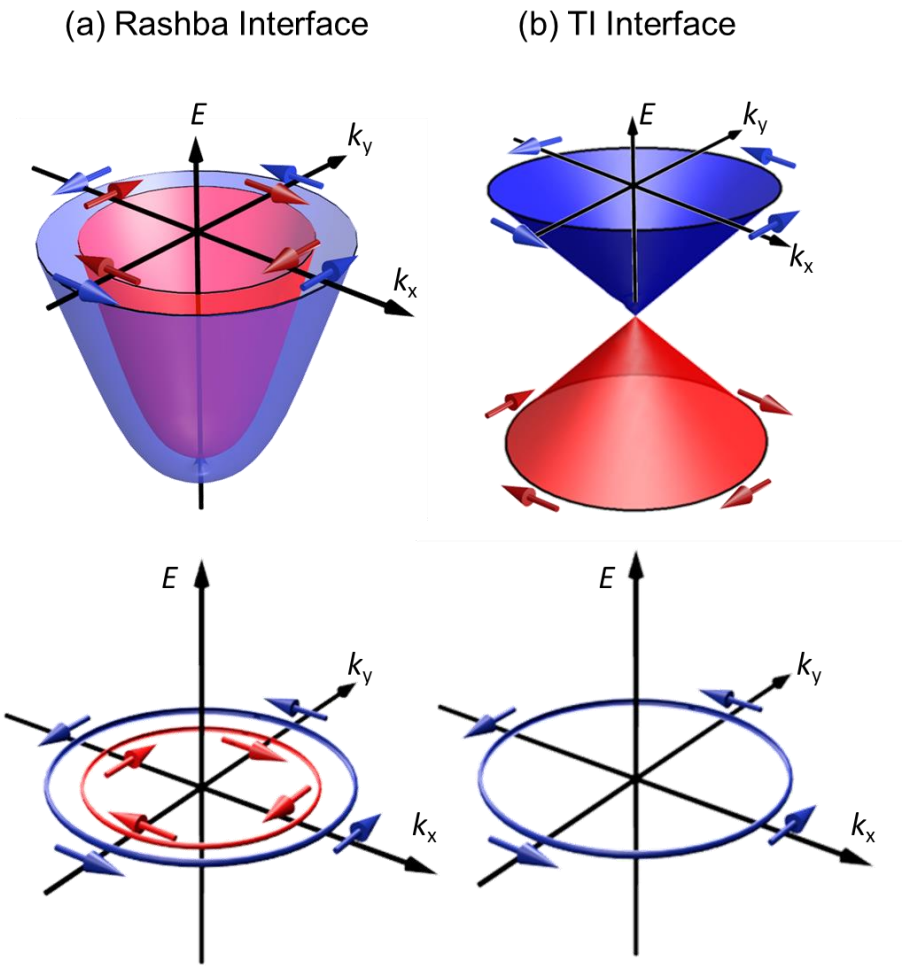

Figure I.7 Schematic illustration of dispersion relationship *E*(*k*) for 2DEG Rashba interfaces (a) and topological insulators (b) at equilibrium. The blue and red arrows indicate the electrons spin polarization. In the bottom are schematized the contours at Fermi level. We can observe two Fermi contours in Rashba interfaces with opposite spin chirality while in TI there is only a single Fermi contour also with spin-momentum locking. This is an example where the contours are circular. In many systems this is not the case, and there are also other bands, either of surfaces or of bulk.

The Edelstein effect can be easier understood in the reciprocal space where we observe the helical spin texture or spin momentum locking is this 2DEG systems. This is schematized in **Figure I.8** for Rashba interfaces (a) and topological insulators (b). Edelstein in 1990 [86], among others before [87–89], proposed that when a charge current Jc is injected in a 2DEG system such as Rashba interface, a nonzero spin accumulation density is automatically generated. An injection of charge current means a variation of momentum; let's suppose Δk along $+k_x$ direction. Due to spin texture or spin momentum locking in these systems, an overpopulation (depletion) of electrons with $+\sigma_y$ ($-\sigma_y$) is created. Note however that for a Rashba system, in the inner contour (red in the **Figure I.8a**) there is a creation of smaller nonzero spin density with opposite spin polarization, $-\sigma_y$. The EE in real space is schematized

in (c). The injected charge current in these 2DEG systems will induce a spin accumulation which can diffuse as a spin current Js into adjacent layers.

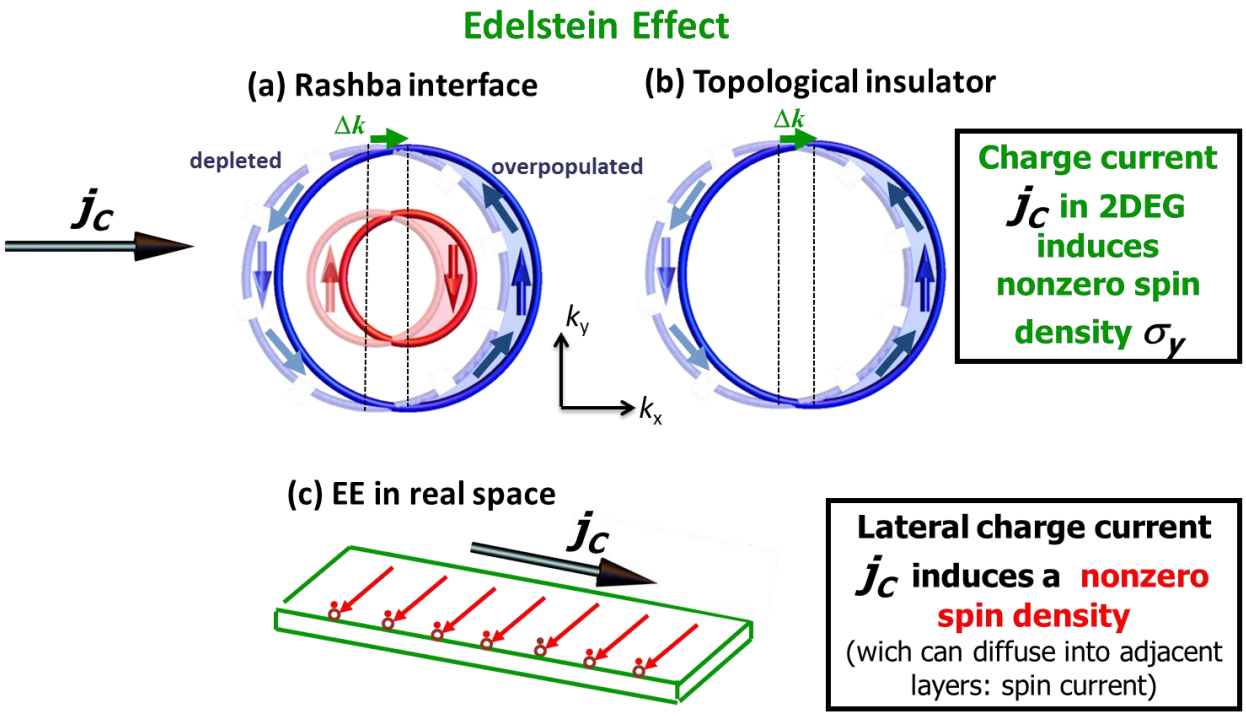

Figure I.8 Schematic of Edelstein effect. In the reciprocal space for (a) a Rashba interface and (b) topological insulators. Edelstein, among others before, proposed that when a charge current Jc is injected in a 2DEG systems, a nonzero spin accumulation density is automatically generated. In the illustrations, the variation of moment, Δ_k, is considered along $+k_x$. Due to spin texture or spin momentum locking in these systems, an overpopulation (depletion) of electrons with $+\sigma_y$ ($-\sigma_y$) is created. The EE in real space is schematized in (c). The injected charge current in these 2DEG systems will induce a spin accumulation which can diffuse as a spin current Js into adjacent layers.

The Inverse Edelstein effect can be also understood analyzing the similar cartoons in the reciprocal space as exposed in **Figure I.9** for Rashba interfaces and topological insulators. We have postulated that the reciprocal of the EE effect also exist and thus when a vertical spin current Js is injected in 2DEG systems, a lateral charge current is induced. This was also previously postulated by Levitotv et al. in 1985 [89]. In the cartoon of **Figure I.9**, the injected spin current Js has a spin polarization $+\sigma_y$. Thus, electrons can only be injected in the $+k_x$ region and extracted from the opposite region, $-k_x$. As consequence there is a shift of Fermi contour which in turns means a variation of moment Δk, along $+k_x$ in the illustration. It turns out that a variation of moment is nothing else that charge current. Thus the vertical injection of the spin current Js generates a lateral charge current in 2DEG systems due to its helical spin texture. This is schematized in the real space in (c). The generated charge current in these 2DEG systems can be detected as a voltage in an open circuit.

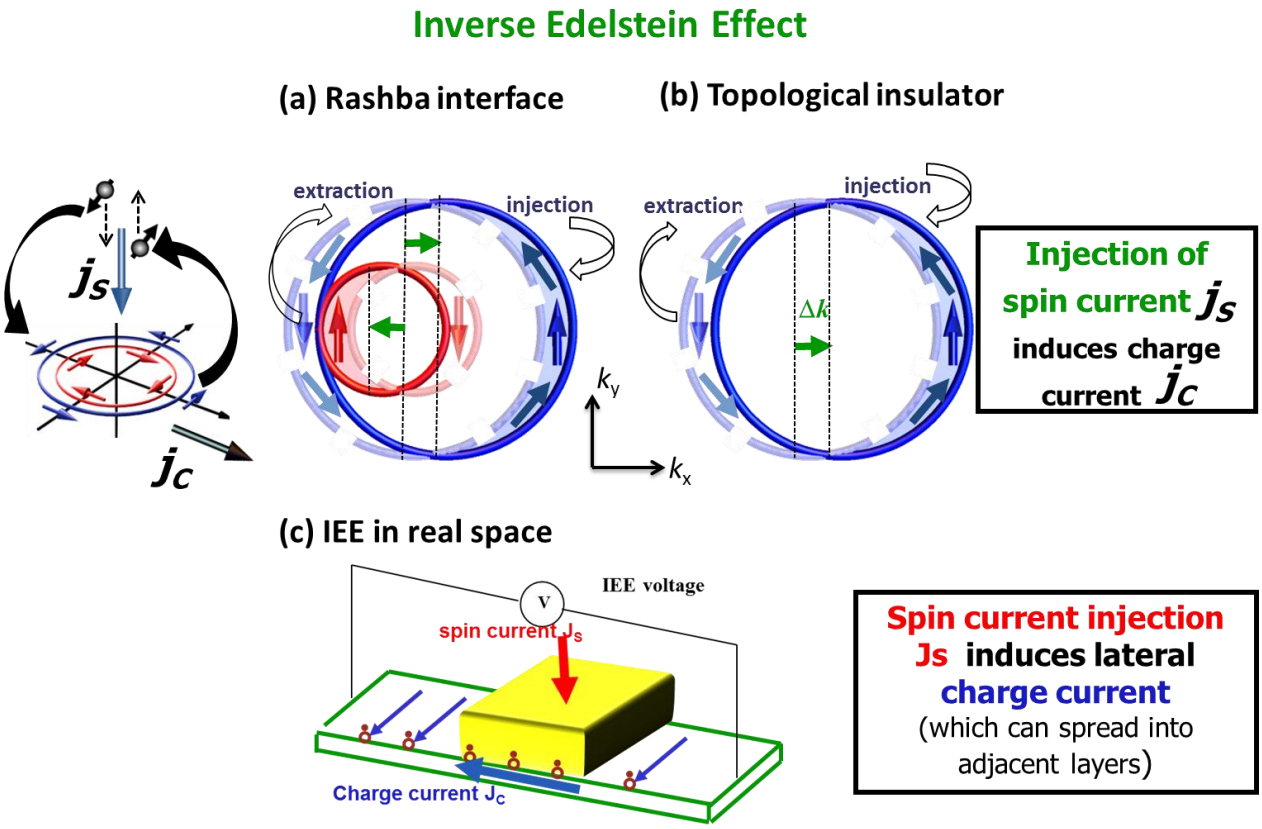

Figure I.9 Schematic of the Inverse Edelstein effect. In the reciprocal space for (a) a Rashba interface and (b) topological insulators. We have postulated that the reciprocal of the EE effect also exist and thus when a vertical spin current Js is injected in 2DEG systems, a lateral charge current is induced. In the illustrations the spin current Js has a spin polarization $+\sigma_y$. Thus, electrons can only be injected in the $+kx$ region and extracted from the opposite region, $-k_x$. As consequence there is a shift of fermi contour which in turns means a variation of moment Δk, along $+k_x$ in the illustration. It turns out that a variation of moment is nothing else that charge current. Thus the vertical injection of the spin current generates a lateral charge current in 2DEG systems due to its spin texture. This is schematized in the real space in (c). The generated charge current in these 2DEG systems can be detected as a voltage in an open circuit.

Efficiency of EE and IEE

The conversion ratio between the charge current into spin current by EE and between spin current into charge current by IEE are now not equivalent as for SHE and ISHE. Moreover, those parameters have now different dimension. As depicted in **Figure I.8**, in the direct effect, a 2D charge current (in A/m) along x flowing in a Rashba interface or at the surfaces of topological insulator generates a transversal 3D spin current (in A/m^2) along z perpendicular to the interface or surface and with a spin polarization σ along +y in the **Figure I.8**. This gives an efficiency ratio in units of 1/length, m^{-1}.This efficiency has been so-called q_{ICS} [90]. On the other hand, for the reciprocal effect, as depicted in **Figure I.9**, if one succeed to inject a 3D vertical spin current Js into this 2DEG having this particularly helical spin texture, a

charge current is generated in this 2DEG. Consequently, this charge current generated is a 2D one. Now the conversion ratio for the reciprocal effect has units of length, namely inverse Edelstein effect length, λ_{IEE} [36,91,92]. The relationship between efficiency in both EE and IEE is not trivial, depending on each particular system, and it will be discussed in chapter III and V. Particularly, a way to link or compare the SHE (ISHE) against EE (IEE) will be discussed in the last section of Chapter IV.

Spin-orbit torque

A particular case of charge to spin conversion- due to spin-orbit coupling- or spin accumulation at a given interface could be exploited to exert a torque to the magnetization of an adjacent magnetic layer. This is known as spin-obit torque (SOT). And it provides new routes to manipulate the magnetization, lowering energy consumption for different kind of devices as for magnetic memories SOT-MRAM. While current spintronics memories are based on spin-transfer torque as depicted in **Figure I.3**, the new SOT-MRAM provides the advantages of increasing durability since the paths for writing and reading operations are separate. For writing operations, where the highest current densities are needed, the current is no longer passed through the tunnel barrier but through the horizontal heavy metal (HM) layer - or interface - which has strong SOC and will produce a spin accumulation or transverse spin current. This spin current might produce a torque on the magnetization of the free FM layer and eventually switch it. Important is then to understand the SOT in FM/HM bilayer systems towards an optimization seeking to obtain the switching of the magnetization only with electric or charge current, to reduce the current and to reduce the power required for such switching. This opens a whole field of research and interface engineering to achieve these aims.

Regardless of the mechanism behind the origin of the SOT, we will discuss even newer concepts beyond SHE and EE in next section and in chapter VI, the magnetization dynamics can be described by the Landau-Lifshitz-Gilbert (LLG) equation allowing for a SOT term $\mathbf{T}_{SOT}$:

$$\frac{d\hat{\mathbf{m}}}{dt} = -\gamma\hat{\mathbf{m}}\times\mathbf{H}_{eff} + \alpha\hat{\mathbf{m}}\times\frac{d\hat{\mathbf{m}}}{dt} + \frac{\gamma}{M_s}\mathbf{T}_{SOT} \tag{1.1}$$

$$\mathbf{T}_{SOT} = \tau_{FL}\hat{\mathbf{m}}\times\hat{\boldsymbol{\sigma}} + \tau_{DL}\hat{\mathbf{m}}\times(\hat{\mathbf{m}}\times\hat{\boldsymbol{\sigma}}) \tag{1.2}$$

where $\gamma = g\mu_B/\hbar$ is the absolute value of the gyromagnetic ratio; g, μ_B and $\hbar$ are the Landé g-factor (2 for free electrons), Bohr magneton, and reduced constant Planck, respectively. $\mathbf{H}_{eff} = -\delta F/\delta\mathbf{M}$ stands for the effective field around which magnetization precession takes place, first term of the Eq. (1.1), and defined as functional derivative of the magnetic energy density F (Gibbs free energy). The dimensionless Gilbert damping parameter is given by α, the saturation magnetization by M_s, and $\hat{\mathbf{m}} = \mathbf{M}/Ms$ is the magnetization unit vector. The second term in Eq. (1.1) accounts for the relaxation of the magnetization towards its equilibrium position. The torque, always perpendicular to the magnetization, is expressed in

two orthogonal components- transversal τ_{FL} and longitudinal τ_{DL} - as displayed in Eq. (1.2), where the unit vector $\hat{\boldsymbol{\sigma}}$ stands for the spin polarization of the spin accumulation or of the injected spin current. The transverse component of the torque, τ_{FL}, is normal to the $(\hat{\mathbf{m}},\hat{\boldsymbol{\sigma}})$ plane while the longitudinal one, τ_{DL}, lies in the $(\hat{\mathbf{m}},\hat{\boldsymbol{\sigma}})$ plane as depicted in

Figure I.10. Additionally, we can see in Eq. (1.2) that the transversal torque τ_{FL}, acts on the magnetization dynamics like an effective field, i.e first term in Eq. (1.1), whereas the longitudinal torque τ_{DL} acts like an effective magnetic damping, i.e second term in Eq. (1.1). Thus, the two torque components τ_{FL} and τ_{DL} are denoted as field-like and damping-like, respectively. Furthermore, we can define effective magnetic fields that drives each components of this SOT, namely H_{FL} and H_{DL}, expressed as:

$$\begin{aligned}\mathbf{H}_{DL(FL)} &= (\boldsymbol{\tau}_{DL(FL)} \times \hat{\mathbf{m}})\frac{1}{\gamma} \\ \mathbf{H}_{DL} &\propto (\hat{\mathbf{m}} \times \hat{\boldsymbol{\sigma}}) \\ \mathbf{H}_{FL} &\propto (\hat{\boldsymbol{\sigma}})\end{aligned} \tag{1.3}$$

We can see that these effective fields are in turn parallel (H_{FL}) or perpendicular (H_{DL}) to the spin polarization σ. We will see some cases where SOT is driven mainly for the SHE to switch a perpendicular magnetization in chapter V. And considering new concepts such as spin Anomalous Hall effect and magnetic Rashba interfaces some preliminary results of self-torque in chapter VI. **Figure I.11** (taken from ref. [93]) presents a summary of the potential functionalities and applications of SOT combining different materials and heterostructures to which I would add Heusler compounds and ferrimagnets.

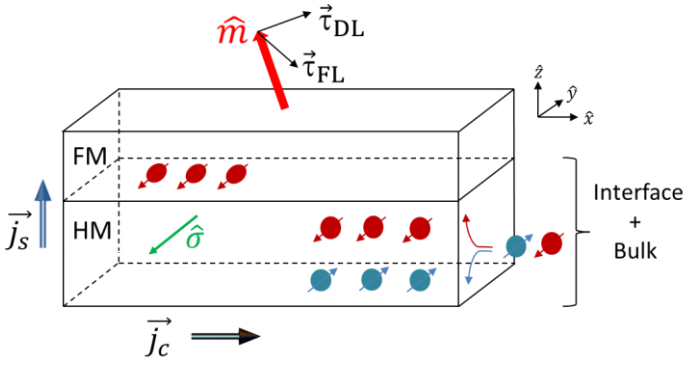

Figure I.10. Graph showing the axes and torques exerted on a magnetization m. It has been considered that the polarization of the spin current or spin accumulation at the origin of that torque is along the y-axis, σ//-y. Courtesy of Heloïse Damas.

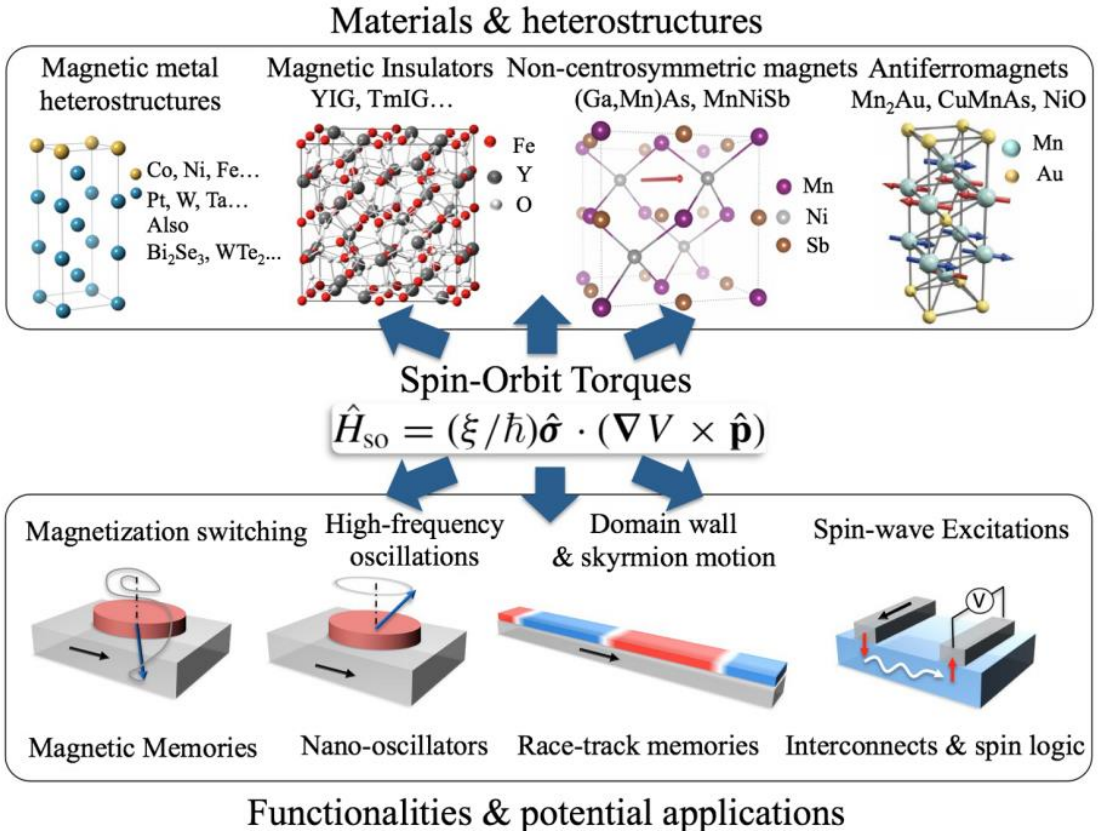

Figure I.11 Materials in which spin-orbit torques have been observed range from metallic heterostructures involving transition metals, topological insulators, and other heavy element substrates to bulk non centro symmetric ferromagnets and antiferromagnets. Spin-orbit torque is a promising candidate mechanism to drive disruptive spintronics devices such as magnetic memories, nano-oscillators, racetrack storage devices, as well as interconnects and spin logic gates. Taken from [93].

To go deeper into some of the aspects described in this chapter some reviews on these topics are references [77] for AHE, [38] for SHE in metals, [94] for SHE and EE (called inverse spin galvanic effect in this review), and [93] for SOT.

II. Spin-to-charge current conversion in bulk

This chapter is devoted to the experimental studies of the ISHE. This is to show some techniques that allow using ISHE to quantify some relevant spintronics parameters as spin Hall angle, spin diffusion length and interfaces properties (spin memory loss or transparency). I will describe first the results on lateral spin valve, then using spin pumping ferromagnetic resonance to finally show some perspectives using longitudinal spin Seebeck effect.

Lateral spin valve

I feel lucky to have done my first postdoc in Grenoble where I started to discover new concepts such as spin current, spin Hall effect and so on. Particularly the study in nano devices thanks to the expertise in electronic lithography of my former boss, Laurent Vila. During my first post doc I have started to study devices based on so-called lateral spin valve (LSV). This device based on magnetic nanostructures is formed by two parallel ferromagnetic electrodes which are joined by a non-magnetic (NM) transverse wire as represented in **Figure II.1**. When an electric current I (charge current) flows through an FM/NM interface there is a spin accumulation which can be relaxed in the NM wire generating a spin current [95,96]. This spin current can be detected on the second FM/NM interface using a non-local voltage V measurement [48,73,97–102]. This non-local voltage V, normalized by the injected current I into the other FM/NM interface is so called spin signal, R or R_{NL}.

The amplitude of this spin signal is calculated by the difference between the signal when the two FM electrodes have their magnetizations parallel to each other and when they are anti-parallel. Usually this spin signal is a few mOhm and depends on the FM and NM materials used, the quality of the FM/NM interfaces, the distance between the two interfaces, the geometry (mainly width) of the nanowires and the temperature.

This type of nano device was used in the 1980s to show the injection of spin into some metals. Later, it was possible to show SHE [48] in metals for the first time based on these devices[1]. For this purpose a third HM nanowire with strong SO coupling, typically Pt, is nanostructured in parallel and between the FM nanowires. Part of the spin current flowing in the NM crossover nanowire is then absorbed by this new HM nanowire and detected by the ISHE in the HM itself. The reciprocal experiment can also be performed: to do so, the charge current is circulated in the HM nanowire, which through the SHE will produce a transverse spin current that is injected into the NM nanowire and detected in one of the NM/FM interfaces. For further reading on these devices and effects one can have a look for example at

[1] For this work SV has been granted the Young Scientist Award of the IUPAP Magnetics Section in 2009.

the following reviews [39,103] or recent studies in metal [73,104,105]. The development and research with these devices requires access to the state of the art in electronic lithography techniques. Also, the whole process of lithography requires various stages making it difficult to have clean FM/NM and HM/NM interfaces. Without being exhaustive, some groups that work exploiting these devices are in Groningen (Van Wees' group), Tokyo (Otani's group), Chalmers U. (Dash's group), Nanogune (Casanova and Hueso's group), ICN2 (Valenzuela's group) and in Spintec-Grenoble (my former boss' group). Next I will show and describe briefly one of my main and first contributions in this type of devices [106].

To my knowledge, the highest spin signal amplitude reported in these types of devices is 2.5 Ω at 4.2 K using different materials for the FM electrodes [107]. In that work one FM electrode was CoFe and the other one was NiFe. The NM channel was Al and AlOx tunnel barrier was used at the FM-Al interfaces. Other values are < 10 Ohm in the non-local system of FM-NM-FM system with transparent or ohmic contact at the interfaces. In our case, I measured 168 mΩ of amplitude at 77 K using NiFe-Al-AlOx-NiFe LSV [106]. If there is not that oxide, the signal is just 24 mΩ for transparent (without barrier) contacts [100].

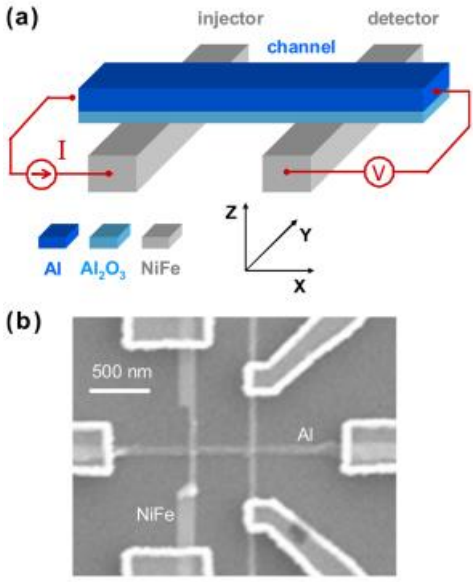

Figure II.1. (a) Scheme of a central part of a lateral spin valve (LSV). The drawn electrical connections correspond to a non-local measurement. (b) SEM image of a LSV. Taken from [106].

Thus, we have shown that this spin signal is strongly amplified when a barrier, such as AlOx, is added between the NiFe/Al interfaces, because the relaxation of the spin accumulation on the FM injector itself is reduced. In other words, the AlOx barrier reduces the back-flow of spin accumulation from the NM wire to the FM wire. Furthermore, we have taken advantage of this large spin signal and the appropriate aspect ratio of the nanowires (thickness and width around 50 nm each), to demonstrate that it is possible to manipulate the orientation of the spin arriving at the FM detector in all three spatial dimensions through Hanle effect experiments, **Figure II.2**. We have obtained the angle between the NiFe magnetization and the applied field taking advantage of AMR curves and then we have used these angles to fit the Hanle curves, **Figure II.3**. This 3D control is also very interesting for technological applications.

More recently, exploiting FM/NM interface of a LSV structure, it has been shown that a pure spin current is injected into a nonmagnetic wire only when a domain wall is pinned at the constriction [108].

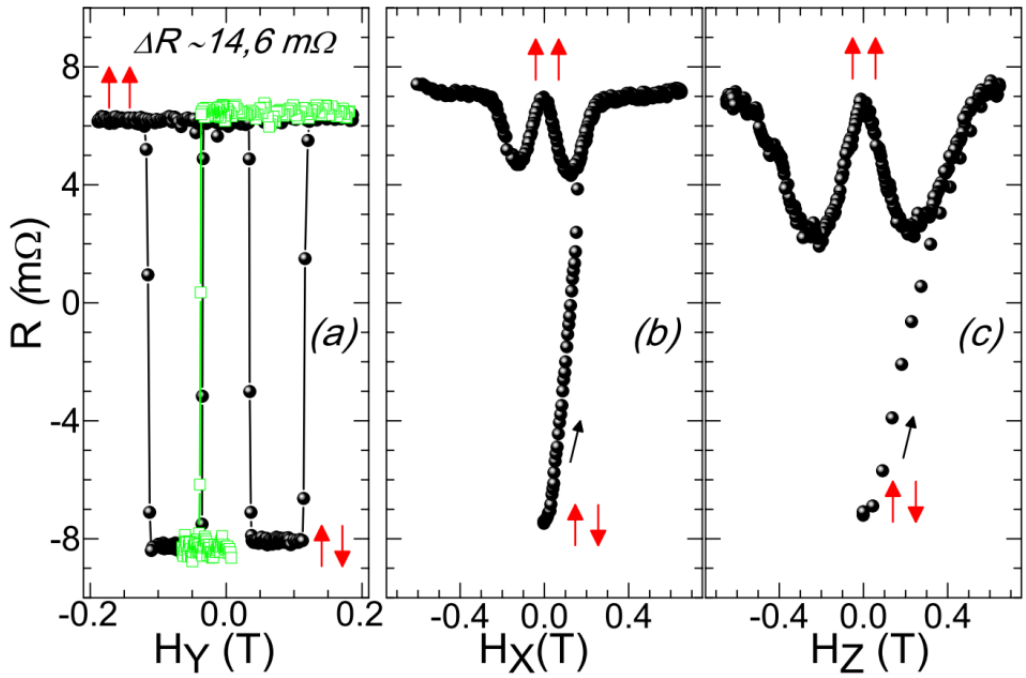

Figure II.2 Nonlocal measurement (black dots) obtained on a FeNi/AlOx/Al LSV, where the magnetic field H is applied along the FeNi wires, H//Y (a), along the Al transversal channel, H//X (b), and along the normal to both nanowires, H//Z (c). The small red arrows represent the relative magnetization between the two NiFe nanowires in parallel or anti-parallel states. Green open squares in (a) is a minor loop allowing reaching the antiparallel state. The distance between the ferromagnetic wires is 350 nm. (a) is the typical measurement in LSV while (b) and (c) the electrons also precess around the applied field, and this type of curve accounts for the Hanle effect. Both Hanle curves starting from parallel and antiparallel configuration are shown in each case. The measurements were performed at 77 K, and the resulting spin signal amplitude is around 14.6 mΩ in all the three measurements. Taken from [106]

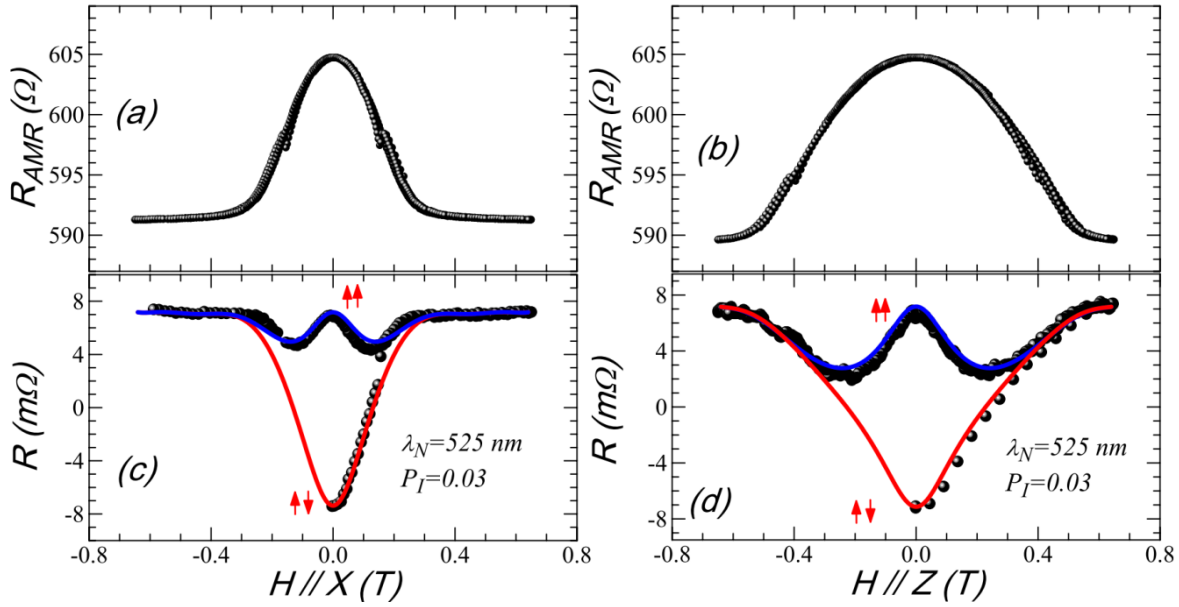

Figure II.3 Anisotropic magnetoresistance curves of the NiFe wires when the external magnetic field is applied along the X (a) and Z (b) directions. These curves can be adjusted by the typical dependence, $R_{AMR}(H) = R_{\perp} + (R_{\perp} - R_{\parallel})\cos\theta^2(H)$, to obtain the angle between the NiFe magnetization and the applied field. This angle will then be used to fit the Hanle curves at (c) and (d), the equations are not shown. With such an experiment we can obtain the spin diffusion length in the NM cross channel of Al, and the spin polarization P_I in the FM/AlOx/Al. In (d) the spin precession in the Al channel is around H_Z while in (c) is around H_X which has been shown for the first time in this study. Taken from [106]

II.1 Inverse spin Hall Effect (ISHE) by spin pumping ferromagnetic resonance (SPFMR)

One of the methods to evaluate relevant spintronics parameters like spin Hall angle, spin diffusion length and even interface properties is the so-called spin pumping based on ferromagnetic resonance. Its use has been widely spread because of the ease of the technique, and, in general, the ease of its analysis. Usually the magnetic damping constant is measured, but in my opinion that measurement is a first step since the origin of the damping enhancement can be due to many other causes besides the spin pumping effect, namely defects due to poor sample quality. The most complete experiment in addition to the damping measure is the measurement of spin pumping voltage. In this section we will discuss the spin pumping voltage when its origin is in volume (due to the inverse spin Hall effect), and in the next chapter we will discuss the spin pumping voltage when its origin is due to spin-charge conversion in two-dimensional system interfaces.

In the next sub-section I will first describe the ferromagnetic resonance (FMR), and then turn to the spin pumping phenomenon.

Ferromagnetic resonance (FMR)

Ferromagnetic resonance (FMR) is a well-established technique for more than six decades to characterize ferromagnetic (FM) systems. The numbers of magnetic moments that are detectable in an FMR experiment are in the order of 10^{10} – 10^{14}, depending on the linewidth of the signal. This corresponds to a film thickness in the range of a single atomic layer. Due to its high sensitivity, FMR has been widely used for the study of FM metallic thin films and more recently FM insulator magnetic thin films. The technique can also be used to study the coupling between FM films separated by a non-magnetic spacer layer.

In a typical ferromagnetic resonance experiment the sample is placed in a microwave cavity (the use of coplanar waveguides, CPW, has become more popular in the last two decades). Two fields are then applied perpendicular to each other: an alternating field, h_{rf}, of constant frequency and a dc field, H. The dc field is swept while the amplitude and frequency of the alternating field stay fixed. When the system reaches the resonance condition, the injected microwave power is strongly absorbed by the sample. This result in a peak or valley of absorption in a power absorbed vs. field sweep. The motion of the magnetization M of the sample in an FMR experiment can be described by the Landau-Lifshitz equation proposed in 1935 [109] extended with the Gilbert damping term in 1955 [110] (LLG equation) which is written now as

$$\frac{d\hat{\mathbf{m}}}{dt} = -\gamma\hat{\mathbf{m}}\times\mathbf{H}_{eff} + \alpha\hat{\mathbf{m}}\times\frac{d\hat{\mathbf{m}}}{dt} \qquad (2.1)$$

The first right-hand term of equation (2.1) describes the precession of magnetization in an effective magnetic field H_{eff} that includes the external field, the demagnetizing field and fields

of magnetic anisotropies. $\mathbf{H}_{\text{eff}}$ is given by the functional derivative of the magnetic energy density F (Gibbs free energy), $\mathbf{H}_{eff} = -\delta F / \delta \mathbf{M}$. The second right-hand term in equation (2.1) is a dissipative term describing the damping of the magnetization precession. The main intrinsic contribution to the Gilbert damping constant in FM thin films arise from the spin-orbit coupling and d-band of 3d FM. Others intrinsic mechanism includes: i) Eddy currents induced by the magnetization precession and its dissipation is proportional to the conductivity and the square of the FM thickness [111] which contribution may be negligible for FM films below 10 nm. ii) Phonon drag by direct magnon-phonon scattering [112]. The phonon Gilbert damping for Ni crystal was estimated to be $\alpha_{\text{phonon}} \sim 0.001$ Woltersdorf (ref). The phonon drag damping contribution will be then weaker in Fe, Co, and Py because magnetostrictive effects are weaker in those materials than in Ni. It might be illustrative to mention the model proposed by Heinrich et al. [113,114] based on the interaction of s-p like electrons with localized d spins which work well for NiFe. They have shown that for this contribution the damping reads:

$$\alpha_{\text{s-d}} = \frac{\chi_{\text{p}}}{\gamma M_s} \frac{1}{\tau_{\text{sf}}}, \qquad \chi_{\text{p}} = \mu_{\text{B}}^2 N(\varepsilon_F) \tag{2.2}$$

where χ_p is the Pauli susceptibility for itinerant electrons (in the order of 3-9×10^{-6} for 3d transition metals), τ_{sf} is the spin flip relaxation time (~3×10^{-14} s for NiFe but ~4×10^{-12} s for Co), and $N(\varepsilon_F)$ is the density of states at the Fermi level. The experimental damping value for NiFe is about 0.005 which agrees well with eq. (2.2). Moreover, the s-d relaxation is indirectly proportional to the momentum relaxation and it is expected that damping constant scale with resistivity as shown experimentally in ref. [115] . However, s-d interaction does not contribute to pure 3d FM metals as τ_{sf} is very slow. Extrinsic contributions to the magnetic damping includes inhomogeneities, impurities or doping, two-magnon scattering, spin pumping which be discussed in the next sub-section) and spin-orbit torque which will be discussed in next chapter. The role of SOC in the contribution of the damping constant has been highlighted theoretically and experimentally by Mankovsky et al. [116] where they have shown that the increase of NiFe damping is more important with 5d impurities than 3d. The lowest damping has been measured in the insulator ferrimagnetic Yttrium Iron Garnet (YIG), with a value of damping about 10^{-5}. In metals, bulk Fe has a damping about 2×10^{-3}. Recently, an "ultra-low" damping of 0.002 has been reported in $Co_{0.25}Fe_{0.75}$ alloy [117], and more recently in our group at IJL-Nancy a record of low damping < 10^{-4} in epitaxial Heusler compounds was achieved [118]. Furthermore, even in polycrystalline Heusler compounds we show experimentally a low damping < 10^{-4} [119].

Resonance Condition

Smit and Beljers [120] derived a general formula for the resonance condition in a ferromagnetic material from equation (2.1) considering an undamped motion and assuming small deviations of the magnetization from its equilibrium position. The solution obtained was expressed in terms of the partial derivatives of the total free energy density F with respect to the polar angle, θ, and azimuthal angle, ϕ, of the magnetization vector (**Figure II.4**). It reads:

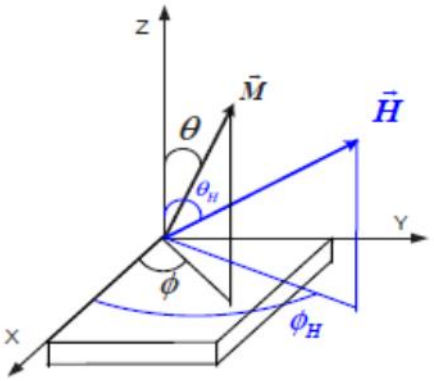

Figure II.4. Geometry used to describe the angles that *M* and *H* have with the x, y, and z axes.

$$\left(\frac{\omega}{\gamma}\right)^2 = \frac{1}{M_s^2 \sin^2\theta}\left[\left.\frac{\partial^2 F}{\partial\theta^2}\right|_{\theta_0,\phi_0}\left.\frac{\partial^2 F}{\partial\phi^2}\right|_{\theta_0,\phi_0} - \left(\left.\frac{\partial^2 F}{\partial\theta\partial\phi}\right|_{\theta_0,\phi_0}\right)^2\right] \tag{2.3}$$

where $\omega = 2\pi f$ is the angular frequency of the precession, M_s is the saturation magnetization and the partial derivatives of free energy are evaluated in the equilibrium angles of magnetization, i.e. $\partial F/\partial\theta|_{\theta_0,\phi_0} = 0$ and $\partial F/\partial\phi|_{\theta_0,\phi_0} = 0$.

Knowing the free energy density of the system and using equation (2.3) it is possible to calculate analytically or numerically the frequency dispersion relationship, *f*, depending on the applied magnetic field.

The magnetic anisotropies of a ferromagnetic material can then be calculated from the adjustment of the angular dependence of its ferromagnetic resonance spectrum. The FMR spectra can be studied in two different geometries. The first is by rotating the magnetic field dc in the plane of the samples (IP) while the second is by varying the H field from the plane to the direction normal to the plane of the samples (OOP).

Determination of magnetic anisotropies in oxide films

As an example of the powerful tool that is FMR I present here the results of a pseudo-cubic perovskite oxide film $La_{0.25}Sr_{0.25}MnO_3$ (LSMO) on $SrTiO_3$ (STO) substrate[2]. I grew these films by magnetron sputtering with a substrate temperature of 750°C. **Figure II.5** shows various in-planes FMR spectra performed at 150 K.

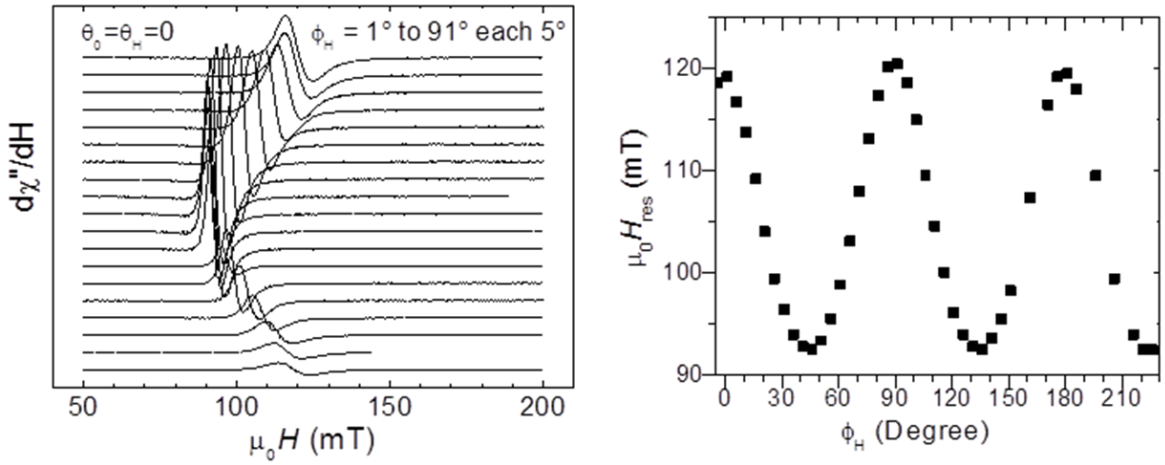

Figure II.5. (a) FMR spectra measured at 150 K on a LSMO(60 nm) film performed using a X-band resonance cavity (*f*~9.6 GHz). Each spectrum was recorded with the external magnetic field applied in-plane and for different values of ϕ_H as depicted. (b) Resonance field in-plane angular dependence after analyzing the measurements in (a).

After the analysis of the curves (fitting) we can obtain among others parameters the resonance field H_{res} which is displayed in **Figure II.5b**. Based on the results of the angular variations of the resonance field, a free energy density given by the following expression is proposed

$$F = -\mathbf{M}.\mathbf{H} + 2\pi M_s^2 \cos^2\theta + (K_{1\perp} - 2K_{2\perp})\cos^2\theta + K_{2\perp}\cos^4\theta + \frac{K_{cub}}{4}\left(\sin^2(2\theta) + \sin^4\theta\sin^2(2\phi)\right) + K_{uni}\sin^2\theta\cos^2(\phi) \quad (2.4)$$

where the first term is Zeeman's energy and the second term takes into account the shape anisotropy. The third and fourth terms include the contribution of a uniaxial anisotropy with hard axis perpendicular to the film plane. $K_{1\perp}$ and $K_{2\perp}$ denote the corresponding first and second order anisotropy constants, respectively. The fifth term describes the magnetocrystalline anisotropy of the system, of cubic symmetry (K_{cub}). The last term

[2] These are "unpublished" results of my doctoral thesis. My thesis, in Spanish, is available at http://ricabib.cab.cnea.gov.ar/245/

represents a uniaxial anisotropy existing within the plane of film whose hard axis (if $K_{uni} > 0$) is parallel to the crystalline axis [100].

By solving in a self-consistent way the equation (2.3) using the expression (2.6) of the free energy we can adjust the values of the anisotropies present in the film. This is done numerically. From the IP angular variation, **Figure II.6a**, we obtain $K_{eff\perp} = 2\pi M_s^2 + K_{1\perp} + 2K_{2\perp}$, K_{cub} and K_{uni}. Complementing this information with the data of the OOP angular dependence, **Figure II.6b**, we can get independently $K_{1\perp}$ and $K_{2\perp}$, if we know M_s. The results of this example are summarize in Table I.

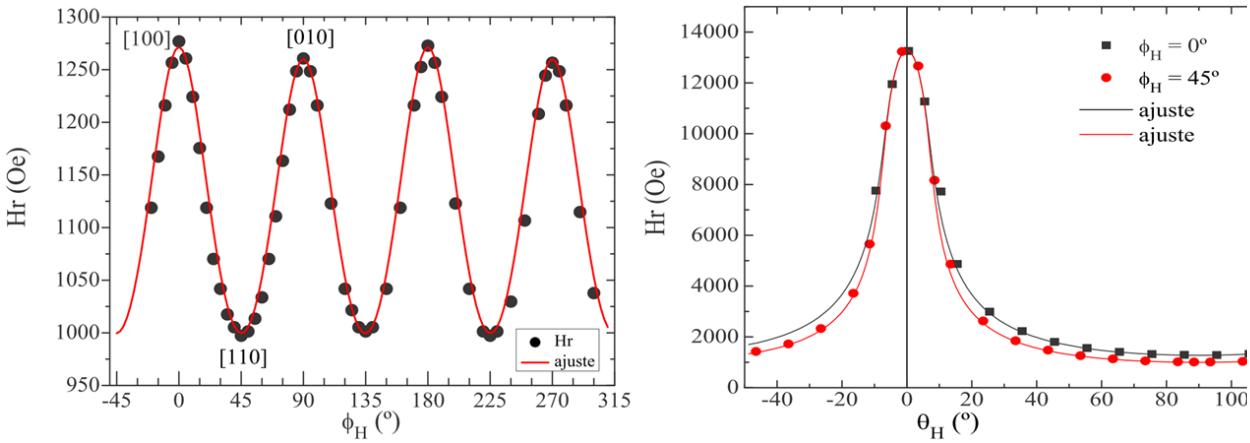

Figure II.6. IP (a) and OOP (b) angular dependence of resonance field at 150 K on a LSMO(60 nm) film performed using a X-band resonance cavity (*f*~9.6 GHz). Data points are experimental values and lines are numerical fits using eq. (2.3) and (2.5). In square brackets are shown the corresponding crystalline axes in (a). Two perpendiculars plane to the film were carried out to get the data points in (b).

IP	**OOP**			
K_{uni} **(erg/cm^3)**	K_{cub} (erg/cm^3)	$K_{1\perp}$ +2 $K_{2\perp}$ (erg/cm^3)	$K_{1\perp}$ (erg/cm^3)	$K_{2\perp}$ (erg/cm^3)
2(1) 10^3	-4.1(3) 10^4	5.6(3) 10^5	7.7(3) 10^5	-1.0(3) 10^5

Table II.1 Anisotropy constants of an LSMO thin film at 150 K determined by the IP and OOP angular dependence.

Spin Pumping FMR

The "modern" or "standard" theory of spin pumping has been developed by Y. Tserkovnyak and co-workers based on the concept of spin current in 2002 [121]. It is based on the first notions of the exchange of the itinerant electrons s of a non-magnetic layer with the localized

electrons "d" of the magnetic layer in an FM/NM interface pointed out by Silsbee, Janossy and Monod in the late 70s [122]. On the experimental side, the increase of damping has been reported also since the 80's [123], and systematically in Cu/NiFe/Cu and Pt/Cu/Pt at the beginning of the 2000's by Mizukami and co-workers [124–126].

The spin current $\mathbf{I}_s$ pumped form the FM layer generates a torque, $\tau_{sp} = -\hat{\mathbf{m}} \times \mathbf{I}_s \times \hat{\mathbf{m}}$. Note that $\mathbf{I}_s$ has units of torque. In a FM/NM bilayer, at the FMR condition, the precession of the magnetization creates an out of equilibrium spin accumulation at the FM/NM interfaces which in turns can be diffused as transversal spin current Js. This spin current is usually written in the following form

$$js = \frac{\hbar g_r^{\uparrow\downarrow}}{4\pi} \int_0^{\frac{2\pi}{\omega}} (\hat{\mathbf{m}} \times \frac{d\hat{\mathbf{m}}}{dt}) dt \tag{2.7}$$

where $g_r^{\uparrow\downarrow}$ is the real part of spin mixing conductivity and $\omega=2\pi f$ is the RF field pulsation. We consider here only the real part of $g^{\uparrow\downarrow}$ since the imaginary part would affect the Landé g factor which is not affected in typical FM/NM systems. We can recognize the dissipative or damping term in the LLG equation. In fact, this spin pumping term modifies the LLG equation as follows:

$$\frac{d\hat{\mathbf{m}}}{dt} = -\gamma \hat{\mathbf{m}} \times \mathbf{H}_{eff} + \alpha \hat{\mathbf{m}} \times \frac{d\hat{\mathbf{m}}}{dt} + \alpha_{sp} \hat{\mathbf{m}} \times \frac{d\hat{\mathbf{m}}}{dt} \tag{2.8}$$

where α_{sp} takes into account the enhancement of the Gilbert damping coefficient due to the spin pumping effect. It reads:

$$\alpha_{sp} = \frac{g \mu_B g_{eff}^{\uparrow\downarrow}}{4\pi M_S t_{FM}} \tag{2.9}$$

where $g_{eff}^{\uparrow\downarrow}$ is the real part of the *effective* spin mixing conductance and t_{FM} is the ferromagnetic layer thickness. The period of the precession of the magnetization is of the order of ns much greater than the momentum relaxation time in the metals, of the order of fs. It can then be considered that the electrons in the non-magnetic metal layer and far from the FM/NM interface are in equilibrium.

The magnitude of the spin current pumped from FM layer and injected at the FM/NM interface can be evaluated using eq. (2.7) and the linearization of LLG equation as was performed by Smit and Beljers in 1955 [120]. Thus, it is considered a small variation $\delta\hat{\mathbf{m}}$ around the equilibrium position of the magnetization, i.e. $\delta\theta << \pi$ around θ_0. This was performed first by Ando et al. to account for the spin current [127,128] and it is found in units of A/m^2:

$$j_{s0}^{\text{eff}} = \frac{g_{eff}^{\uparrow\downarrow}\gamma^2\hbar\ h_{rf}^2}{8\pi\ \alpha_{\text{F/N}}^2}\left[\frac{4\pi M_s\gamma + \sqrt{(4\pi M_s\gamma)^2 + 4\omega^2}}{(4\pi M_s\gamma)^2 + 4\omega^2}\right](2e/\hbar) \tag{2.10}$$

where $\alpha_{\text{F/N}}$ stands for the total damping in the FM/NM bilayer. As experimentally this damping value includes all possible effects on the dynamics of the magnetization (back flow spin pumping, spin memory loss or transparency, etc), this spin current on the interface will be called *effective* spin current injected at the interface. The spin current given in eq. (2.10) has unit of A/m^2. This spin current decays along the z direction (normal to the FM/NM interface) following the Vale-Fert drift diffusion model. In this model the steady-state transverse spin electrochemical potential $\mu_s = \mu_\uparrow - \mu_\downarrow$ can be expressed as $\nabla^2\mu_s = \mu_s / l_{\text{sf}}$ where l_{sf} is the spin diffusion length of the NM layer. Considering that the non-magnetic layer has a thickness t_{N}, it has been shown for bilayers [51,57,128,129]:

$$j_s(z) = j_{s0}^{\text{eff}}\frac{\sinh[(z - t_{\text{N}})l_{\text{sf}}}{\sinh[(t_{\text{N}})l_{\text{sf}}} \qquad 0 \le z \le t_{\text{N}} \tag{2.11}$$

The same model can be extended for three layers, i.e. FM/NM1/NM2 (references). The detail of our calculation can be found in the supplementary material of ref. [57]. The result gives for each layer:

$$\begin{aligned} j_{\text{sN1}}(z) &= j_{s0}^{\text{eff}}\frac{r_{\text{sN2}}^{\infty}\sinh\left[\frac{t_{\text{N1}}-z}{l_{\text{sf}}^{\text{N1}}}\right]\cosh\left[\frac{t_{\text{N2}}}{l_{\text{sf}}^{\text{N2}}}\right] + r_{\text{sN1}}\cosh\left[\frac{t_{\text{N1}}-z}{l_{\text{sf}}^{\text{N1}}}\right]\sinh\left[\frac{t_{\text{N2}}}{l_{\text{sf}}^{\text{N2}}}\right]}{r_{\text{sN2}}^{\infty}\cosh\left[\frac{t_{\text{N2}}}{l_{\text{sf}}^{\text{N2}}}\right]\sinh\left[\frac{t_{\text{N1}}}{l_{\text{sf}}^{\text{N1}}}\right] + r_{\text{sN1}}\cosh\left[\frac{t_{\text{N1}}}{l_{\text{sf}}^{\text{N1}}}\right]\sinh\left[\frac{t_{\text{N2}}}{l_{\text{sf}}^{\text{N2}}}\right]} \qquad 0 \le z \le t_{\text{N1}} \\ j_{\text{sN2}}(z) &= j_{s0}^{\text{eff}}\frac{r_{\text{sN1}}\sinh\left[\frac{t_{\text{N1}}+t_{\text{N2}}-z}{l_{\text{sf}}^{\text{N2}}}\right]}{r_{\text{sN2}}^{\infty}\cosh\left[\frac{t_{\text{N2}}}{l_{\text{sf}}^{\text{N2}}}\right]\sinh\left[\frac{t_{\text{N1}}}{l_{\text{sf}}^{\text{N1}}}\right] + r_{\text{sN1}}\cosh\left[\frac{t_{\text{N1}}}{l_{\text{sf}}^{\text{N1}}}\right]\sinh\left[\frac{t_{\text{N2}}}{l_{\text{sf}}^{\text{N2}}}\right]} \qquad t_{\text{N1}} \le z \le t_{\text{N2}} \end{aligned} \tag{2.12}$$

where $r_{\text{N1}} = \rho_{\text{N1}}l_{\text{sf}}^{\text{N1}}$ and $r_{\text{N2}}^{\infty} = \rho_{\text{N2}}l_{\text{sf}}^{\text{N2}}$, are the spin resistance of NM1 and NM2 layer, respectively. ρ stands for the electrical resistivity.

Spin Pumping Voltage by ISHE

The first experimental measurement of spin pumping voltage was presented by Rezende's Brazilian group in 2005 [130], and then by a Japanese group in 2006 [131] with the

interpretation of spin pumping plus ISHE[3].The spin current injected into the NM layer might be converted into a charge current due to ISHE if the NM layer has large enough SOC. The charge current produced generates an electric field that counterbalances it since in an open circuit there is no flow of electric current. In an open circuit such a produced charge current can be detected through a voltage. **Figure II.7** shows a schematic diagram summarizing all these effects: FMR, spin pumping and ISHE. To calculate the measured dc voltage, or the produced charge current let's start with the relationship due to the ISHE between js and jc:

$$\mathbf{j}_C(z) = \theta_{SHE}\left[\mathbf{j}_S(z) \times \boldsymbol{\sigma}\right] \tag{2.13}$$

where θ_{SHE} is the spin Hall angle, $\mathbf{j}_S$ is the injected spin current which is perpendicular to the interface (along *z*) with a spin polarization $\boldsymbol{\sigma}$ (along the $\pm x$ axis given by the applied external magnetic field dc). The dc electric field created to compensate such induced charge current is then directed along *y*, *Ey*. Taking into account the shunting in the FM layer, we have:

$$\left(\sigma_F t_F + \sigma_N t_N\right) E_y = -\theta_{SHE} \int_0^{t_N} j_S(z)\,dz \tag{2.14}$$

where σ_F (σ_N) is the conductivity of FM (NM) layer. Note that $\sigma_F t_F + \sigma_N t_N = R_{sh}^{-1}$, is the inverse of the sheet resistance of the full FM/NM stack bilayer. In the experiment one measures the dc voltage $V_{SP\text{-}ISHE} = E_y L$ along the length *L* of the sample of width *W*. The charge current I_C is nothing else than $V_{SP\text{-}ISHE} / R$ where $R = R_{sh} L / W$ is the total resistance of the sample. Both quantities read:

$$\begin{aligned} V_{SP\text{-}ISHE} &= L R_{sh}\, \theta_{SHE} l_{sf}^N \tanh\left(\frac{t_N}{2 l_{sf}^N}\right) j_{S0}^{eff} \\ I_C &= \frac{V_{SP\text{-}ISHE}}{R} = W\, \theta_{SHE} l_{sf}^N \tanh\left(\frac{t_N}{2 l_{sf}^N}\right) j_{S0}^{eff} \end{aligned} \tag{2.15}$$

The same procedure can be performed for FM/NM1/NM2 three-layer. Let's consider that the NM1 layer has a weak SOC, i.e. we disregard ISHE in this layer, and that only in the NM2 layer we have spin-charge conversion, one gets then:

[3] For this work ES has been granted the Young Scientist Award of the IUPAP Magnetics Section in 2009.

$$V_{\text{SP-ISHE}} = LR_{\text{sh}}\,\theta_{\text{SHE}} l_{\text{sf}}^{\text{N2}} \tanh\left(\frac{t_{\text{N2}}}{2l_{\text{sf}}^{\text{N2}}}\right) j_{\text{S0}}^{\text{eff}} \frac{r_{\text{sN1}}}{r_{\text{sN2}}^{\infty} \coth\left[\frac{t_{\text{N2}}}{l_{\text{sf}}^{\text{N2}}}\right] \sinh\left[\frac{t_{\text{N1}}}{l_{\text{sf}}^{\text{N1}}}\right] + r_{\text{sN1}} \cosh\left[\frac{t_{\text{N1}}}{l_{\text{sf}}^{\text{N1}}}\right]}$$

$$I_{\text{C}} = \frac{V_{\text{SP-ISHE}}}{R} = W\,\theta_{\text{SHE}} l_{\text{sf}}^{\text{N2}} \tanh\left(\frac{t_{\text{N2}}}{2l_{\text{sf}}^{\text{N2}}}\right) j_{\text{S0}}^{\text{eff}} \frac{r_{\text{sN1}}}{r_{\text{sN2}}^{\infty} \coth\left[\frac{t_{\text{N2}}}{l_{\text{sf}}^{\text{N2}}}\right] \sinh\left[\frac{t_{\text{N1}}}{l_{\text{sf}}^{\text{N1}}}\right] + r_{\text{sN1}} \cosh\left[\frac{t_{\text{N1}}}{l_{\text{sf}}^{\text{N1}}}\right]}$$

(2.16)

One can see that the measured voltage is proportional to the length of the sample and independent of the width. In other words, if the intensity of the radio frequency field h_{rf} remains constant in a certain region, it is advisable to have a sample with the longest possible L in order to increase the signal of the detected voltage and with the smallest possible width, in order to have a homogeneous rf field over the sample. The latter is actually convenient for reducing spurious signals such as anisotropic magnetoresistance (AMR) and anomalous and planar Hall effects (AHE, PHE). The spin pumping voltage is a symmetrical Lorentzian around the resonance field, H_{res}. This signal can be accompanied by other symmetric and anti-symmetric contributions (PHE, AHE and AMR) [132]. In a typical experiment, where the power and frequency of the microwave are fixed and the external magnetic field dc is swept, the overall relationship of the voltage in the experiment is equal to that of the FMR voltage, and is given by the linear combination of a symmetric and antisymmetric Lorentzian plus an offset:

$$V_{\text{measured}}(H) = V_{\text{offset}} + V_{\text{sym}} \frac{\Delta H^2}{\Delta H^2 + (H - H_{res})^2} + V_{\text{anti}} \frac{(H - H_{res})\Delta H}{\Delta H^2 + (H - H_{res})^2} \tag{2.17}$$

where ΔH is the half width at half maximum (HWHM) of the FMR line. If we perform frequency dependence, one can obtain the damping constant and the effective magnetization saturation using the well-known expressions:

$$\left(\frac{2\pi f}{\gamma}\right)^2 = (H + H_K)(H + H_K + 4\pi M_{\text{eff}}) \tag{2.18}$$

$$\Delta H = \Delta H_0 + \left(\frac{2\pi f}{\gamma}\right)\alpha \tag{2.19}$$

Depending on the FMR experimental setup, the derivative of the power absorbed is sometimes measured, dP_{abs}/dH. In this case the signal can be fitted with the derivative of expression given by eq. (2.17). In addition, the peak-to-peak linewidth ΔH_{pp} is usually used in this signal. In this case, to determine the damping there is a factor of $2/\sqrt{3}$ in eq. (2.19) since $\Delta H_{\text{pp}} = \frac{2}{\sqrt{3}}\Delta H$.

There are some features that allow to identify that the measured voltage is only (or mainly) due to spin pumping. Namely:

- it is purely symmetrical around the resonance field
- it changes sign upon change of sign of *H*
- it is zero when *H* is applied perpendicular to the plane of the sample
- it changes sign upon change of stacking order FM/NM by NM/FM
- it changes sign when NM layer is replaced by another one of material with opposite spin Hall angle (i.e. Ta and Pt)

Some of these characteristics are exemplified in **Figure II.7** which validates that the signal we measure in our new experimental setup is well due to spin pumping.

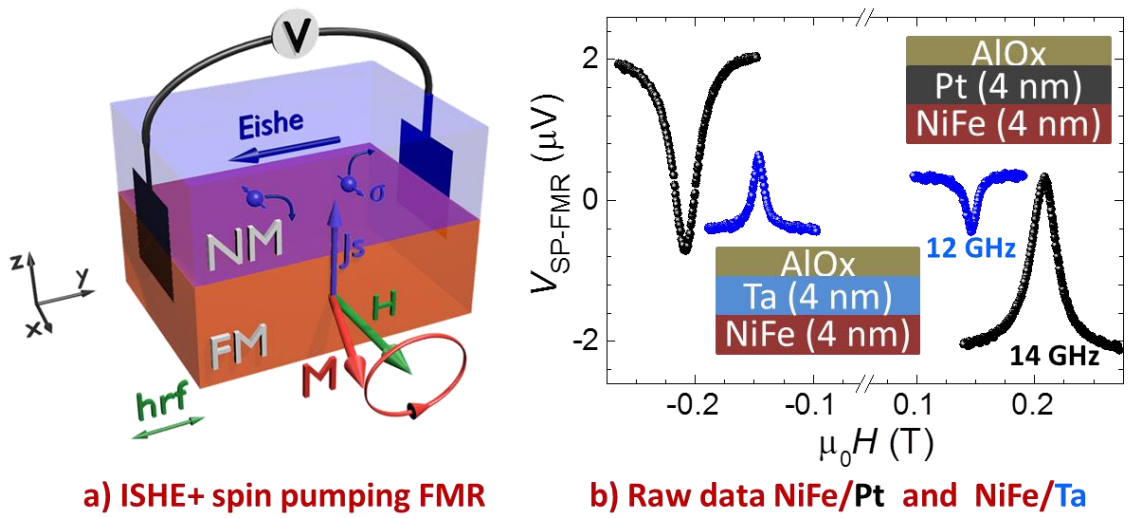

Figure II.7. (a) Schematic of spin pumping - FMR and voltage detection by ISHE on NM/FM bilayer. At resonance condition of FM layer, a spin current Js is injected into the NM layer and converted in $J_c \propto \theta_{SHE}(Js \times \sigma)$ due to ISHE (detected as a voltage in an open circuit). θ_{SHE} is the spin Hall angle and accounts for the SCC conversion efficiency of SHE and ISHE. (b) Raw data examples. The SP-FMR voltage is a symmetric Lorentzian curve around the resonance field. Its sign changes upon field ($\sigma \rightarrow -\sigma$), stacking order ($J_s \rightarrow -J_s$) and sign of θ_{SHE}.

In what follows I will summarize some of my main results during my 9 years of research in France thanks to spin pumping experiments which I could set up in Grenoble (using EPR cavity), Palaisseau (using grounded coplanar wave guide, GCPW), and finally in Nancy (using CPW).

Spin memory loss

As mentioned, I believe that FMR measurements alone might not be enough to obtain spintronics parameters such as spin diffusion length since damping enhancement could be polluted by other contributions, particularly inhomogeneities. One research we carried out was the comparison between Co/Pt bilayers and Co/Cu/Pt trilayers. We measured the damping and the charge current produced as a function of the thickness of the Pt layer as shown in **Figure II.8**.

Previously, the analysis of ISHE and spin pumping FMR was carried out with the above-mentioned models. That is, considering that the interfaces were perfectly transparent to the injection of the spins. However, one finds different values of the spin Hall angle if the NM layer is attached with different FM layer such as NiFe or CoFeBo or Co. Similarly, one finds different values if one inserts a "transparent" layer (material with weak SOC) like Al or Cu layer of a much lower thickness than its spin diffusion length. So, evidently, interfaces play a role as well. We then consider the depolarization of the spin current on the interface due to the so-called spin memory loss (SML). From spin-transport and magnetoresistance experiments on metallic multilayers, it is well established that metallic interfaces dissipate spin current by SML. The physical parameter governing such SML processes is given by the spin-flip parameter δ that specifies the probability $P=\left[1-\exp(-\delta)\right]$ of a conduction electron flipping its spin direction as it traverses a FM/NM interface. One can consider the SML on the interface by an artificial intermediate layer I (I per interface). Then $\delta = t_{\mathrm{I}} / l_{\mathrm{sd}}^{\mathrm{I}}$ can be viewed as the ratio between the effective interfaces thickness t_{I} and the interface spin diffusion length l_{sf}^{I}, which become short with disorder. Developing a three-layer F/I/N model as depicted in **Figure II.9** we can then calculate the correction factor due to the SML. Following the analysis previously shown, we have in eq. (2.16)

$$I_{\mathrm{C}} = W\,\theta_{\mathrm{SHE}} l_{\mathrm{sf}}^{\mathrm{N2}} \tanh\left(\frac{t_{\mathrm{N}}}{2l_{\mathrm{sf}}^{\mathrm{N}}}\right) j_{\mathrm{S0}} \frac{r_{\mathrm{sI}}}{r_{\mathrm{sN}}^{\infty} \coth\left[\frac{t_{\mathrm{N}}}{l_{\mathrm{sf}}^{\mathrm{N}}}\right] \sinh\left[\delta\right] + r_{\mathrm{sI}} \cosh\left[\delta\right]} \tag{2.20}$$

$$R_{\mathrm{SML}} = \frac{r_{\mathrm{sI}}}{r_{\mathrm{sN}}^{\infty} \coth\left[\frac{t_{\mathrm{N}}}{l_{\mathrm{sf}}^{\mathrm{N}}}\right] \sinh\left[\delta\right] + r_{\mathrm{sI}} \cosh\left[\delta\right]} \leq 1 \tag{2.21}$$

where the factor on the right represents the correction due to the SML, R_{SML}. The parameters δ and the spin resistance at the interfaces, r_{sI} are known in few interfaces at low temperature. In recent years some values have been reported but there is still a lack of experimental values in some common interfaces used in spintronics, i.e NiFe/Pt and NiFe/Cu or CoFeB/Pt, etc.

In our work in 2014 we have considered for Co/Pt and Cu/Pt the values shown in Table II.2. Using those values we could determine an "intrinsic" value of θ_{SHE} for Pt at 0.056±0.010.

This means that the R_{SML} factor is 0.553 in the Co/Pt bilayer. Using the same principle, and our Co/Cu/Pt trilayer model, considering as transparent the Cu layer since its thickness $t_{Cu} << l_{sf}^{Cu}$, we have the same result. That is, an effective value equal to 0.056*R_{SML} where now R_{SML} is 0.35 for Co/Cu/Pt using the values in Table II.2. This explains well why the saturation level of the charge current is lower in the three-layer Co/Cu/Pt than in the two-layer Co/Pt (the higher the R_{SML} value, the more transparent the interface).
However, the values we used are experimentally reported values at 4.2 K. Recently, this year 2020, there is a calculation of these parameters as a function of temperature [133]. The SML value decreases with increasing temperature as does the interface spin resistance. Considering these new values, the new calculation for the spin Hall angle of Pt would give 0.09 as shown in Table II.3Table II.1.

System	δ	2AR* (fΩm²)	2AR (fΩm²)	$r_{sI} = r_b / \delta$ (fΩm²)	Ref.	R_{SML} [57]
Co|Cu	0.25	1.0	-	2.0	[134]	
Cu|Pt	0.9	-	1.5	1.7	[135]	
Co|Pt	0.9	1.5	-	1.66	[136]	0.56
Co|Cu|Pt	1.2		-	0.85		0.35

Table II.2 Values of δ, r_b=AR* for F|N interfaces (r_b=2AR for $N_1|N_2$ interfaces) and r_{sI} as reported in the literature (at 4.2 K), or calculated for trilayers [57].

We can draw the conclusion of our paper [57] where we pointed out the role of the interfaces in the spin current transmission and quantification of spintronics parameters:

- NM thickness dependence of magnetic damping constant: $\alpha(t_{NM})$ is not enough to determinate l_{sf}^{NM}
- NM thickness dependence of charge current: $I_C(t_{NM})$ is suitable to determinate l_{sf}^{NM}
- Considering transparent interfaces we just estimate an "effective" spin Hall angle: $\theta_{SHE}^{eff} = \theta_{SHE} \times R_{SML}$ & $R_{SML} \leq 1$
- Consequently, using different FM material we will measure apparently different spin Hall angle of NM layer.

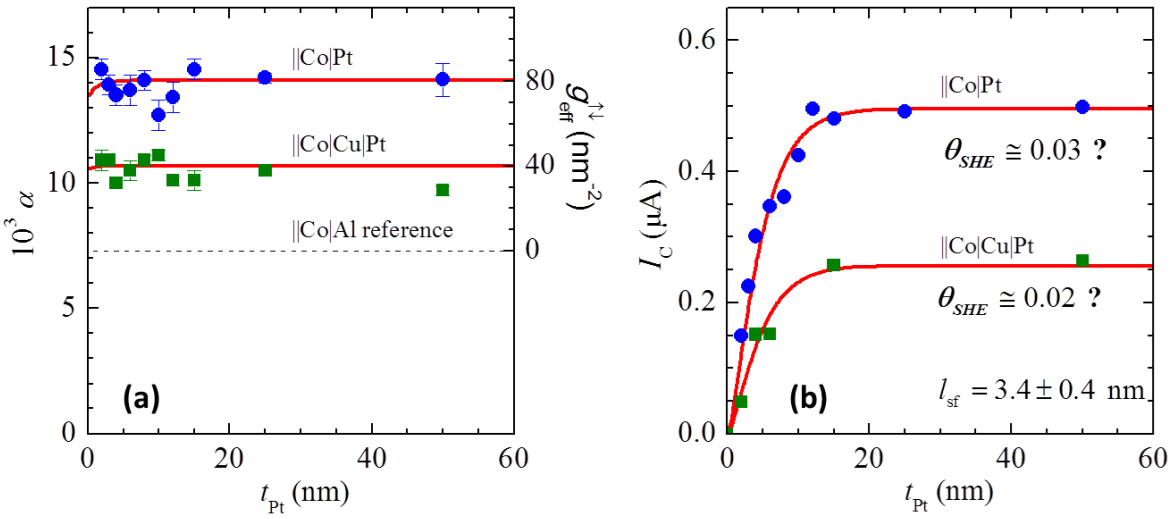

Figure II.8. Platinum thickness dependence of the damping constant α (a) and charge current I_C (b) for ||Co(15 nm)|Pt(*t*) (filled blue circles) and charge currents ||Co(15 nm)|Cu(5 nm)|Pt(*t*) (filled green rectangles). The value of θ_{SHE} for Pt seems different in bilayers and trilayers if we consider that interfaces are totally transparent. Thus, these values are effective values that are in convolution with the properties of the interfaces. We can also see that the characteristic scale length in the evolution of the damping and the charge current are not the same. The spin diffusion length can only be extracted from the evolution of the charge current (eq. (2.15)). The resistivity of Pt is 17.3 ± 0.6 μΩ.cm, resulting in l_{sf}=3.4 ± 0.4 nm as displayed in (b).

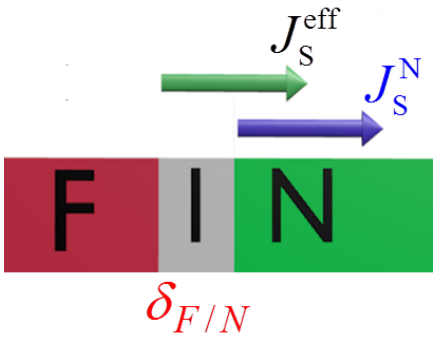

Figure II.9. Overview of the model used to describe that the interfaces are not transparent to spin injection. Within an FM/NM bilayer it is considered an I interface, and is analyzed as a fictitious FM/I/NM three-layer (FIN in the scheme). So the current that actually reaches the NM layer is an effective current after "losing" something in the interface and that also takes into account the back flow.

System	δ	AR* (fΩm²)	$r_{sI} = r_b / \delta$ (fΩm²)	R_{SML}	θ_{eff}	Ref.	θ_{SHE}
Co|Pt	0.88	0.85	1.7	0.57	0.031	[57]	0.054
NiFe|Pt	0.78	0.78	1.56	0.61	0.04	[52]	0.066
NiFe|Pt-(b)	0.92	0.95	1.03	0.48	0.04	[52]	0.083

Table II.3 Values of δ, r_b=AR* for F|N interfaces, and r_{sI} as theoretically calculated much recently at 300 K [133]. The NiFe/P-(b) stands for lattice-disorder only in the theoretical calculation. The experimental effective values θ_{eff} are those reported in the indicated references.

In Table II.3 I show the newly calculated interfacial parameters at room temperature for the NiFe/Pt and Co/Pt interfaces. Taking these values into account, the "intrinsic" value $\theta_{SHE} = \theta_{SHE}^{eff} / R_{SML}$ of Co/Pt would be similar as we have reported before. But now we can compare with NiFe/Pt. The R_{SML} would be 0.61 or 0.48 when only lattice-disorder is considered. For NiFe/Pt system with R_{SML}=0.48 the effective θ_{SHE} should smaller than in Co/Pt, and there are several reports in literature in this situation. In contrast, if $R_{SML}^{NiFe/Pt} = 0.61$, the effective θ_{SHE} measured should be smaller than in Co/Pt, and there are also several reports supporting this claim.

Spin memory loss (SML) or spin transparency T_s?

After our report [57], there was another report by Zhang et al. [137] with the same idea that there is a loss of spin injection at the interfaces and a parameter needed to account for that loss. They called this parameter spin interfacial transparence, T_s. And they used the opposite technique, STFMR (which will be discussed in the next chapter) to explain the differences in values between NiFe/Pt and NiFe/Cu/Pt and Co/Pt for example. Then, most reports using the STFMR technique use T_s, and some reports using spin pumping or using an effective spin Hall angle mention SML. The idea of spin T_s is the depolarization on the interface due to the mismatch in the band structures in the two metals on either side of the interface, without any loss of spin polarization at the interface. I think this is including in the spin mixing conductance developed by Tserkyovnav and the effective $g_{eff}^{\uparrow\downarrow}$ one measure experimentally. The equations for both models are:

$$\theta_{SHE}^{eff} = \theta_{SHE} \times R_{SML} \quad \& \quad R_{SML} = \frac{r_{sI}}{\rho_{sN} l_{sf}^{N} \coth\left[t_N / l_{sf}^{N}\right] \sinh\left[\delta\right] + r_{sI} \cosh\left[\delta\right]} \leq 1$$

$$\theta_{SHE}^{eff} = \theta_{SHE} \times T_s \quad \& \quad T_s = \frac{g^{\uparrow\downarrow} \tanh\left[t_N / 2 l_{sf}^{N}\right]}{g^{\uparrow\downarrow} \coth\left[t_N / l_{sf}^{N}\right] + \frac{\sigma_N}{l_{sf}^{N}} \frac{h}{2e^2}} \leq 1 \qquad (2.22)$$

The question that arises is: which model to use? Both speak of effective spin Hall angle. However, their equations are different because although the R_{SML} and T_s are similar they are not identical. There is still work to be done to reconcile the two models.

Dispersion of spin diffusion length and spin Hall angle values

More recently, Tao et al. [138] presented a study where they calibrate the effective spin current injected into the interface by magnetoresistance measurements. However, as in Feng et al. [139] where they use the same method to determine j_{s0}^{eff} injected by spin pumping, Tao et al. report high values of l_{sd} and small values of θ_{SHE}. It is not clear whether this is related to the method they use to calibrate j_{s0}^{eff}. In Tao et al., they split the effective spin Hall angle measured with an SML model based on the work of Kai Chen and Shufeng Zhang [140]. That is, they do not take an artificial interfacial layer, but the factor (1-δ) to account for the amount of spin current loss at the interface while we use R_{SML}. However, they do use equivalent expression for j_{s0}^{eff} as given in Eq. (2.10) considering $g_{eff}^{\uparrow\downarrow}$ which is what we measure using Eq. (2.9). Another difference, following the model of Chen and Zhang and the experimental work of Feng et al., is that they normalize the ISHE voltage only by the resistance of the HM layer and not the total resistance as we do. It seems to me that these two points, the method of measuring j_{s0}^{eff} with magnetoresistance at the microwave resonance condition, and the way they account for the charge current production are the main reasons for the difference between their and our results. The equivalent expression for j_{s0}^{eff}, the one used by Tao et al. [138] and Feng et al. is shown below in Eq. (2.24).

As we can see, there is therefore still a work to be done around all these studies. In an FM/HM system one can use both methods of normalization of the spin pumping voltage, normalized by the total resistance or normalized by the resistance of the HM layer, to obtain the produced charge current, and thus quickly see if they produce the same l_{sf}.

There is a paper that reports the same values of spin Hall angle for Pt using both techniques, SPFMR and STFMR, but that is after considering some corrections [141]. I think the effective values, that is without adjustments or corrections, reported by SPFMR or STFMR should be the same (injection of spin from the FM layer to NM would suffer the same loss as if injected from the NM layer to the FM layer).

The SML coefficients for different interfaces of interest in spintronics are unfortunately not known. One might infer what FM/NM interface is more or less transparent to spin injection by comparison. For example, in NiFe/Pt one finds by ISHE-SPFMR effectives values below 2% for the $\theta_{SHE\text{-}eff}^{NiFe/Pt}$ in studies from the groups of Saitoh [142] and about 4% in the studies of Rezende's group [52]. As we can see, there is no easy to do a straightforward comparison. One would need to make his/her own benchmark.

ISHE-SPFMR in alloys: $Au_{1-x}W_x$ and $Au_{1-x}Ta_x$

One of the objectives in spintronics is the exploration for materials with high efficiency coefficients in the interconversion of spin and charge currents. It has been proposed in that sense that alloys of light and heavy metals, i.e. of metals with weak and strong spin-orbit coupling, can possess extraordinary large spin Hall angles due to resonant scattering [68]. There are several theoretical papers with predictions in that sense as mentioned already in Chapter I, i.e. new alloys of Cu or Au host doped with impurities such as C, Bi or Os, in order to enlarge the SHE efficiency due to resonant asymmetric scattering by impurities [68,69] as proposed already in 1981 [67]. Thus, we have studied $Au_{1-x}W_x$ alloy for many years and most recently the Au_{x1}-Ta_x alloy. We have combined the method described at the beginning of this chapter, lateral spin valves with SHE or ISHE absorption of an alloy bar, and the ISHE spin pumping method, **Figure II.10**. The $AuW_{0.07}$ alloy reaches an effective spin Hall angle $\theta_{\text{SHE-eff}}^{AuW\,0.07} = 0.10$, a spin diffusion length $l_{\text{sf}}^{AuW\,0.07} = 2$ nm, and a resistivity $\rho_{\text{AuW0.07}} \cong 59$ μΩ.cm at 300 K. The variation of resistivity at 10 K is less than 3%, so the spintronics parameters of this alloy measured at 10 K and 300 K are practically the same [73]. In our study we also seek to discern between extrinsic contributions to SHE. The skew scattering SHE resistivity is proportional to the longitudinal one, $\rho_{xy} \propto \rho_{xx}$ and give an θ_{SHE} independently of ρ_{xx}. This has been reported for CuIr ($\theta_{\text{SHE}}^{\text{CuIr}} = 0.02$), CuBi ($\theta_{\text{SHE}}^{\text{CuBi}} = -0.24$), and CuPb ($\theta_{\text{SHE}}^{\text{CuPb}} = -0.13$) [70,72,143]. However, the side-jump and the intrinsic mechanism from Berry curvature in the conduction band give the same dependence, $\rho_{xy} \propto \rho_{xx}^2$, and $\theta_{\text{SHE}} \propto \rho_{xx}$. This intrinsic contribution was observed in the AuPt alloy $\theta_{\text{SHE}}^{\text{AuPt}} = 0.3$ [144].

Our results show that the spin Hall angle for AuW_x changes proportionally to the longitudinal resistivity up to x=0.12 then decreases and become negative for x=0.028. This behavior is explained by the skew scattering contribution, and for the competition with the SHE of W which has a negative θ_{SHE}. In the case of $AuTa_x$ the spin Hall angle also increases linearly with its resistivity. The values found for the spin Hall angle in $AuTa_x$ are higher than in AuW_x and with the advantage of having smaller resistivity. Theoretical support shows that intrinsic and skew scattering contributions are much smaller than the values measured experimentally in AuTax. Considering the side-jump contribution we found values in good agreement with our experimental results. Thus, in $AuTa_x$ alloys the side-jump contribution is predominant and can lead to values of $\theta_{\text{SHE-eff}}^{\text{AuTa0.1}} = +0.50$ with moderate resistivity values ($\rho_{\text{AuTa0.1}} \leq 85$ μΩcm). This study was the first one to provide experimental evidence of the contribution of side jump scattering to the spin Hall effect [75].

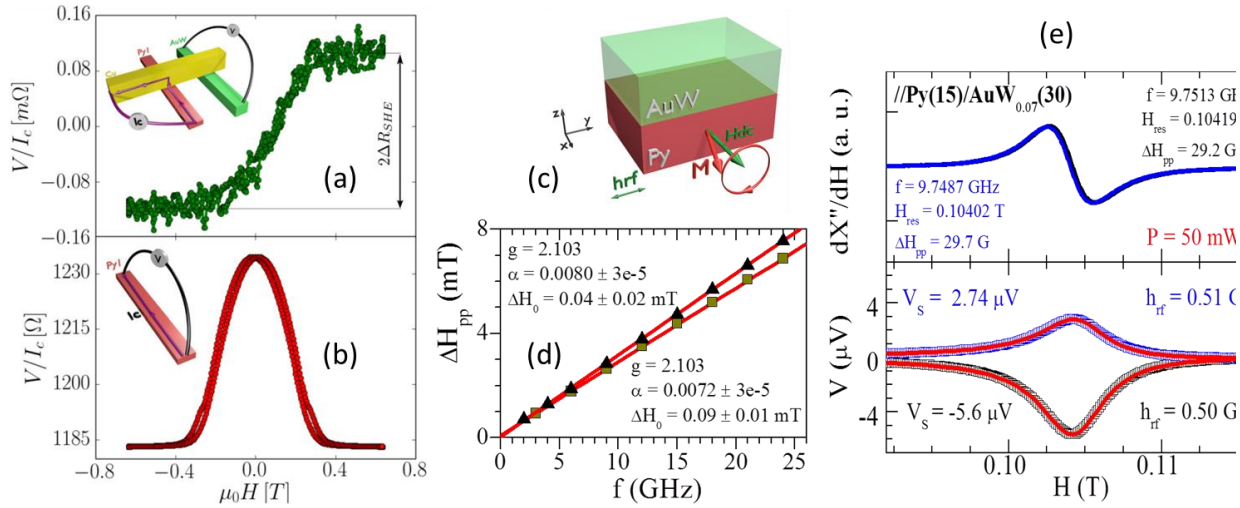

Figure II.10. (a) ISHE absorption experiment in $AuW_{0.07}$ 100 nm width nano-wire with (b) AMR signal of the Py ferromagnetic injector, both measured at 10K. Insets show schematic representations of experimental configuration. The external field is applied along the Cu channel (yellow bar). (c) Schematic of a Py(15 nm)/$AuW_{0.07}$(30 nm) bilayer at the FMR condition. (d) ΔH_{pp} frequency dependence and Gilbert damping determination on Py/AuW bilayer and Py reference. (e) Simultaneously measurement of FMR spectrum (top) and spin pumping voltage (bottom) performed in a resonant cavity. Two cases are shown, when in plane field is positive and when it is negative (or turned 180°). Adapted from [69].

ISHE-SPFMR in semiconductors: n-Ge

High efficiency values of charge current conversion into spin current are found in the heavy metals due to the strong SOC. However, this also reduces the characteristic length l_{sf} which hinders the creation of devices using these heavy metalss as channels to transport the spin current. Semiconductors, on the other hand, have a weak SOC, consequently a small θ_{SHE} but a long l_{sf}, which can reach the order of microns. The main obstacles to achieve spin injection in semiconductors is the conductivity mismatch between the ferromagnetic electrode and the semiconductor for which tunnel barriers were proposed [145–147]. This brings other problems such as paramagnetic impurities in the tunnel barriers [148], interface states [149] and surfaces roughness [150]. Experimentally, the electrical spin injection in Si was shown in 2007 [151,152], and for Ge in 2011 [153]. My contribution to the study in Ge was performed in Grenoble with Mathiew Jamet and his group. We used non-local measurements on 3-terminal devices to measure relaxation times and spin diffusion length in the semiconductor channel, and combined them with spin pumping voltage measurements. Although the SOC coupling in semiconductors is weak, the ISHE-spin pumping technique allows detecting spin injection in semiconductors thereby overcoming the impedance problem. Thus, it has been

reported ISHE and spin pumping results in GaAs in 2011 [154], in p-Si in 2012 [155], and in p-Ge in 2013 [44]. We reported it for nGe in 2012 [46] and 2013 [156].

We use the same device for both non-local measurements and spin pumping voltage. The multiterminal device we used for electrical measurements is shown in **Figure II.11a**. The full stack Ta(5 nm)/$Co_{60}Fe_{20}B_{20}$(5 nm)/MgO(3 nm) has been grown by sputtering and annealed on germanium-on-insulator wafers [46]. A thin MgO tunnel barrier was inserted to circumvent the conductivity mismatch and partly alleviate the Fermi level pinning by reducing the interface states density [15–17] which leads to a modest Schottky barrier height at the MgO/n-Ge interface. Conventional optical lithography was used to define three-terminal devices made of a tunnel spin injector in between two Ohmic contacts made of Au(250 nm)/Ti(10 nm).

On these devices we perform i) I-V measurements to determine the R_sA spin resistance-area product, ii) back-gate voltage dependence of the Hanle (H//z) and inverted-Hanle (H in-plane and parallel to the FM injector electrode) curves. Relaxation times and spin diffusion length in the conduction band, l_{sf}^{cb}, can be obtained from these experiments. The temperature dependence shows a transition at 150 K of the normalized spin signal, ΔV/V(T=50 K). This transition is interpreted as a transition from the spin accumulation in the interface states at low temperature to the spin injection in the n-Ge conduction band at high temperature. Using the two-step tunneling process through interfaces states, i.e. sequential tunneling trough localized states at the MgO/Ge interface states [149,157], we can use the product R_sA to obtain the spin diffusion length in the n-Ge since $R_sA=(V_s/I)A=(TSP\times l_{sf}^{cb})^2\rho/t_{Ge}$ following the spin diffusion model where TSP ≈0.65 is the tunnel spin polarization on a symmetric magnetic tunnel junction CoFeB/MgO/CoFeB. From the results, $l_{sf}^{cb}\approx 1.5$ μm was obtained with a weak dependence of the back-gate voltage up to ±0.5V. Independently, Hanle curves give the spin lifetime $\tau_{sf}^{cb}=400\pm100$ ps at room temperature which yields $l_{sf}^{cb}\approx 1.3\,\mu$m in very good agreement with R_sA results. As mentioned, on these devices we also perform ISHE-spin pumping measurements, **Figure II.11b**. The temperature dependence shows that there is no signal at low temperature and it starts to appear around 150 K in perfect agreement with the former experiments [46]. Furthermore, at room temperature we perform a thorough study of the ISHE-spin pumping signal, magnetic damping, and magnetic anisotropies including out-of-plane angular dependence, reference and control samples and annealing processes. In a control sample, when we perform similar measurements in devices without MgO barrier, we detect well the FMR spectrum but there is not ISHE-SP voltage. Our results show that $g^{\uparrow\downarrow}=1.0\times10^{18}$ (0.6×10^{18}) m^{-2}, and $\theta_{SHE}=0.0011$ (0.00044) for the annealing (not annealing) sample.

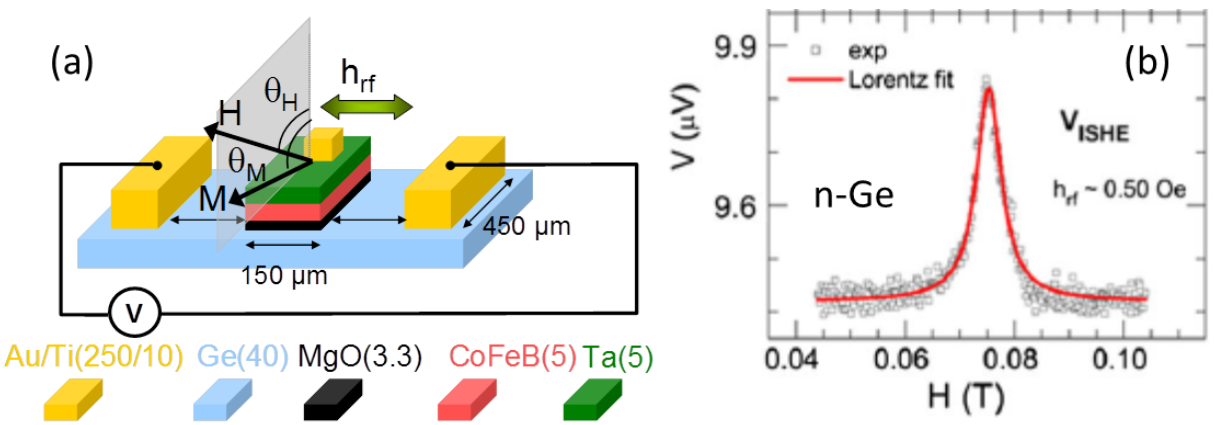

Figure II.11. (a) Schematic of the multiterminal device used for ISHE SP-FMR and FMR measurements along with the angular position definition and the h_{rf} radio frequency field. The thickness of each layer is given in nm between parentheses. (b) Spin pumping voltage peak due to spin injection and ISHE in the conduction band of n-Ge channel at the FMR condition of CoFeB layer. Note: although the amplitude (< 1µV) is much smaller than in HM, the experimental setup in a resonant cavity and this method still allows detecting ISHE signals from materials with weak SOC.

Ongoing research at IJL

New SP-FMR setup

I am very pleased that after several years we have converged on the development of an experimental setup to measure ISHE SP-FMR in Nancy. We use here a probe station with planar field and rf and dc probe contacts. I was quickly able to obtain some results but these were qualitative and very difficult to reproduce because of the connection with the rf and dc contacts using an external GCPW antenna. Now, in close collaboration with my colleague Sébastien Petit-Watelot, we have developed a method where the CPW antenna is integrated in the last step of the lithography allowing to reproduce the measurements more easily and to reduce the surface of the sample for each device but increasing the detected signal. An example of such a device to mesure spin pumping voltage is depicted in **Figure II.12**. In addition, these devices are oriented in different directions every 45° which is particularly special for epitaxial samples. Furthermore, we have designed different blocks for other experiments such as magnetotransport, Hall measurements, SOT, ST-FMR, spin Seebeck and spin Nernst effects; some of which will be detailed in the following chapters. It results then a range of devices for different experiments based on spin-orbitronics from the same sample with enough area (>10x10 mm^2).

Figure II.12. (a) Picture of a SPFMR device which consists of a slab of the systems under study with an insulator cap and an antenna was deposited on top. (b) The same device with rf (GSG) and dc connections. The dc is to detect the spin pumping voltage, and rf to inject the rf current in the antenna. The dc field is applied along x-axis and perpendicular to the slab which is along y-axis as depicted in the figure.

We have already a submitted a paper. It is a study on CoFeB/Pt and CoFeB/Ir. We were able to determinate the spin diffusion length of Pt and Ir by the HM thickness dependence. The values agree with previous reports, and particularly with the Elliot-Yaffet scattering mechanism. That's the product of resistivity and spin diffusion length is a constant. We have measured for Pt, $\rho_{\mathrm{Pt}} \times l_{\mathrm{sf}}^{\mathrm{Pt}} \approx 59$ fΩ.m^2 and for Ir, $\rho_{\mathrm{Ir}} \times l_{\mathrm{sf}}^{\mathrm{Ir}} \approx 59$ fΩ.m^2. Moreover, by comparison, we have estimated the spin Hall angle of Ir, $\theta_{\mathrm{SHE}}^{\mathrm{Ir}} \cong 0.25 \times \theta_{\mathrm{SHE}}^{\mathrm{Pt}}$. Using our previous results [57], we know that the effective spin Hall angle times the spin diffusion length is also a constant, mostly independent of experimental setup and sample quality. For Pt, it reads $\theta_{\mathrm{SHE\text{-}eff}}^{\mathrm{Pt}} \times l_{\mathrm{sf}}^{\mathrm{Pt}} \approx 0.2$ nm. We have obtained then, $\theta_{\mathrm{SHE\text{-}eff}}^{\mathrm{Pt}} = 0.07$ and $\theta_{\mathrm{SHE\text{-}eff}}^{\mathrm{Ir}} = 0.02$.

The quantification of the charge to spin current conversion efficiency $\theta_{\mathrm{SHE}}^{\mathrm{eff}}$ relies on precise knowledge of the spin-current injected into the FM/NM or FM/HM interface. For this we use eq. (2.10). There are many material-dependent parameters that can be obtained from the frequency dependence, such as M_{eff} (= M_{s} for thick FM layers, i.e. > 15 nm), and magnetic damping constant. However, a key parameter is the h_{rf} field amplitude, which depends on the experimental setup. One way to obtain this parameter is by measuring the power absorbed, ΔP_{abs}, by the sample in the resonance condition. The relationship is known [158], and it is given by:

$$\Delta P_{abs} = \upsilon_{\mathrm{mag}} \mu_0 h_{\mathrm{rf}}^2 (2\pi f) \chi'' = \upsilon_{\mathrm{mag}} \mu_0 h_{\mathrm{rf}}^2 \frac{\gamma M_s}{4\alpha} \left[\frac{M_s\gamma + \sqrt{(M_s\gamma)^2 + 4(2\pi f)^2}}{\sqrt{(M_s\gamma)^2 + 4(2\pi f)^2}} \right] \qquad (2.23)$$

That means to carry out another series of FMR measurements without changing a single cable or connector in the setup where it was measured ISHE- spin pumping. Since the magnetic volume υ_{mag} under the CPW is small, this approach requires the magnetic susceptibility of the samples to be large enough to ensure that the FMR signal strength is above the experimental detection limit. This means this approach works for samples with large *M* and low damping. Another way is to use the magnetoresistance of the spin pumping slab. If we consider that we are at the limit of small conical angles of precession θ_c, where $\sin\theta_c \cong \theta_c \cong h_{rf} / (2\Delta H) \approx h_{rf}\gamma / (2\alpha\omega)$, eq. (2.10) can be rewritten as follows:

$$j_{s0}^{eff} = \frac{\hbar\omega}{4\pi} g_{eff}^{\uparrow\downarrow} \sin^2(\theta_c) \left[2\omega \frac{M_s\gamma + \sqrt{(M_s\gamma)^2 + 4\omega^2}}{(M_s\gamma)^2 + 4\omega^2} \right] (2e/\hbar) \tag{2.24}$$

where the amplitude of the conical angle of precession can be determined by other series of measurements. For this purpose, a small dc current, i_{dc}, is applied in the spin pumping slab to obtain the variation of the resistance or voltage in the FMR condition (same power and frequency as that used for ISHE-spin pumping). The voltage of this slab as function of magnetic field will have also a Lorentzian shape around the resonance field. The amplitude of this measurement will be V_0/i_{dc}. In addition a standard AMR measurement is needed (*R* vs H_{dc} perpendicular allows to obtain that), that is without any rf applied. The maximum change in dc magnetoresistance is $\Delta R_{AMR} = R_{\parallel} - R_{\perp}$ where $R_{\parallel}$ ($R_{\perp}$) is resistance of the FM slab in the saturate state when H_{dc} is applied parallel (transverse) to the applied current direction. The amplitude V_0/i_{dc} together with the AMR allows obtaining the conical angle as follows [139,159,160]:

$$\theta_c = \sin^{-1}\sqrt{\frac{V_0}{I_{dc}\Delta R_{AMR}}} \tag{2.25}$$

We have then two methods or protocols to quantify the spin Hall angle (or the figure of merit in 2D systems that will be studied in the next chapter). Although it requires another set of measurements, it is worth the effort to be able to quantify precisely and not remain only in the qualitative or semi-quantitative analysis. Besides, it will be useful to compare if the magnetoresistance method is at the origin of the large values of spin diffusion length reported

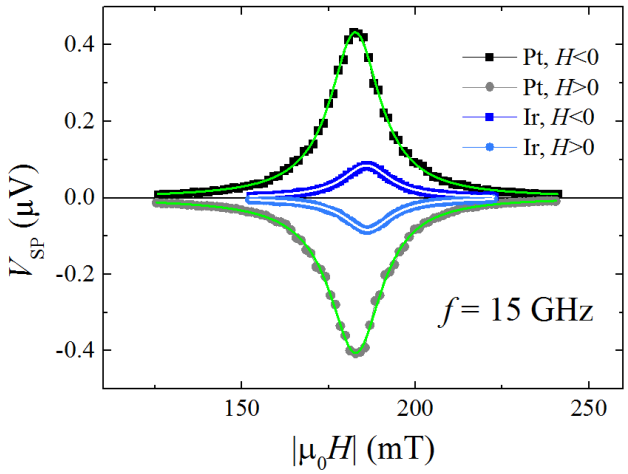

Figure II.13. Raw data SPFMR voltage in SiO_2//CoFeB/Ir and SiO_2//CoFeB/Pt. We can observe that the signal is symmetric around resonance field, and both systems exhibit the same sign, that is Pt and Ir have the same sign of spin hall angle.

FM/NM and YIG/Pt

We have other ongoing studies such investigating YIG/Pt with two different growth directions, [001] and [111] and measurements along different in-plane crystalline directions. Although YIG/Pt is one of the most studied systems, a comparison in different crystalline orientations in the same study has not yet been reported to my knowledge. In addition, this system will serve to underpin others studies where there is also a ferromagnetic insulator (FMI).

Spin Seebeck and spin Nernst effects combined with ISHE

Other ways to produce spin current is by the interaction between phonons and magnons [161,162]. Thus, ideally in a FMI material to rule out other possible contributions, a temperature gradient ∇T produces a spin current J_s . The first effect discovered is the spin Seebeck or longitudinal spin Seebeck effect (SSE) [27]. Here, the spin current generated is parallel to the temperature gradient, $Js \| \nabla T$. If a HM layer with strong SOC is attached to the FMI layer, J_s injected into the HM layer will produce a transversal charge current due to the ISHE, $J_c \propto J_s \times \sigma$. This charge current can be measured as a voltage produced in an open circuit [163]. Note that the symmetry of this phenomenon is very similar to that of the anomalous Nernst effect, ANE, where the voltage produced is proportional to the vector product between the temperature gradient and the magnetization, $\mathbf{E}_{\mathrm{ANE}} \propto \nabla T \times \mathbf{M}$. However, ANE can be measured on a single FM layer while LSSE needs a FM/HM bilayer to be measured in combination with ISHE on the HM layer. More recently, the spin Nernst effect has been reported experimentally in 2017 independently by two groups [164,165]. In this case the spin current generated is transverse to the temperature gradient and proportional to the so-called spin Nerst angle, θ_{SN} . Thus is $J_s \propto \theta_{\mathrm{SN}}(\nabla T \times \sigma)$. Again, by combining with HM layers for detection through its ISHE, a voltage produced in an open circuit can be measured. All these effects, a temperature variation that generates a spin current which in turn produces a voltage in certain geometry, can be exploited to recycle the energy we waste through heat.

III. Spin-to-charge current conversion at interfaces

This chapter is dedicated to the experimental studies of what we have called Inverse Rashba-Edelstein effect or Inverse Edelstein effect. As it was mentioned, it is also known as spin galvanic effect. I will describe first the general method using again spin pumping voltage at FMR condition. Then, I will describe some of my main results and contribution to the field which was triggered with our results in Ag/Bi Rashba interface. Finally, I will show some ongoing studies and perspectives using longitudinal spin Seebeck effect.

III.1 Inverse Edelstein Effect (IEE) by spin pumping ferromagnetic resonance (SPFMR)

At the resonance condition, the FM layer is able to inject a spin current j_s^{eff} out of the FM layer. Now, if this spin current reaches an interface with strong SOC and spin texture such as a Rashba interface, or an interface with a topological insulator or semimetal, it will be converted efficiently in a transversal charge current. j_s^{eff} is a 3-dimensional (3D) spin current (in A/m^2) but now the charge current generated in this exotic interfaces will be a 2-Dimensional charge current (in A/m) as depicted in **Figure I.9** and **Figure III.1**. The amount of the spin current injected at the interface hold the same relation as shown in eq. (2.10), and the 2D charge current will be given by the total current normalized by the total resistance R and the width W of the sample, along x-axis in Figure III.1(b). The efficiency or figure the merit now has units of 1/length. The detailed relations are given in the following expressions:

$$j_s^{eff} = \frac{g_{eff}^{\uparrow\downarrow}\gamma^2\hbar\ h_{rf}^2}{8\pi\ \alpha_{F/N}^2}\left[\frac{4\pi M_s\gamma + \sqrt{(4\pi M_s\gamma)^2 + 4\omega^2}}{(4\pi M_s\gamma)^2 + 4\omega^2}\right](2e/\hbar) \tag{3.1}$$

$$I_C^{2D} = \frac{V_{IEE}}{W\,R} \tag{3.2}$$

$$\frac{I_C^{2D}}{j_s^{eff}} = \lambda_{IEE} \tag{3.3}$$

The efficiency λ_{IEE} is proportional to the Rashba coupling for Rashba interface, and the Fermi velocity of the topological states for TI materials, times the relaxation time [36,91,92,166]. Note that this relaxation time is not only spin relaxation time or momentum relaxation time but both since they are locked [167]:

$$\lambda_{IEE} = \frac{\alpha_R}{\hbar}\tau \quad \text{for Rashba interfaces}$$
$$\lambda_{IEE} = \upsilon_F \tau \quad \text{for TI} \tag{3.4}$$

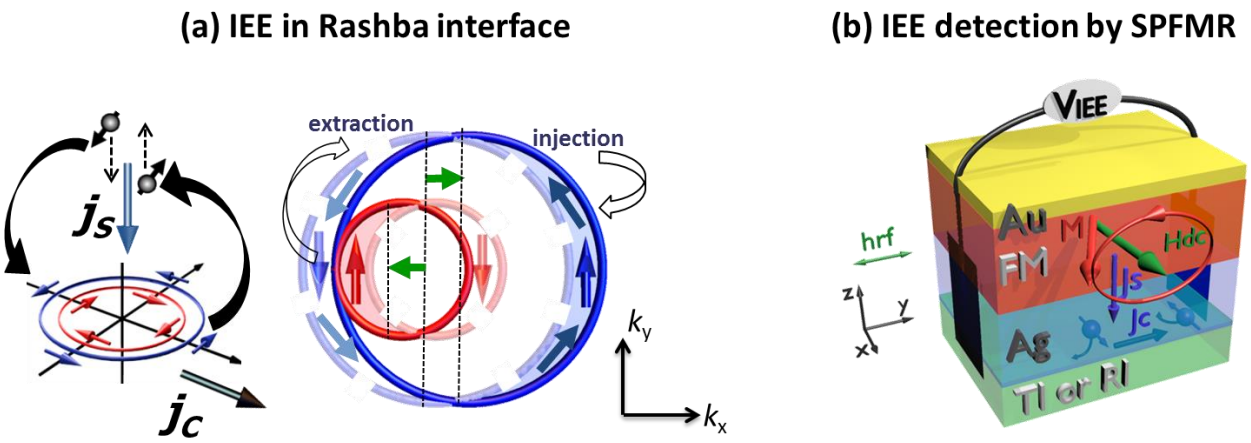

Figure III.1 (a) Inverse Edelstein effect in the reciprocal space for a Rashba interface (for topological insulators there is not the inner red Fermi contour). We have postulated that the reciprocal of the EE effect also exist and thus when a vertical spin current Js is injected in 2DEG systems, a lateral charge current is induced. In the illustrations the spin current has a spin polarization $+\sigma_y$. Consequently, electrons can only be injected in the $+k_x$ region and extracted from the opposite region, $-k_x$. As consequence there is a shift of Fermi contour which in turns means a variation of moment Δk, along $+k_x$ in the illustration. It turns out that a variation of moment is nothing else that charge current. Accordingly the vertical injection of the spin current generates a lateral charge current in 2DEG systems due to its spin texture. (b) IEE detection in the real space thanks to a spin pumping ferromagnetic experiment. The generated charge current in these 2DEG systems can be detected as a voltage in an open circuit.

IEE-SPFMR at Rashba Interfaces

I will mention below my contribution and results in the studies carried out in Ag/Bi [36], $SrTiO_3/LaAlO_3$ [168], and [111]Ge/Fe [169]. Besides, I also carried out a spin pumping study in [111]GeTe [170].

Ag/Bi Rashba interface

I carried out this study during my first post-doctoral position in Grenoble in collaboration with Prof. Fert in Palaiseau CNRS-Thales and José María De Teresa in Zaragoza. The Ag/Bi interface is one of the Rashba interfaces with the highest Rashba coefficients with a value of $\alpha_R = 3.05\,\text{eV}\text{Å}$. It has been predicted theoretically and shown experimentally using ARPES in

1/3 Bi layer on [111]Ag substrate [171]. Furthermore, all Bi surfaces have been shown to be Rashba interfaces. For instance, [111]Bi has $\alpha_R = 0.56$ eVÅ [172].

We have studied different systems. The 15 nm of NiFe reference sample, and the NiFe/Ag and NiFe/Bi control samples; and the main system which consist of //Bi/Ag/NiFe [36]. A summary of our main results are displayed in **Figure III.2**.

The signal in NiFe and NiFe/Ag is mostly antisymmetric around the resonance field, and both have the same magnetic damping constant. This indicates that there is no spin pumping effect on the NiFe/Ag bilayer. This was to be expected since the Ag thicknesses used (between 5 and 20 nm) are much smaller than the spin diffusion length of Ag. It can therefore be concluded that Ag and the NiFe/Ag interface are transparent for spin injection. And of course as there is no spin pumping effect, there is no charge production in the Ag layer.

In the NiFe/Bi bilayer control sample, an increase in the magnetic damping constant is observed, which would indicate a possible spin pumping effect. This is verified by the symmetrical voltage around the resonance field but once it is normalized by the resistance of the sample; the charge current produced is small and comparable to other reports [173].

In the main system, Bi/Ag/NiFe, an increase in the magnetic damping constant is also observed, as well as a symmetrical voltage around the resonance field that normalized by its resistance accounts for a higher production of charge current. This is our main result. Ag thickness dependence between 5 and 20 nm gives similar results with the same charge production (0.5 μA/G^2, normalized by the square of the radio frequency field). We interpreted these findings as the IEE effect we had predicted with an efficiency $\lambda_{IEE}^{Ag/Bi} \approx 0.2-0.3$ nm. Actually, there was a previous demonstration of the effect by S.D. Ganichev and co-workers in 2002 using semiconductor quantum wells along with optical means and electrical detection. They called the phenomenon spin galvanic effect [174]. As I have mentioned many times in the conferences to which I have had the honor of being invited, one does not have to believe in our results. And that's the beauty of science. Other groups in the community will be able to validate or contradict our results and interpretations. This work on Ag/Bi quickly triggered many studies related to Rashba interface (and topological insulators) in the spintronics community. I believe that the evidence to support the scenario we have proposed is clear.

Here I summarize some points that, following the eq. (3.4), support our findings:

The Rashba coupling α_R strength: As mentioned, the Ag/Bi interface has one of the highest Rashba coefficients. Zhang et al. [175] showed that the charge current produced in Ag/Sb is much smaller than in Ag/Bi which agrees with our theoretical model described by eq. (3.4).

The Rashba coupling α_R sign: Two interfaces or systems with α_R of opposite signs are anticipated to produce spin pumping voltage (and charge current) also of opposite signs. Thanks to the community of surfaces and ARPES, it is known that the Ag/Bi interface has α_R with the opposite sign than the Cu/Bi interface [176]. In the work of Karube et al. they show that the Ag/Bi_2O_3 and Cu/Bi_2O_3 interfaces produce opposite sign signals [177].

The stacking order of the Rashba interface: Indeed, this is equivalent to changing the sign of the α_R alpha coefficient. The origin of the α_R coefficient is the electric field at the Rashba interface. One can imagine that if we change the stacking order, A/B to B/A, the electric field at each interface is opposite which leads to a sign of the opposite α_R coefficient in each case. This has been verified by studies of positron beams at the Ag/Bi and Bi/Ag interfaces where the authors observe spin accumulation of opposite signs in the samples with opposite stacking order [178]. In other collaboration between French and Spanish research groups, also using spin pumping, the authors show that the sign in Fe/Ag/Bi is opposite to the sign of the sample in Fe/Bi/Ag [179]. Note that the Fe layer always remains on the same side, and only the order of the Bi and Ag layers was inverted. Moreover, a more recent demonstration seems to me to show the IEE unequivocally. In that study, epitaxial samples with small Bi thickness (3 nm) are analyzed by considering that the spin current reaches the Ag/Bi interface either by passing through the Ag layer or the Bi layer first. The experiment is by THz emission, that is, a fs laser pulse excites the sample on the side of the FM layer generating a spin current. This spin current is converted into charge current by ISHE in HM or by IEE in Rashba interfaces or TIs. The electrical signals they observe in Fe/Bi/Ag and Fe/Ag/Bi have opposite signs [29]. Their main results are shown in **Figure III.3**. Again, I take this result as an irrefutable proof of the IEE.

Now that the IEE scenario has been consolidated, we can quickly move on to study other Rashba or TIs systems.

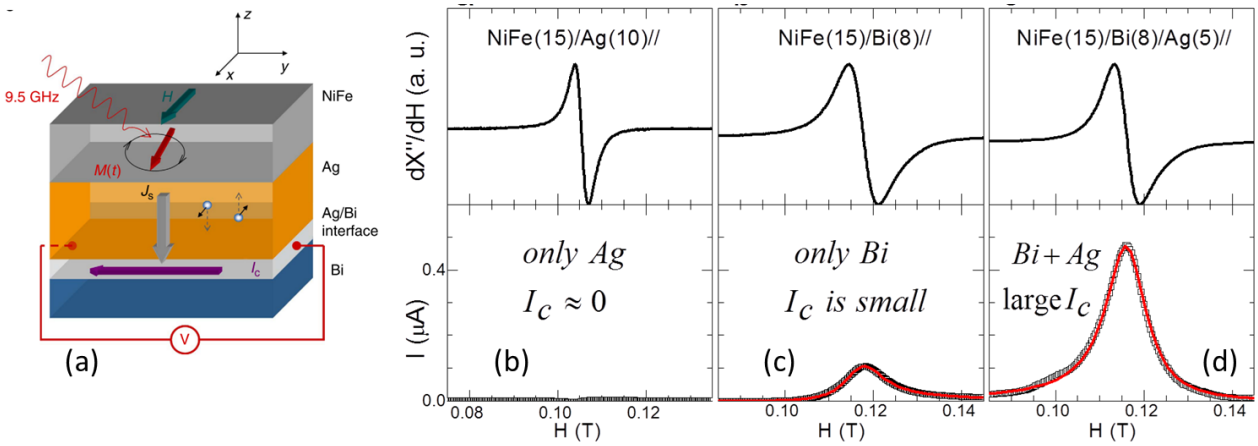

Figure III.2 (a) Schematic of the main sample in the study, //Bi(8)/Ag(t)/NiFe(15). (b-f) Simultaneously measurements of the FMR spectrum (the derivate) in top panels and the spin pumping voltage in bottom panels performed in a Bruker resonant cavity for the samples depicted. The NiFe/Ag control sample shows that Ag and NiFe/Ag interface are transparent for spin injection. The NiFe/Bi control sample shows a spin pumping effect and charge current production which is small in comparison with the main sample where the Ag/Bi Rashba interface produces charge current more efficiently due to IEE. Adapted from [36]

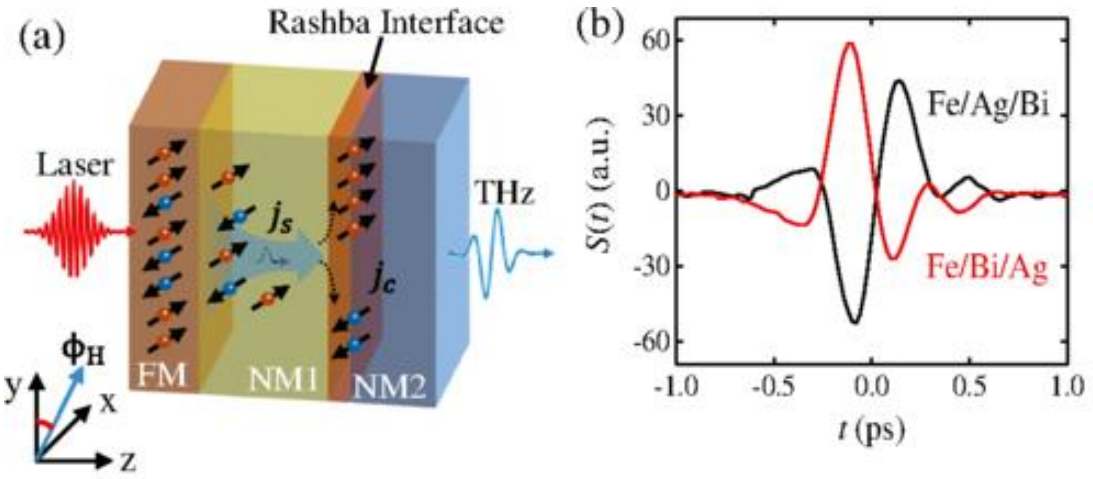

Figure III.3 (a) Schematic of the THz emission experiment. An fs laser shines the sample on the FM side generating a spin current js which is converted in a transversal charge current jc of THz range. (b) The THz emission on epitaxial Fe(2nm)/Ag(2nm)/Bi(3nm) and Fe(2nm)/Bi(3nm)/Ag(2nm) has opposite sign. Taken from [29]**. In my opinion this is nice new evidence that supports the IEE scenario.**

$SrTiO_3/LaAlO_3$ oxide Rashba interface

This study started during my post-doc at UMPhi CNRS-Thales. It was a good coincidence. There is a consolidated group in oxides led by Agnés Barthelemy and Manuel Bibes. At the same time as I was doing my post-doc, Edouard Lesne was doing his PhD on the LAO/$SrTiO_3$ system. It was natural then that Edouard and I became interested in conducting a study similar to that of Ag/Bi on this oxide Rashba interface.

The $LaAlO_3/SrTiO_3$ (LAO/STO) system is quite well known to the oxide community. Despite the fact that $SrTiO_3$ and $LaAlO_3$ are band insulators alone; the STO/LAO interface has metallic states [180,181]. Conductive tip atomic force microscope (cAFM) evidences the quasi-two-dimensional nature of the conduction [182,183]. For the existence of 2DEG in LAO/STO a minimum LAO thickness of 4 unit cells was required. However, it was shown that when you have an FM layer over the LAO layer, that threshold is reduced [184]. It was also known that the spin accumulation in the LAO/STO interface could be tuned with a backgate voltage [185]. Essentially, we wanted to address two questions: Would we observe spin pumping voltage, would the effect on this interface be larger? Would this signal be tunable by a backgate voltage?

In order to answer these questions, samples of STO//LAO(t)/NiFe(15)/Al(3) were prepared by pulsed laser deposition, PLD, for LAO, and sputtering for the NiFe and Al layers. The PLD and sputtering chamber were interconnected, so the LAO/NiFe interface remained clean. The samples were cut in slabs of 2.6x0.4 mm^2 for the spin pumping experiments. These slabs were glued with Ag paint on the sample holder which was placed inside the resonant cavity. The

contact of the Ag paint allows the application of the backgate voltage. It was also known that, thanks to temperature-dependent magnetotransport characterizations, 2DEG manifests itself at low temperature. The main SPFMR measurements were then performed at 7 K.

An outline of the sample is shown in **Figure III.4**. The reference sample, LAO/NiFe, has an antisymmetric signal. However, the STO/LAO/NiFe system shows a symmetrical voltage around the resonance field of the NiFe. As the dielectric constant of STO is huge (300 at low temperature compared to MgO or SiO2 which is around 10), the resonant cavity can be highly disturbed when the RF power is switched on. To avoid such disturbance, a fairly low rf power was used (less than 10 mW instead of the usual 100 or 200 mW). The signal was then normalized by the total resistance of the sample and the squared rf field (or the rf power used). This normalized signal allows comparison with other systems directly, and estimation of its figure of merit, λ_{IEE} . We found out that the signal is highly tunable by the backgate, and that it reaches giant values with $\lambda_{IEE}^{LAO/STO} = 6.4$ nm for V_{BG}=+125 V, 20 times more than the measured value in Ag/Bi.

The question that arises now is how it is possible to have a much stronger effect on STO/LAO than on Ag/Bi if the α_R constant in STO/LAO (3×10^{-12} eVm) is much smaller than in Ag/Bi (3.5×10^{-10} eVm).

Considering the simple model given by eq. (3.4), we see that the efficiency of the IEE is not only proportional to the α_R coefficient but also to its relaxation time. While in the Ag/Bi interface the relaxation time is quite low (1-10 fs) due to the Ag channel, the relaxation time in the STO/LAO interface is much higher (~1 ps). This explains, at least qualitatively, the high efficiency observed in LAO/STO. Of course, the band structures in LAO/STO are much more complex than a circular contour Fermi we have considered in the derivation of eq. (3.4).

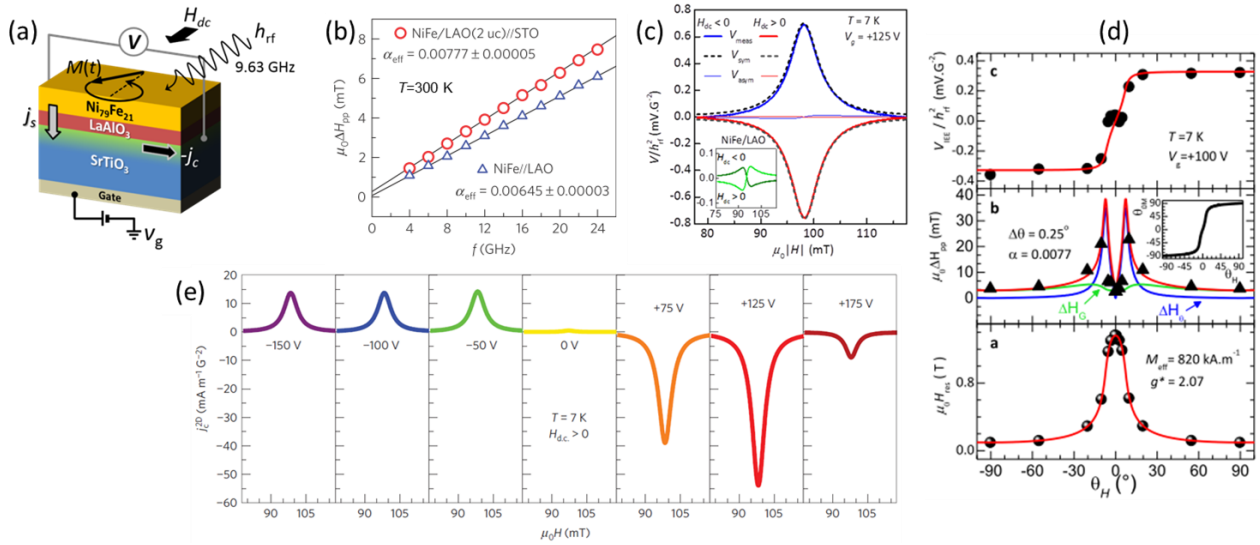

Figure III.4 (a) Schematic of the STO//LAO/NiFe sample along with contacts to detect the spin pumping voltage at the resonance condition and apply the backgate voltage. (b)B broadband frequency dependence of the same sample and LAO//NiFe reference sample performed at room temperature. It allows us to estimate the spin mixing conductivity. (c) Spin pumping voltage detected in the main sample at 7 K and backgate of +125 V. The signal is reversed upon a reversal of magnetic field. The inset shows the signal in the reference sample which is antisymmetric, so not spin charge conversion in this reference sample. (d) OOP angular dependence of the SPFMR voltage carried out at 7 K and with a backgate of +100 V. The top panel show the amplitude with agrees with all the features of a spin pumping and IEE voltage (signal change sign with sign of magnetic field and is zero when magnetic field is applied perpendicular to the film plane). The middle panel shows the OOP angular dependence of the linewidth which allows us to determine the magnetic damping constant. It turned out that we have found the same value as for room temperature. The inset is the equilibrium angular position of the NiFe magnetization. The bottom panel shows the dependence of the resonance field which allow us to estimate the effective magnetic saturation. (e) Backgate dependence of the 2D charge current production normalized by the square of the rf field.

Other studies were quickly reported on LAO/STO. In Song et al. [186] and Wagg. et al. [187] they showed the effect at room temperature which vanished at low temperature [186]. In the first case the 2D charge current produced seems to be much smaller than in our study (0.5 uA/m). We cannot normalize by the strength of the rf for a more direct comparison since that value is not reported. In the other study, Wang et al. performed the opposite experiments, conversion of charge current into spin current by STFMR (technique to be described in the next chapter). They reported an efficiency equal to 0.63 nm. Another difference between both studies and our study is that in order to deposit the FM layer in those studies, the sample was exposed to air. There are however other studies where they show, as we do, that the effect is observed at low temperature and goes away at room temperature [188].

Fe/Ge interface

The presence of sub-surface states had already been reported in 2012 [189] and 2013 [190] for [111]Ge interface by Yoshiyuki Ohtsubo and co-workers. In another SPFMR study conducted mainly by Simon Oyarzun during his post-doctorate in Grenoble under the supervision of Matthieu Jamet, we were able to observe the presence of Rashba states on the [111]Ge/Fe interface. Spin pumping experiments similar to those described in the previous sections were conducted and a nice spin pumping signal at 20 K was observed which vanishes at room temperature. A good control experiment was using [001]Ge as a substrate instead of [111]Ge. In the case of [001]Ge/Fe, the FMR spectrum is well observed but no spin pumping signal is measured. This validates the results observed in [111]Ge/Fe. Results which were further explained theoretically, in collaboration with S Blugel and his group at Juliech, as hybridized states at the semiconductor/metal interface having both exchange and SOC [169]. Almost at the same time the Rashba interface was reported in another semiconductor/Fe interface. In this case it was in [001]GaAs/Fe investigated by STFMR method [191].

IEE-SPFMR in Topological Insulators

A high efficiency in the interconversion of charge current and spin current in topological insulators is anticipated due to their spin-momentum locking as described in chapter I. Many studies report investigations into some nominally TI materials. Most of the studies were using Bi_2Se_3. Below is a list of some previous work or almost parallel to our work on α-Sn.

Shiomi et al. reported a spin pumping voltage at low temperature in $Bi_{1.5}Sb_{0.5}Te_{1.7}Se_{1.3}$/NiFe, below 20 K [192]. At room temperature the measured signal is ascribed to thermal effects. Indeed, the voltage measured remains with the same sign for positive and negative applied magnetic field. Also, at low temperature, below 3 K, Song et al. [193]reported some signal in SmB_6/NiFe but it seems to be inconsistent with the expected temperature dependence of the topological surfaces states in SmB_6 which has been shown to be more complex using FMI such as YIG, SmB_6/YIG [194].

There are several studies in Bi_2Se_3. In the system Al_2O_3//Bi_2Se_3/NiFe(20nm)/SiO_2 the thickness dependence of Bi_2Se_3 was reported and an ISHE-like behavior was observed (cf. eq.(2.15)). They reported a spin diffusion length of 6.2 nm and a spin Hall angle of 0.009 for Bi_2Se_3 [195]. Then another study was reported on InP//Bi_2Se_3/CFB(5nm)/MgO [196]. Here again ISHE was reported to be dominant. Furthermore, it is observed that the quality of the interface is critical to obtain the best results. Thus, for nominally identical samples, spin pumping voltage signals were measured with amplitudes that fluctuated by more than an order of magnitude. The spin Hall angle varies accordingly between 0.026 and 0.34. On the other hand, a theoretical work was reported where they show that metallic FM layers in contact with the TI Bi_2Se_3 is detrimental to the TSS since there is a hybridization of the TSS with the bands of the metals that destroy their helical spin texture [197]. Consequently, if there is no helical spin texture, there will be neither EE nor IEE. An alternative is then to use an FMI like the YIG. And that was reported in GGG//YIG/Bi_2Se_3/MgO [198]. A higher spin pumping

voltage was observed in YIG/Bi_2Se_3 than in YIG/Pt, however after normalization, the IEE efficiency is small (0.0035 nm). Although in all the experimental works just mentioned the Bi_2Se_3 layer was epitaxial and deposited by MBE, there is still much work to be done to improve the quality of the interfaces and to avoid exposure of the sample to air before the deposition of other layers. More recently, spin pumping results have been reported for Bi_2Se_3 or (Bi,Se) based compounds deposited by sputtering. In sputtered samples it is most likely that the signal is due to the ISHE of Bi, which itself has a strong SOC, and not due to the IEE.
We have also tried to study Bi_2Se_3 in collaboration with the INSP institute. Unfortunately the ex situ deposition of the FM layer did not give the best results. A huge FMR linewidth was observed (which one might think would be due to a large spin pumping effect), however the effective magnetization was lower than usually measured in the FM layers. This is characteristic of a poor quality FM layer. It was also verified by the absence of a large symmetrical signal when I measured the voltage at the resonance condition in the resonant cavity.

α-Sn single element topological insulator

Liang Fu and C. Kane theoretically predicted the existence of topological states in Bi_2Se_3 and α-Sn in 2007 [199]. While Bi_2Se_3 was rapidly obtained and Dirac cone verified by ARPES, it was not until 2013 [200–202] and 2014 [203] that epitaxial a-Sn films were obtained whose ARPES spectra show a linear relationship. Among these works is that of Yoshi Othsubo and collaborators in the Cassiope line of the Soleil synchrotron. They showed that α-Sn TSS have a Fermi velocity of $\upsilon_F = 7.3\times10^5$ m/s (equivalent to 4.8 eVÅ) for thicknesses between 24 and 30 atomic monolayers (ML) of α-Sn. Our project was then to explore the possibility of using this single TI for spintronics. To do this we need to know if the TSS or the Dirac cone survives when another layer is added to the free surface of the TI. So, together with Yoshi, we reproduced the α-Sn film that shows the Dirac cone. This was a good first result. Then the question we wanted to tackle was whether the Dirac cone would hold when we deposited on top of it Fe or Ag for our spin pumping experiments.
To make a long story short, **Figure III.5** presents our main results related to ARPES and spin pumping voltage. The sample to which Fe was added directly no longer shows the Dirac cone (not shown in the figure). However, the sample where Ag is added still shows the TSS even up to Ag thicknesses of 1.2 nm. Then in the same sample the Ag deposition was continued up to 2 nm and then Fe protected with Au as outlined in **Figure III.5(c)**. A reference sample without α-Sn was also deposited. The sample of α-Sn in direct contact with Fe was also finished for study as a control sample. The FMR study shows a higher damping in the sample with α-Sn (0.028) than the reference sample (0.0062). As shown in **Figure III.5(d)**, the voltage at the Fe resonance condition, normalized by the resistance of the sample, is practically zero in the reference sample as in the α-Sn sample in direct contact with Fe. The latter result is perfectly consistent with the ARPES result where the Dirac cone disappeared. However, in the sample with Ag between α-Sn and Fe, where the persistence of TSS was

clearly observed, a large signal is observed. This spin pumping voltage signal is the highest ever measured at room temperature in the same setup.

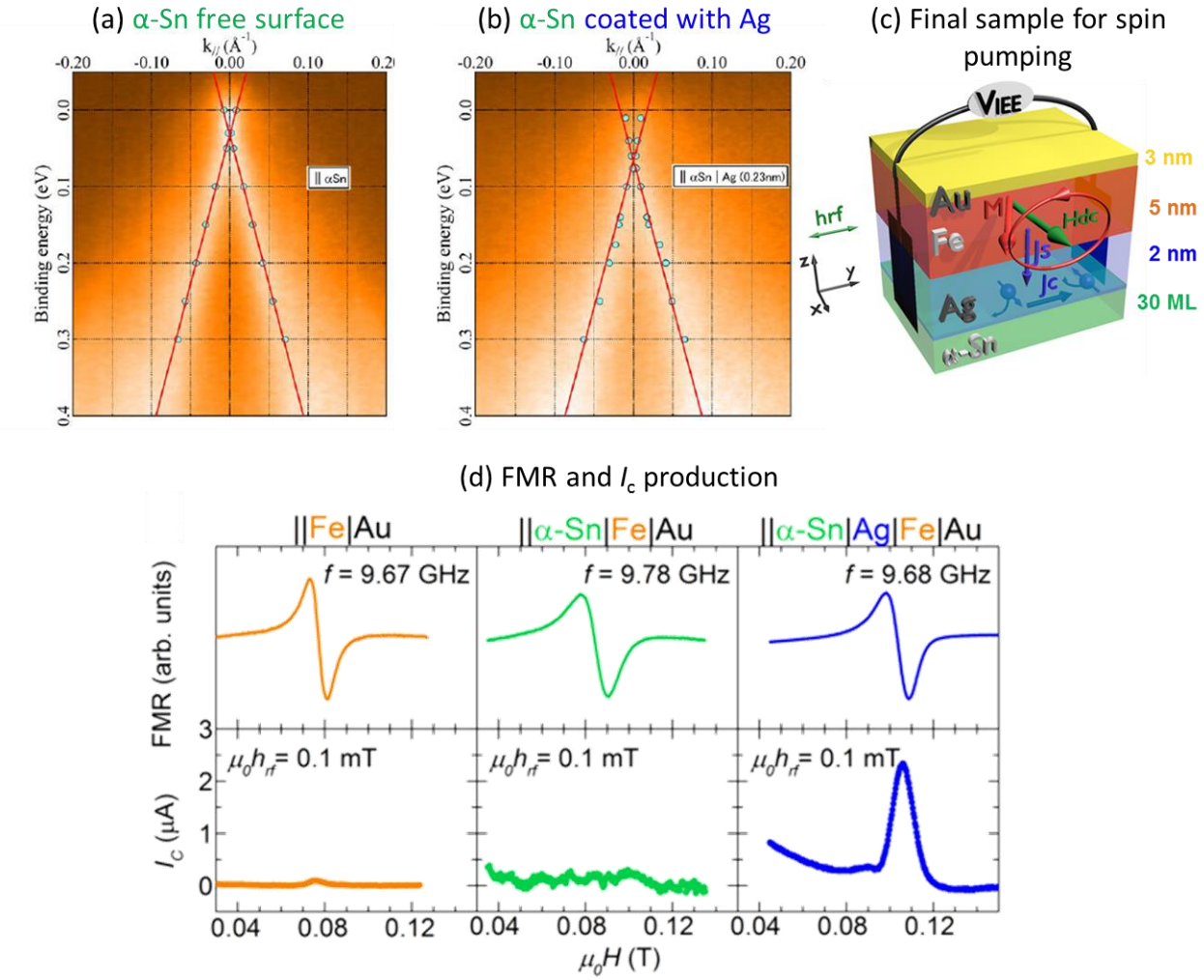

Figure III.5 IEE in single TI α-Sn. (a) ARPES spectrum in α-Sn(30ML) free surface. (b) ARPES spectrum in α-Sn(30ML) coated with Ag. The Dirac cone with small down shift of Dirac point is visible up to 1.2 nm –thick Ag. The image is for 0.23 nm Ag. (c) The deposition of Ag, Fe and Au layer is performed for the spin pumping experiments as displayed. (d) Simultaneously measurement of FMR spectrum (top panels) and spin pumping voltage normalized by the whole resistance sample (bottom panels). The charge current production happens only in the sample with Ag in between α-Sn TI and Fe in perfect agreement with ARPES results. Adapted from [91].

We can see that the charge current produced is more than 2 μA for our InSb//α-Sn/Fe/Au sample, for CoFeB/Pt it is in the order of 0.5 μA as well as for Ag/Bi. If we now quantify its efficiency we have $\lambda_{IEE}^{\alpha\text{-Sn/Ag}} = 2.1\text{nm}$ at 300 K. As we know the Fermi velocity because we have measured the Dirac cone, we can estimate the effective relaxation time τ. This gives $\tau = 3.7$ fs, much lower than the α-Sn free surface (ps). This is explained by the presence of Ag which adds a relaxation channel strongly reducing τ. We can then summarize some conclusions of this work:

- Large I_c^{2D} production at α-Sn/Ag
- Ag is useful to keep surface states of TI
- But Ag reduces τ
- A next step might be the use of insulating barrier to increase τ

However, concerning the last point, in addition to the challenge of depositing a barrier on an α-Sn epitaxial film, the material selected is also important. Other more recent theoretical work shows the existence of TSS and bulk bands (Γ_8^+) near the Fermi level. Even lower than E_F there are other surface states (TSS2) and more bulk bands (Γ_7^- and Γ_7^+) [204]. By changing the interface, playing with the tension (e.g. thickness), or applying a gate it would be possible to tune different contributions by changing the E_F.
Our experimental work in ref. [91] was performed in slabs with the in-plane crystallographic orientation along the (100) direction. Unfortunately, as the [001]InSb substrate used is quite fragile and has a small gap, no further experiments could be performed (i.e. along other crystalline directions or dc magnetotransport).

Ongoing research at IJL

As I mentioned in the previous chapter, in these almost 5 years that I am in Nancy I have dedicated a lot of time and energy to optimize the setup to measure SPFMR. We are getting new results. We have collaborations with different colleagues, mainly with Yoshi Othsubo (U. Osaka) to study more Rashba and TI interfaces. As well as with Felix Casanova and Luis Hueso (Nanogune) to study sputtered BiSe compounds. It is worth mentioning that a young research project ANR (French funding agency) has been granted to me to study TI. I hope we will get more results soon.

IV. Charge-to-spin current conversion

This chapter is dedicated to direct effects: conversion of a charge current into a spin current in both 3D and 2D systems. In addition, it is experimentally devoted to methods based on FMR. In the last few years in Nancy I have invested quite a lot of time and energy in developing the experimental set-up and analysis. We already have three publications and other studies underway. Other method such as SOT magnetization switching will be discussed in chapter V.

IV.1 Charge-to-spin current conversion in bulk

In this first part I will discuss the results that are given due to the conversion in the bulk, i.e. the SHE. I will make a first introduction of the technique and its variants as well as of the different analyses there are, and then I will present the results that we have already published.

Spin-torque ferromagnetic resonance (STFMR) at FM/HM

Like SPFMR, the STFMR method is also widely used. Both are based on the FMR condition and are in some ways the opposite effects. While in SPFMR a spin current is injected from the FM layer into the adjacent layers, in STFMR a charge current is injected from the adjacent layers into the FM layer. Both methods allow quantifying spintronics parameters such as spin diffusion length, spin Hall angle and effective spin mixing conductivity in an FM/HM system. However, there is still a controversy about the reported values. Usually, higher values are reported by STFMR than by SPFMR.

The method is based on the spin transfer torque developed in the 2000's in tunnel junctions [205–208]. In 2011, L. Lu and collaborators [209] on the one hand and Fan et al. [210] on the other hand used this technique to study SOT in the FMR condition of a FM/HM bilayer based system. **Figure IV.1** shows a picture with a schematic of our STFMR based setup. There are different alternatives or options of the method. I will list here those that we use the most based on the development of the ref. [209]. Spin-torque ferromagnetic resonance is also known as spin-orbit FMR (SO-FMR), or spin diode. In this method we inject directly the microwave frequency charge current in the FM/HM slab which is converted into a rf or oscillating spin current inside the HM layer due to the SHE. Therefore an oscillating spin current is injected from HM into FM layer. The oscillating charge current flowing in the HM layer generates an oscillating Oersted field h_{Oe} into the FM layer driving the magnetization dynamics inducing precession of its magnetization. Additionally, the oscillating spin current injected into the FM layer exerts two orthogonal torques, namely, a damping-like torque (τ_{DL}) and a field-like torque (τ_{FL}) manipulating the magnetization precession. The Oersted and field-like effectives fields, and torques have the same symmetry, i.e $\tau_{Oe} \| \tau_{FL}$. Owing to the anisotropic magnetoresistance (AMR) effect, the oscillating magnetization gives rise to a time-dependent resistivity which mixes with the rf current and

results in a rectified dc voltage. This oscillatory radiofrequency resistance mixed with the rf current allows, at the resonance condition, dc voltage detection across the FM/HM slab using a bias tee [209–213]. The dc voltage is picked up at 45° of the applied H_{dc} (**Figure IV.1**). The dc voltage as function of magnetic field H_{dc} is composed of a mix between a symmetrical Lorentzian function and an antisymmetric one around the resonance field H_{res} and has the same shape as described in eq. (2.17). An example of such raw data is shown in **Figure IV.**4 for a SiO2//Pt(5)/NiFe(4)/AlO_x(3) sample. We can see that broadband frequency dependence allow the determination of M_{eff} and magnetic damping α as in classical FMR experiments. The amplitude of each contribution is V_{sym} and $V_{anti.}$ The equation for STFMR reads:

$$V_{\text{measured}}(H) = V_{\text{offset}} - \frac{1}{4}\frac{dR}{d\theta}\frac{\gamma I_{\text{rf}}\cos\theta}{\Delta H(2\pi df/dH)\big|_{H=H_{\text{res}}}}\left[\left(S\frac{\Delta H^2}{\Delta H^2+(H-H_{res})^2}+A\frac{(H-H_{res})\Delta H}{\Delta H^2+(H-H_{res})^2}\right)\right]$$

$$S = \frac{\hbar}{2e}\frac{J_s}{\mu_0 M_s t_{\text{FM}}}$$

$$A = h_{\text{Oe}}\left[1+\frac{M_{\text{eff}}}{H}\right]^{1/2} \approx \frac{J_c t_{HM}}{2}\left[1+\frac{M_{\text{eff}}}{H}\right]^{1/2} \tag{4.1}$$

where R is the resistance of the FM/NM slab, θ is the angle between current and magnetization, f is the resonance frequency, h_{Oe} is roughly estimated as $h_{Oe} = J_c t_{HM}/2$, and I_{rf} is the total rf current flowing in the FM/NM slab.

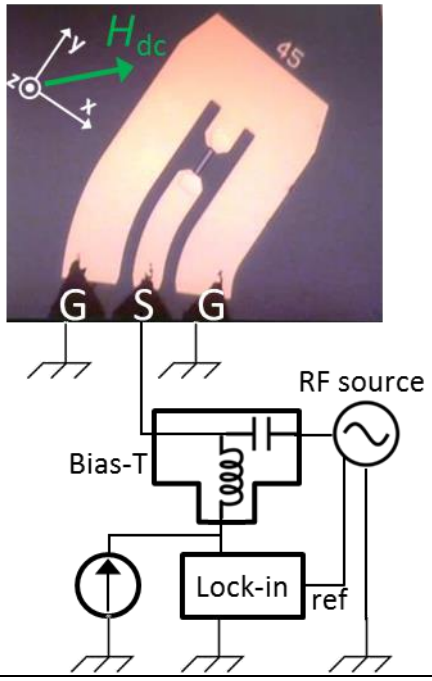

Figure IV.1Picture of a STFMR device along with a schematic of our spin-orbit driven FMR based measurements. The stripe in the middle of the pictogram has dimensions $W\times L$=10×60 μm² and is along the y-axis. The rf frequency and input power are fixed and injected after a bias-T with GSG rf connections. The dc magnetic field H_{dc} is swept. H_{dc} is applied at 45° of the stripe for optimal detection [209,214]**. The rf power is modulated at 433 Hz and the voltage V_{mix} signal is picked-up after the bias-T using a lock-in. To look for the variation of the FMR linewidth as a function of dc bias current, additional dc current source is included as illustrated.**

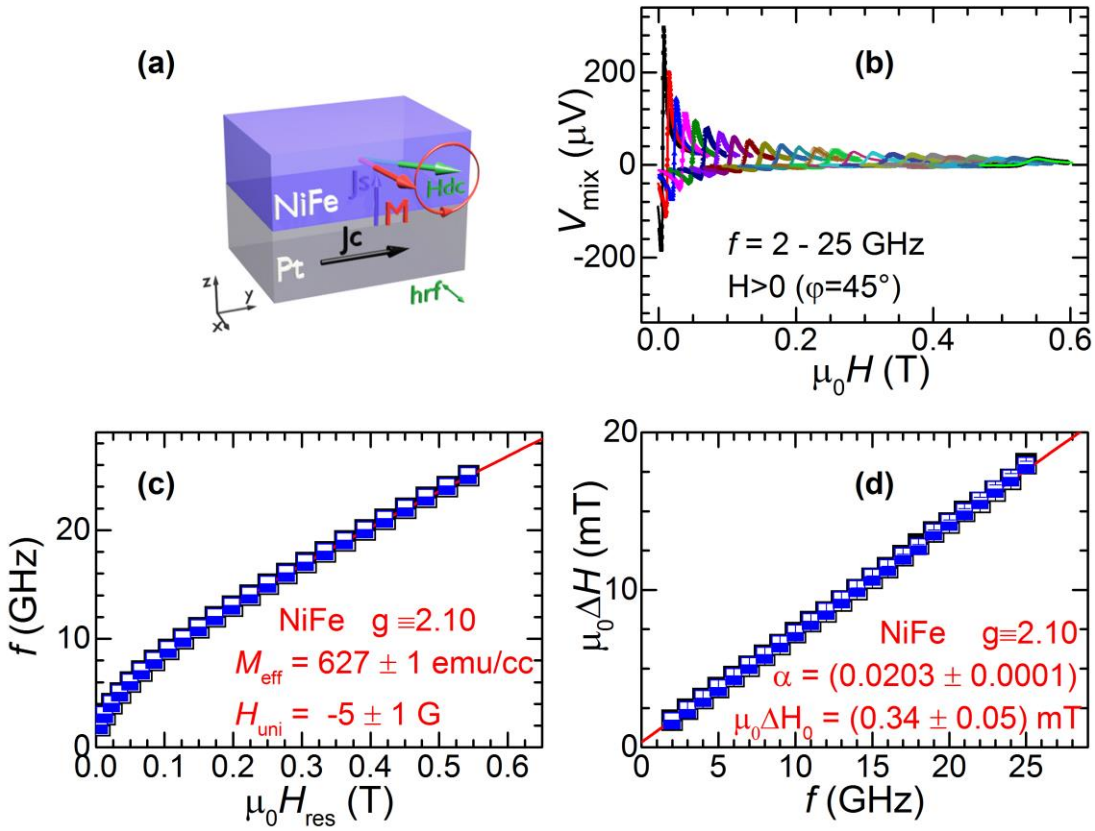

Figure IV.2 M_{eff} and damping determination in Pt/NiFe by STFMR. (a) Schematic of bilayer at FMR condition. Oscillating charges current J_c in Pt generates an oscillating spin current J_s which in turns exert a torque and manipulated the NiFe precesion magnetization. (b) Raw STFMR data of V_{mix} and fit with Eq.(4.4). Frequency dependence of H_{res} (c) and linewidth ΔH (d) for the determination of M_{eff} and damping constant α, respectively. Equation (2.18) is used in (c) and Eq. (2.19) in (d). *Unpublished*

Line shape analysis. In a first approximation, using the last equation, if we take the ratio of the symmetric amplitude over the anti-symmetric one, we have:

$$\frac{J_s}{J_c} = t_{FM} t_{HM} \frac{V_{sym}}{V_{anti}} \left[1 + \frac{M_{eff}}{H} \right]^{1/2} \tag{4.2}$$

This equation has been widely used to report spin Hall angle ignoring many times the approximations. For example, if the symmetric contribution, V_{sym}, is small the error in the fit of the experimental curve will be large. Furthermore, we see that it is proportional to the product of the FM and HM layer thicknesses $t_{FM} t_{HM}$, so for thick samples with $V_{sym} << V_{anti}$ one can report misleading and overestimated values of J_s / J_c. An example using the eq. (4.2)

to estimate θ_{SHE}^{eff} is given in for the same NiFe/Pt sample in **Figure IV.3**. There is also a dependence on HM thickness, which is given by:

$$\frac{J_s}{J_c} = \left(\frac{J_s}{J_c}\right)_{max} \left[1 - \mathrm{sech}(t_{HM} / l_{sf}^{HM})\right] \quad (4.3)$$

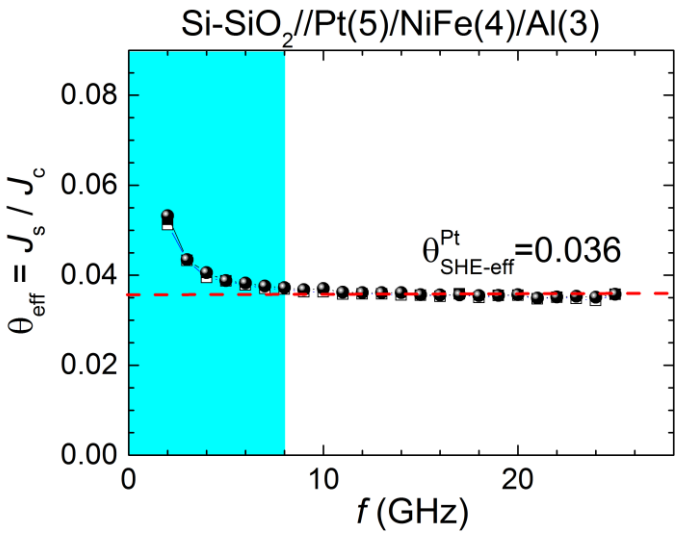

Figure IV.3 Estimation of effective spin Hall angle of Pt in Pt/NiFe sample using the lineshape analysis given by the eq. (4.2). We can see that for frequencies *f*< 8GHz (light blue shaded area), the value is not constant and consequently not reliable. *Unpublished*.

However, even so, Kondou *et al.* [211], and Ganguli *et al.* [212], showed experimentally that $(J_s / J_c)_{max}$ depends linearly with the thickness of the FM layer in this STFMR line shape method.

The most common approximations often overlooked using the line shape analyses are:

i) In the symmetric contribution, the contribution of spin pumping is neglected, Vsp<<Vsym

ii) In the antisymmetric amplitude only the contribution of the Oersted field is considered neglecting the effective field due to field like torque that, for instance, might originate from the SHE or Rashba interface.

iii) The above equations were developed taking a macrospin or single domain model. That is, the precession of the magnetization is considered to be homogeneous. It is often seen in the literature that low frequencies (< 6 GHz) are used to estimate the spin Hall angle of an HM layer using Fe, Co or CoFeB in their system. In these materials the resonance field at those frequencies may be smaller than the saturation field of the FM layer. Consequently, the precession of the magnetization is not homogeneous.

Several studies have been reported where these approaches are addressed. Among them I mention here the one given recently (2019) by Skowronski et al. [215]. I mention also our

contributions, Guillemard et al. [214] and Liu et al. [216], where we highlight and have shown experimentally the importance of reaching homogeneous precession, $H_{res}>H_{sat}$ condition, to get reliable values. In another recent work, they also deal with magnetic anisotropies and the effect on the alignment of magnetization with the applied magnetic field [217]. If one takes the equations described above at low frequency measurements, the values obtained to account for the spin Hall angle might be high but not real. Taking into account these considerations, the above equations can be rewritten as:

$$V_{\text{measured}}(H) = V_{\text{offset}} + V_{\text{sym}}\frac{\Delta H^2}{\Delta H^2 + (H-H_{res})^2} + V_{\text{anti}}\frac{(H-H_{res})\Delta H}{\Delta H^2 + (H-H_{res})^2} \tag{4.4}$$

$$\begin{aligned} V_{\text{sym}} &= -\frac{1}{4}\frac{I_{\text{rf}}\Delta R\sin(2\varphi_0)}{(2H+M_{\text{eff}})\mu_0}\frac{2\pi f}{\gamma}\frac{h_{\text{DL}}}{\Delta H} \\ V_{\text{anti}} &= -\frac{1}{4}\frac{I_{\text{rf}}\Delta R\sin(2\varphi_0)}{(2H+M_{\text{eff}})\mu_0}\frac{2\pi f}{\gamma}\left[1+\frac{M_{\text{eff}}}{H}\right]^{1/2}\frac{h_{\text{FL}}+h_{\text{Oe}}}{\Delta H} \end{aligned} \tag{4.5}$$

$$H_{\text{sat}} < H_{\text{res}} \rightarrow \quad \theta_{\text{SHE}}^{eff} = \frac{J_s}{J_c} \cong \frac{V_{\text{sym}}}{V_{\text{anti}}}\frac{e\mu_0 M_s t_{\text{Fe}} t_{\text{Pt}}}{\hbar}\left[1+\frac{4\pi M_{\text{eff}}}{H_{\text{res}}}\right]^{1/2}\frac{1}{1+\frac{h_{\text{FL}}}{h_{\text{Oe}}}} \tag{4.6}$$

where ΔR is the time-independent component of the resistance, which contains terms from both spin Hall magnetoresistance, SMR, and AMR [215], and φ_0 is the angle between the sample and the dc applied field, usually 45° as depicted in **Figure IV.1**. The above equation is more realistic for estimating the ratio J_s/J_c from the analysis of the shape of the measured STFMR line. In addition, the damping-like spin Hall efficiency $\xi_{\text{DL}}^{\text{HM}}$, and the damping-like effective field, h_{DL}, reads:

$$\begin{aligned} h_{\text{DL}} &= -\frac{\hbar}{2e}\frac{j_c^{\text{HM}}}{\mu_0 M_s t_{\text{FM}}}\xi_{\text{DL}}^{\text{HM}} \\ \xi_{\text{DL}}^{\text{HM}} &\approx \theta_{\text{SHE}}^{\text{HM}}\left(1-\operatorname{sech}\frac{t_{\text{HM}}}{l_{\text{sd}}^{\text{HM}}}\right)\frac{g_{eff}^{\text{HM}}}{1+g_{eff}^{\text{HM}}} \end{aligned} \tag{4.7}$$

And $g_{\text{eff}}^{\text{HM}}$ is the dimensionless real part of the effective spin mixing conductance $g_{eff}^{\uparrow\downarrow}$ which is given in eq. (2.9). g_{eff}^{HM} reads:

$$g_{\text{eff}}^{\text{HM}} = \frac{2e^2}{\hbar}\rho_{\text{HM}} l_{\text{sd}}^{\text{HM}} g_{eff}^{\uparrow\downarrow}\coth\left(\frac{t_{\text{sd}}^{\text{HM}}}{l_{\text{sd}}^{\text{HM}}}\right) \tag{4.8}$$

Analysis of symmetrical amplitude. If we look at eq. (4.1) we see that the symmetric amplitude depends on the oscillating spin current produced, *Js*, multiplied by the total I_{rf}

current injected. If additional measurements are performed the magnetoresistance can be obtained to know $dR/d\theta$ and calibrate I_{rf}. $2\pi df/dH$ is known from FMR condition or much simpler from Kittel law in a polycrystalline FM film. Considering a parallel resistance model, it is possible to obtain J_c flowing in the HM layer from I_{rf} and consequently to estimate J_s/J_c. Equivalently, using equation (4.5), h_{DL} can be estimated if all parameters determining the symmetric amplitude are known. Usually the spin hall angle is considered or determined as:

$$h_{DL} = -\frac{\hbar}{2e}\frac{j_c^{HM}}{\mu_0 M_s t_{FM}}\tilde{\theta}_{SHE}^{HM} \tag{4.9}$$

where $\tilde{\theta}_{SHE}^{HM}$ is introduced as a kind of effective value and to distinguish from a more proper determination given in eqs. (4.7) and (4.8) [215].

Regarding the calibration of the total I_{rf} current, there are different options. One way is by measuring the power input with an VNA and considering the impedance Z of the device, I_{rf} can be estimated. However, if we do not use a VNA but an rf generator with lock-in detection, that could imply changing some rf cable or connectors and consequently altering the rf losses in the circuit. Another method is to take advantage of the Joule heating effect. To do so, taking advantage of the bias-T, $R(I_{dc})$ is measured to see the variation of the resistance with the current due to the Joule effect. Then, using a small dc current, the rf current is also injected at a certain fixed frequency, but varying power. By comparing the resistance variations, I_{rf} can be calibrated under the same measurement conditions (for a given frequency and power). An example is shown in

Figure IV.4.

In this way, we have two options to determine I_{rf} that together with other measures allow us to determine h_{DL} or J_s/J_c more reliably. V_{anti} amplitude analysis could be performed similarly. Considering, in a first approximation, that the Oersted field is $h_{Oe} = J_c t_{HM}/2$, h_{FL} can then be estimated by analyzing V_{anti} amplitude.

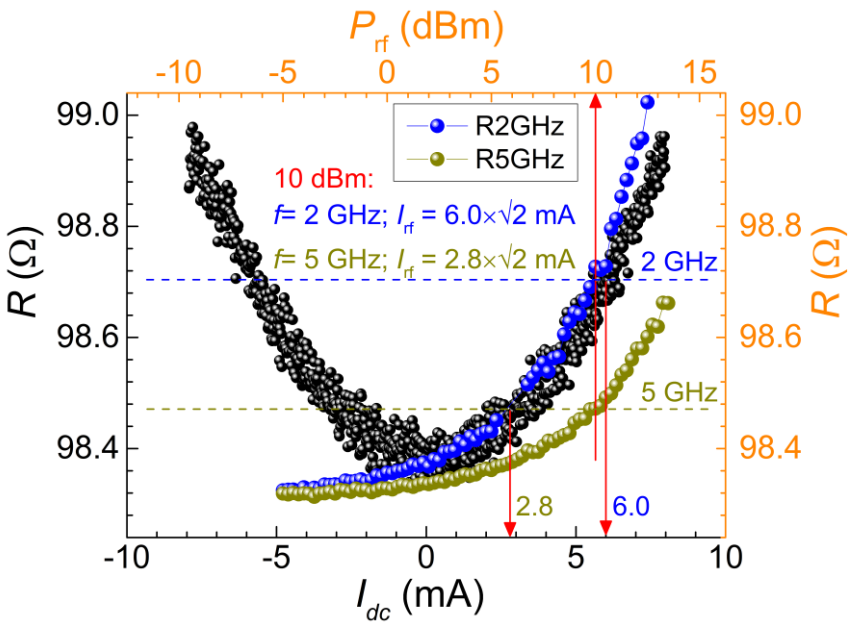

Figure IV.4 Example of the calibration of the I_{rf} current at a certain frequency and power by taking advantage of the variation of the resistance with the I_{dc} current due to the Joule heating effect. In the example we see that for an injected rf power of 10 dBm the current $I_{rf} = 6.0\sqrt{2} = 8.5$ mA for 2 GHz and $I_{rf} = 2.8\sqrt{2} = 3.9$ mA for f=5 GHz.

Modulation of damping

If in the STFMR experiment we also add a dc current, this will generate a spin dc current that will be added to the effect of the oscillating current. Depending on the sign of the dc current and its polarization, a torque will be exerted that will alter the dynamics of the precession of the magnetization. The action of the DL torque is manifested by the variation of the linewidth and the one of the FL torque by the variation of the resonance field as shown in the work of Petit-Watelot et al. for tunnel junctions [206]. However, care must be taken to work on the linear part or subtract the heating part by Joule effect as pointed out in that work. In a FM/HM bilayer, the expression that allows to calculate θ_{SHE}^{eff} from the variation of the linewidth with the total dc current I_{dc}, $d\Delta H / dI_{dc}$, is given by [141,206,209]:

$$\left|\theta_{SHE}^{eff}\right| = \frac{2|e|}{\hbar}\frac{\left(H_{res} + \frac{M_{eff}}{2}\right)\mu_0 M_s t_{FM}}{|\sin\varphi|}\frac{g_{FM}\mu_B/\hbar}{2\pi f}\frac{Wt_{HM}}{\zeta_{HM}}\left|\frac{\partial\mu_0\Delta H}{\partial I_{dc}}\right| \quad (4.10)$$

where g_{FM} is the Landé g-factor of FM layer, W is the width of the stripe, $\zeta_{HM} = I_{HM}/I_{dc}$ is the ratio of the current flowing in the HM over the total dc current injected, and φ is the angle between the current direction and the dc applied magnetic field which usually is 45° or 225° in our experiments.

The effective field due to the field-like torque can be determined from the shift of the resonance field. In a rough approximation, neglecting thermal effects, it can be estimated as:

$$h_{FL} + h_{Oe} = \sin\varphi \frac{\partial H_{res}}{\partial I_{dc}} \tag{4.11}$$

Figure IV.5 shows the result of the linewidth vs I_{dc} for a NiFe/Pt bilayer. We can see that for a field direction or φ=45° we have a negative slope but when the field is inverted the sign of the slope is also inverted. The result gives an effective angle of 0.03 (unpublished). In **Figure IV.6** the result of the variation of the resonance field H_{res} vs I_{dc} for a NiFe/Pt bilayer is presented. We see that for a field direction or phi=45 we have a slope but when the field is inverted the sign of the slope is also inverted (unpublished).

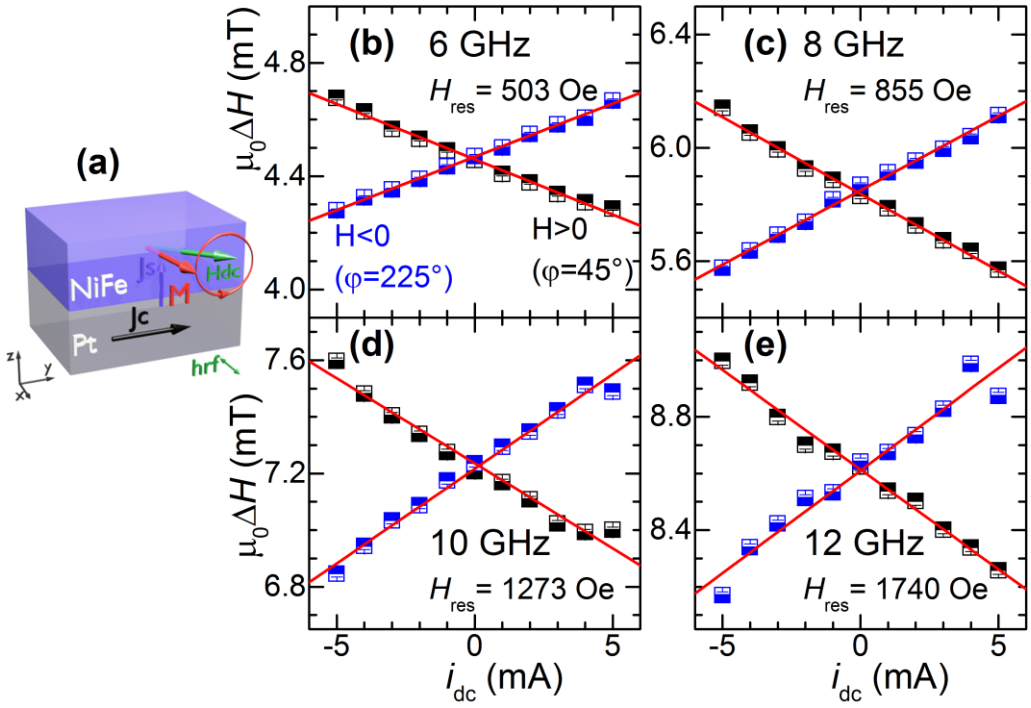

Figure IV.5 Variation of NiFe linewidth vs. total current I_{dc} added in the STFMR experiment at different frequencies between 6 and 12 GHz. The analysis, eq. (4.10), yield an average $\theta_{SHE\text{-}eff}^{NiFe/Pt} = 0.073 \pm 0.005$. *Unpublished*.

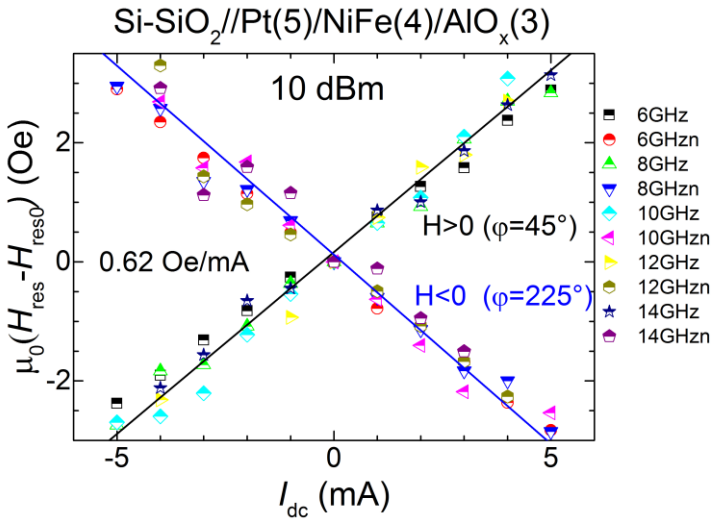

Figure IV.6 Resonance field variation or shift of H_{res} as function of the total I_{dc} current added in the STFMR based experiment. The variation has a positive slop for positive filed, or φ=45°, and negative slop upon reversal of in-plane magnetic field. All the frequencies has the same slope. The linear fit yield 0.62 Oe/mA. Considering h_{Oe}=, then h_{FL}= following the eq. (4.11). *Unpublished*.

IV.2 Research performed at IJL-Nancy

I have developed in Nancy all the experimental work described in this chapter. Using as a base the same FMR equipment, the probe station with the magnetic field in the plane, we have taken advantage of it to configure SPFMR and STFMR.

Thanks to the visiting students, students in our group, and visiting researchers that I have supervised, co-supervised, or collaborated with, we have already had some results published which I mention below.

Independence of Exchange bias anisotropy

This work was done with Hilal Saglam, a doctoral student at the Illinois Institute of Technology and National Argonne Laboratory (USA). She has spent some time in our group under my supervision. The system studied was NiFe/IrMn. Previously, the advantages of using AFM layers had been shown not only to be used as passive components but also have been shown as active ones in spintronics devices [218,219]. Now we wanted to investigate if there was any anisotropy in the spin-orbit torque due to the anisotropy of the exchange bias (EB) imposed by the AFM/FM interface. A summary of the main results is presented in **Figure IV.7**. The samples were grown using rf magnetron sputtering method by Michel Hehn. First we can characterize their magnetic $M(H)$ cycles. In **Figure IV.7a** we can see the typical displacement of the $M(H)$ curve in a EB system in the curve corresponding to the sample of NiFe(6nm)/IrMn(8nm). The shift, which characterizes the EB field, H_{EB}, is uniaxial

and depends on the direction in which the external field is applied. This EB field plays the role of an effective field that adds or subtracts from the resonance field. However, using line shape analysis, no anisotropy is observed in the spin Hall angle and consequently, in the DL torque.

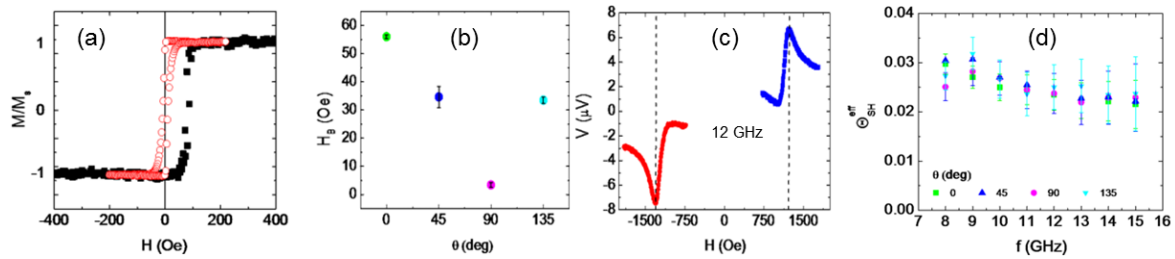

Figure IV.7 (a) Hysteresis cycle of a single NiFe(6) film (red), and NiFe(6)/IrMn(8) bilayer (black). (b) Exchange bias field measured when *H* is applied in-plane according to the directions indicated. (c) STFMR voltage measured at 12 GHz when *H* is applied according to the EB anisotropy axis, θ=0. It is observed that the resonance fields for H<0 and H>0 are displaced by H_{EB} and $-H_{EB}$, respectively. (d) Estimation of θ_{SHE}^{eff} according to directions indicated in (b). We can observe that, within the experimental resolution, there is no anisotropy. Adapted from [220]

This was my first STFMR study reported. We designed our masks, and special care was taken to have the bars along different angles to the EB anisotropy axis. This was already intended for epitaxial samples.

Epitaxial Fe/Pt

In our group, and in our Institute in general, there is the possibility of growing high quality epitaxial samples as well. Taking advantage of this, in collaboration with Stephane Andrieu and his doctoral student, Charles Guillemard, we set out to study epitaxial systems. In order to validate our setup and to obtain relatively simple results, we started with the Fe(6 nm)/Pt(5 nm) system. The sample was grown by molecular beam epitaxy (MBE). First the Fe layer was deposited on the surface of the reconstructed MgO substrate. Then half of the sample was covered to deposit MgO which would give us a true reference sample //Fe(6)/MgO. Then this part of the sample was covered and on the other half Pt was deposited to have the bilayer //Fe(6)/Pt, **Figure IV.8(a-b)**. The area of the Fe/Pt bilayer was lithographed to have the STFMR devices. In the STFMR experiment an rf charge current J_c with power of 10 dBm was injected into the microstrip in the presence of an external field *H*, which is applied in-plane applied at 45° with respect to the microstrip, as shown in **Figure IV.8(c-d)**. In the reference sample the damping constant was measured by typical FMR measurements using a coplanar antenna. Since broadband frequency STFMR measurements also allow obtaining the damping constant in the bilayer, one can estimate the spin mixing conductance using the eq. (2.9). That results in $g_{\text{eff-Fe/Pt}}^{\uparrow\downarrow} = (2.6 \pm 0.5) \times 10^{19}$ nm^{-1}. The highlight of this result is that the

reference Fe layer is exactly the same as the Fe layer in the Fe/Pt bilayer which makes the $g_{\text{eff-Fe/Pt}}^{\uparrow\downarrow}$ result highly reliable. From both STFMR in Fe/Pt and FMR in Fe measurements, we obtain an isotropic damping in the different directions that were measured.

An isotropic result is also obtained in the value of the effective spin Hall angle. Our findings clearly show that the effective spin Hall angle value, $\theta_{\text{eff}}^{\text{Fe/Pt}} = 0.051$, is reliable only when the resonance field is larger than the saturation field. This was confirmed by measurements in SQUID. If we ignore this fact, one can erroneously report high values of $\theta_{\text{eff}}^{\text{Fe/Pt}}$ using the results at low frequencies [214]. The value reported here correspond to a Pt resistivity of $\rho_{\text{Pt}} = 15.6 \pm 0.5$ μΩ.cm, measured independently in a //Fe(6)/Pt(*t*) series with *t* between 1 and 10 nm. For smaller thicknesses, anisotropy of the damping is predicted [221] and recently reported in 0.8 nm of Fe on GaAs substrate [222]. *This work on epitaxial ultrathin FM films is pending for us, as well as the study in Heusler compounds where anisotropic damping is expected even in thick films; i.e. 20 nm.*

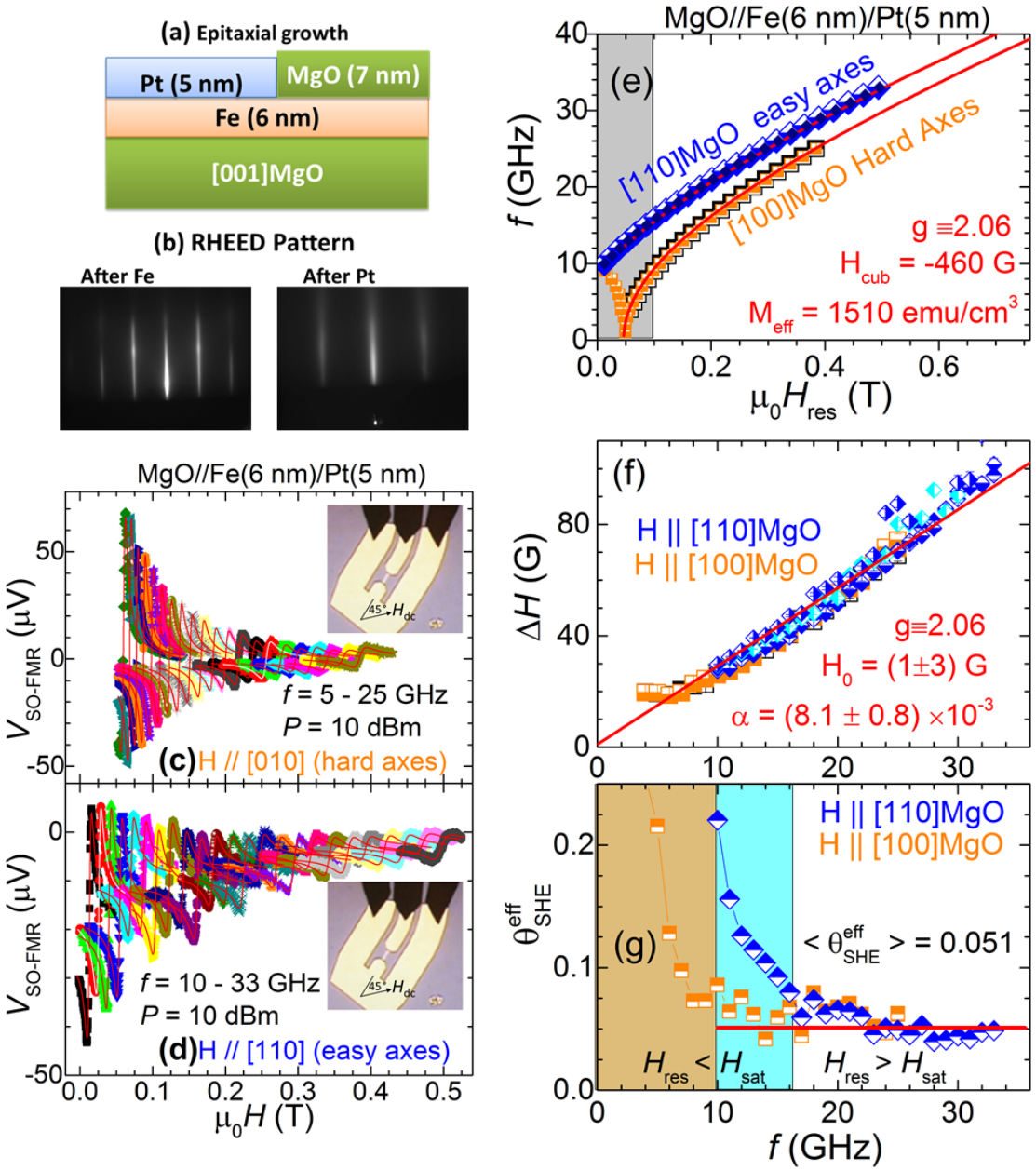

Figure IV.8 Study of spin-orbit torque by FMR in epitaxial Fe/Pt. (a) Schematic of the stacks that have been deposited by MBE. (b) RHEED pattern showing the good quality and 2D growth of Fe as well as the Pt layers. (c-d) STFMR voltages when H is applied in-plane along the hard axes (c) and easy axes (d) crystalline directions. (e)-(g) Results of broadband frequencies to determine the effective magnetization saturation and cubic magnetocrystalline anisotropy field (e), the magnetic damping (f), and the effective spin Hall angle (g). The directions are refers to MgO crystalline axes. The Fe crystalline cell grown rotated by 45° on top of [001]MgO crystalline cell. Adapted from [214].

Ta/Fe/Pt on flexible mica substrate

This study was conducted with Er Liu, a visiting researcher from Nanjing University of Science and Technology (China), who worked with me, for a couple of months in 2018. The project we carried out was about studying the variation of the effective spin Hall angle on flexible substrates, and with different strains. For this purpose, a series of Ta(4nm)/Fe(4 nm)/Pt(5 nm) multilayers were deposited on flexible mica substrates. Besides the SHE contribution of Ta, it was used also as a buffer layer to reduce the roughness of the flexible substrates. During the deposition the substrates are bent and fixed on a homemade mold, as shown in the **Figure IV.9a**. In this way, a compressive longitudinal strain ε is induced in the film when the substrate is flattened after deposition as illustrated. By changing the radius of curvature of the mold, multilayers with compressive strain between 0 and 6.26% are obtained. The magnitude of such induced strain is estimated by $\varepsilon = t_{tot} / 2R$, where R is the radius of curvature of the mold and t_{tot} is the total thickness including both substrate and multilayer.

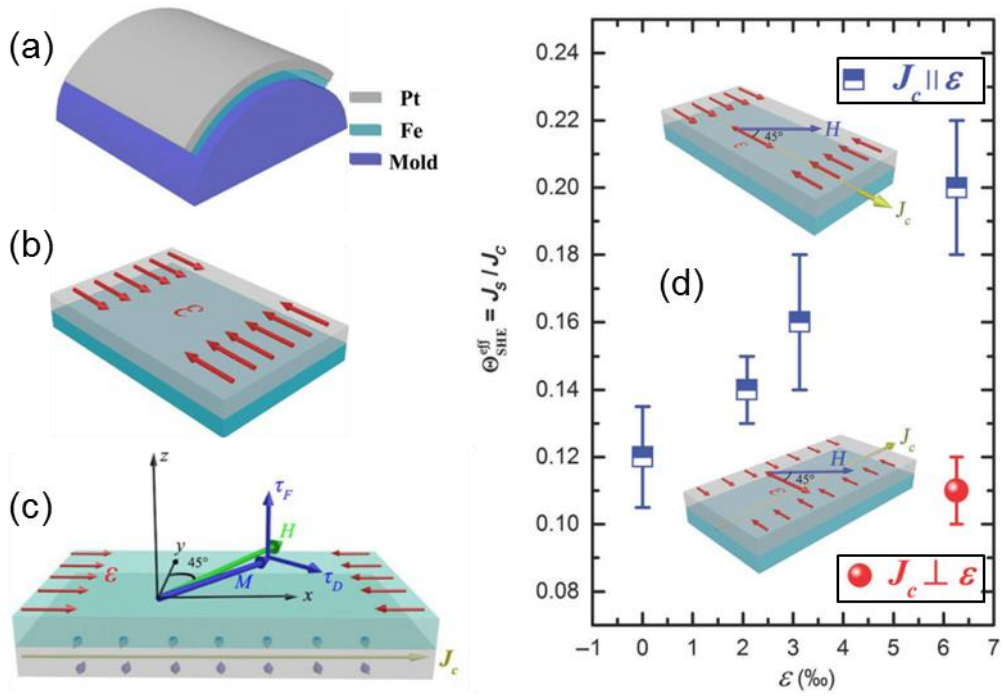

Figure IV.9 (a) The fix of mica on a convex aluminum alloy mold during the film deposition. (b) The flattening afterwards induced a compressive strain ε in the films with direction shown by red arrows. (c) Sketch of the STFMR experimental configuration showing the damping-like and field-like torques, the magnetization *M* and the external field *H*. In this case the micro strip, so the charge current, is parallel to the strain direction, $J_c \| \varepsilon$. (d) Strain dependence of the effective spin hall angle.

The devices for the STFMR study were structured so that the micro strip is parallel, at 45° or perpendicular to the direction of the induced strain ε. As mentioned, in the STFMR experiment, the external field applied is in the plane and at 45° to the micro strip. Our main result is shown in the **Figure IV.9d** where we can observe that, beyond the error bars, the effective spin Hall angle increases almost linearly with increasing strain ε. And in the case of the sample with the highest induced strain, 6.26%, we verify that when measured on the micro strip perpendicular to the strain axis, the result is markedly different, and the same as in the sample where ε=0. This result is also markedly different from the two previous studies where despite EB anisotropy, or cubic magnetocrystalline anisotropy, the effective spin Hall angle was found to be isotropic, for similar thicknesses of the FM and HM layers. We then get an effective overall spin Hall angle that increases from 0.12 to 0.20. This attracts more studies to exploit flexible spintronics.

One perspective of this work is to study the effect of induced stress on SOT-switching. It is a work in progress.

IV.3 Charge-to-spin current conversion at interfaces

I still don't have results of conversion at interfaces using this method. The first results have been in "bulk" to study SHE-SOT as described in the previous section. I will mention some preliminary measures and some studies that could be carried out relatively quickly.

EE-STFMR at Rashba Interfaces and TI

Ag/Bi Rashba interface

Taking advantage of the facilities we have at the IJL, or with external collaborations, one study that could be done is on the Ag/Bi system. To compare, for example, sputtered systems and epitaxial systems. Also compare the results of the two experiments: SPFMR and STFMR. Furthermore, measure the ARPES spectrum before the end of the multi-layer stack deposition for spin-orbitronics experiments in order to make sure if the sample has or does not have the Rashba splitting.

$SrTiO_3/LaAlO_3$ oxide Rashba interface

I maintain collaboration with the oxides group at UMPhi CNRS-Thales. We want to study the direct effect, conversion of charge current into spin current. I have some preliminary measurements with a signal at room temperature. But as the resistance decreases at low temperature, added to the fact that the dielectric constant of the $SrTiO_3$ substrate is huge at low temperatures as mentioned earlier, the signal tends to disappear. At room temperature no effect was observed with the backgate voltage. An ANR project to fund this study is under evaluation.

EE-STFMR in Topological Insulators

In the spintronics-related literature we found several experimental reports claiming that their samples have topological insulators. However, in none of these reports, to my knowledge, has the Dirac cone been measured by ARPES to show interface states unequivocally. Electrical transport measurements were carried out on other samples. I have been pursuing this goal of studying further TI for years. I recently was granted an ANR JCJC project to study it.

IV.4 Compared efficiencies of conversion at interfaces and bulk materials

In a recent publication we have worked on how to compare the efficiencies or figures of merit of spin and charge current interconversions in 3D systems, due to SHE, and in 2D systems, due to EE, and their reciprocals [223]. It is the result of our conferences over several years since 2014. We have seen that in the case of SHE the figure of merit is the spin Hall angle and it is the same for the inverse effect. While the spin to charge current efficiency in systems with spiral spin texture has units of 1/length, and its inverse effect, IEE, has units of length. And the relationship between those two parameters is not simply that one is the reciprocal of the other. Below we write the relationships of these effects:

$$\begin{aligned} \theta_{\mathrm{SHE}} &= j_{\mathrm{s}}^{3D} / j_{\mathrm{c}}^{3D} = \theta_{\mathrm{ISHE}} \\ q_{\mathrm{ICS}} &= j_{\mathrm{s}}^{3D} / j_{\mathrm{c}}^{2D} \\ \lambda_{\mathrm{IEE}} &= j_{\mathrm{c}}^{2D} / j_{\mathrm{s}}^{3D} \end{aligned} \tag{4.12}$$

Charge-to-spin current conversion: Spin Hall effect vs Edelstein Effect. To be able to compare the direct effects, let us remember that, considering transparent interfaces, the transverse spin current produced in a layer of thickness t due to the injected charge current j_{c}^{3D} is:

$$j_{\mathrm{s}}^{3D} = \theta_{\mathrm{SHE}} \left(1\text{-sech}\left[t / l_{\mathrm{sf}}\right]\right) \times j_{\mathrm{c}}^{3D} = \theta_{\mathrm{SHE}} \left(1\text{-sech}\left[t / l_{\mathrm{sf}}\right]\right) \frac{1}{t} \times j_{\mathrm{c}}^{2D} \tag{4.13}$$

Where it has been taken into account that the total current 2D, j_{c}^{2D} , is equal to $t \times j_{\mathrm{c}}^{3D}$. We see that for $t \cong 1.5 l_{\mathrm{sf}}$ we have a maximum conversion, which we call q*:

$$q^{*} = \left(\frac{j_{\mathrm{s}}^{3D}}{j_{\mathrm{c}}^{2D}} \right)_{\max} = 0.38 \frac{\theta_{\mathrm{SHE}}}{l_{\mathrm{sf}}} \tag{4.14}$$

So we get the gain in 2D systems for the direct effect:

$$g_{\mathrm{EE/SHE}} = \frac{q_{\mathrm{ics}}}{q^*} = \frac{2.6 q_{\mathrm{ics}} l_{\mathrm{sf}}}{\theta_{\mathrm{SHE}}} \tag{4.15}$$

Taking typical values for Pt, Ta and W, and considering the value reported for $(Bi_{0.5}Sb_{0.5})_2Te_3$ at low temperature by Kondo et al. [90], we find that the gain is 88.4, 15.6 and 6.1 with respect to Pt, Ta and W, respectively. However, if we consider the shunting factors due to the FM metal layer, the gain factor is reduced to:

$$g_{\mathrm{EE/SHE}}^{\mathrm{shunting}} = \frac{2.6 q_{\mathrm{ics}} l_{\mathrm{sf}}}{\theta_{\mathrm{SHE}}} \times \frac{1}{1+(\rho_{\mathrm{HM}} t_{\mathrm{F}} / \rho_{\mathrm{F}} \lambda_{\mathrm{sf}})} \times \frac{1}{1+(r_{\square}(\mathrm{TI}) t_{\mathrm{F}} / \rho_{\mathrm{F}})} \tag{4.16}$$

Spin-charge current conversion: Inverse Spin Hall effect vs Inverse Edelstein Effect. Recall now that, using classical equations of spin transport, the spin current decays as a function of the depth *z*, $j_{\mathrm{c}}^{3D}(z)$, and the resulting charge current will be:

$$j_{\mathrm{c}}^{3D}(z) = \theta_{\mathrm{SHE}} \frac{\sinh\left[(z-t)/l_{\mathrm{sf}}\right]}{\sinh\left[t/l_{\mathrm{sf}}\right]} \times j_{\mathrm{s}}^{3D} \tag{4.17}$$

where j_{s}^{3D} is the spin current injected at the FM/HM interface. The 2D equivalent charge current density (total current in a unit of layer width) is obtained by integration into the HM layer thickness:

$$j_{\mathrm{c}}^{2D} = \int_0^t j_{\mathrm{c}}^{3D}(z)dz = j_{\mathrm{s}}^{3D} \theta_{\mathrm{SHE}} l_{\mathrm{sf}} \tanh\left[t/2l_{\mathrm{sf}}\right] \tag{4.18}$$

We see now that the maximum conversion is given for $t >> l_{\mathrm{sf}}$ (with $t \approx 3l_{\mathrm{sf}}$ the value of tanh is 0.9), and we define it as $\lambda_{\mathrm{ISHE}}^*$:

$$\lambda_{\mathrm{ISHE}}^* = \left(\frac{j_{\mathrm{c}}^{2D}}{j_{\mathrm{s}}^{3D}}\right)_{\mathrm{max}} = \theta_{\mathrm{SHE}} l_{\mathrm{sf}} \tag{4.19}$$

So we get the gain in 2D systems for the inverse effect:

$$g_{\mathrm{IEE/ISHE}} = \frac{\lambda_{\mathrm{IEE}}}{\lambda_{\mathrm{ISHE}}^*} = \frac{\lambda_{\mathrm{IEE}}}{\theta_{\mathrm{SHE}} l_{\mathrm{sf}}} \tag{4.20}$$

Similarly, if we take typical values for Pt, Ta and W, and using our $\lambda_{IEE}^{\alpha\text{-Sn}}$ value for α-Sn at room temperature, we find that the gain in the IEE is 11.0, 7.8 and 6.2 with respect to Pt, Ta and W, respectively.

Spin Seebeck power generator. Let us now consider that the FM layer is an insulator which if it is exposed to a temperature gradient produces a spin current due to the spin Seebeck effect. We can compare the gain in electrical power of the IEE with respect to the ISHE for the same injected spin current density. The electrical power output scales with the product of the sheet resistance, $r_{\square}$, and the square of the charge current density. The output power gain is:

$$G_{\text{IEE/ISHE}} = \frac{P_{\text{out}}(\text{IEE})}{P_{\text{out}}(\text{ISHE})} = \frac{r_{\square}(\text{TI})}{r_{\square}(\text{HM})} \times \left[\frac{j_c^{2D}(\text{IEE})}{j_c^{2D}(\text{ISHE})} \right]^2 = \frac{r_{\square}(\text{TI})}{r_{\square}(\text{HM})} \times \left(\frac{\lambda_{\text{IEE}}}{\lambda_{\text{ISHE}}^*} \right)^2 \qquad (4.21)$$

Let's consider again the case of α-Sn, $r_{\square} \approx 16$ kΩ, against Pt, Ta and W where $r_{\square} = \rho / t \approx \rho / l_{\text{sf}}$. The gain would be 38000, 917 and 295 with respect to Pt, Ta and W, respectively. Here our prediction of a great advantage using α-Sn TI for power generation.

Shunting by magnetic metallic layer. If the FM layer is metallic, the gain in the inverse effect, IEE vs ISHE, is still maintained. However, the gains of TI or 2D systems estimated in the above equation for power generation are reduced by shunting factors:

$$G_{\text{IEE/ISHE}}^{\text{shunting}} = \frac{r_{\square}(\text{TI})}{r_{\square}(\text{HM})} \times \left(\frac{\lambda_{\text{IEE}}}{\lambda_{\text{ISHE}}^*} \right)^2 \times \frac{1}{1 + (\rho_{\text{HM}} t_{\text{F}} / \rho_{\text{F}} \lambda_{\text{sf}})} \times \frac{1}{1 + (r_{\square}(\text{TI}) t_{\text{F}} / \rho_{\text{F}})} \qquad (4.22)$$

These reduction factors are the most important for heavy metals of large resistivity and short spin diffusion lengths (W, Ta), and even more for 2DEGs of large sheet resistance. Using a typical metal magnetic layer such as CoFeB with and thickness of 5 nm, the gain of α-Sn is reduced to 807, 6 and 1.5 with respect to Pt, Ta and W, respectively.

V. Spin-orbit torque

In this chapter I discuss my results on the switching of magnetization with current. This is one of the ultimate goals for magnetic memory applications. Before discussing my results, I present a summary of some techniques, models or expressions used to describe magnetization switching.

V.1 Field-like and Damping-like SOTs

In Chapter I the LLG equation was already mentioned including the SOT term with its two orthogonal components, damping-like (DL) and field-like (FL). Below I briefly describe the approximations or models used to describe or quantify the efficiency of SOT using SOT-switching or current-induced magnetization switching.

Current induced magnetization switching

Typically, in a FM/HM bilayer where the FM layer has the magnetization naturally aligned perpendicular to the plane of the sample, the combination of a strong current density and a small magnetic field H_x parallel or anti-parallel to it allows switching this magnetization. The DL torque is responsible for switching this magnetization. Lee et al. [224] demonstrated an approach to estimate the critical current in such systems considering that DL is originated mainly by the SHE:

$$J_{\text{switch}} \approx \frac{2e}{\hbar}\frac{t_F}{\theta_{\text{SHE}}^{\text{eff}}}\left(K_{\text{eff}} - \frac{\mu_0 H_x M_s}{\sqrt{2}}\right) \tag{4.23}$$

where K_{eff} is the effective perpendicular anisotropy. However, sometimes the model is also used where only the critical current is considered, and not the field in the plane, H_x.

Anomalous Hall angle θ_{AHE} and spin Hall angle θ_{SHE}

As mentioned in Chapter I, the anomalous Hall effect (AHE) present in magnetic materials is also a result of spin-orbit coupling. In a Hall bar of length L and width W, the detected transverse voltage V_{xy} across a distance W is the result of a conversion of longitudinal charge current j_x into a transverse charge current j_y. The anomalous Hall angle θ_{AHE} gives the ratio between the transverse electric field, E_y, over the longitudinal electric field, $E_x = V_{xx}/L$. E_y is formed by the accumulation of charges j_y, due to the injection of charge current j_x. Thus, in a single magnetic layer, the expression allowing the quantification of θ_{AHE} is:

$$\theta_{AHE} = \frac{V_{xy}}{V_{xx}}\frac{L}{W} = \frac{R_{AHE}}{R_{xx}}\frac{L}{W} = \frac{\Delta R_{AHE}}{\rho_{xx}}t \tag{4.24}$$

And in a FM/NM bilayer or multilayer with just a single FM layer, the ratio is:

$$\theta_{AHE} = \frac{V_{xy}}{V_{xx}}\frac{L}{W}\left[1+\frac{\sigma_{NM}t_{NM}}{\sigma_{FM}t_{FM}}\right] = \theta_{AHE} = \frac{R_{AHE}}{\rho_{FM}}t_{FM}\left[1+\frac{\sigma_{NM}t_{NM}}{\sigma_{FM}t_{FM}}\right]^2 = \frac{R_{AHE}}{\rho_{FM}}t_{FM}\frac{1}{\xi_{FM}^2} \tag{4.25}$$

where $\sigma_i=1/\rho_i$ stands for the longitudinal conductivity of each layer. The expression has been rewritten in terms of the Hall resistance, R_{AHE}, and the longitudinal resistivity of the FM layer. It is worth to note that the factor in square brackets is the reciprocal of the shunting factor of the FM layer due to the presence of NM one, ξ_{FM}. The ratio of the current flowing in FM over the total current injected in the bilayer is $\xi_{FM}=I_{FM}/I$. This ratio ξ_{FM} was already used in Modulation of damping section in Chapter IV.

The relationship for determining the spin Hall angle θ_{SHE} has been seen in different experiments, i.e. spin pumping, ST FMR, etc. Also we can use the *R*(i) cycles in systems with magnetization out-of-plane using the critical current or switching current, eq. (4.23). In this way, we can quantify for example from a $R_{AHE}(H_z)$ cycle, in addition to the coercive field and the amplitude of the effect, its Hall angle θ_{AHE}. And if current-induced magnetization switching is observed, from *R*(i) cycle we can quantify the critical current, and the spin Hall angle θ_{SHE}. We can thus compare in the same system, the Hall angle, charge-to-charge conversion, and the spin Hall angle, charge-to-spin current conversion. An example of this will be presented in the following sections.

V.2 Pt/(Co/Ni)$_3$/Al system

During my post-doc at UMPhi CNRS/Thales, besides continuing with spin-charge current conversion by spin pumping, I also started to study magnetization switching together with Joao Sampaio, Nicolas Reyren, Jean-Marie George and co-workers. For this we looked for a system with out-of-plane magnetization, and the HM layer with strong SOC. The selected system was Si-SiO2//Pt/(Co/Ni)N/AlOx.

Anomalous Hall Effect and SOT-switching in Pt/(Co/Ni)$_3$/Al(5)

The samples were grown by Sophie Collin using the magnetron sputtering technique. We varied the repetition of the Co/Ni period, and the thickness of the Pt to obtain their respective resistivities. I obtained 32.1 μΩcm for Co/Ni and 20 μΩcm for Pt. The saturation magnetization measured by SQUID was M_s= 540 kA/m^2. The samples were then patterned in Hall bars with a width between 4 and 20 microns. I deduced the effective magnetic anisotropy constant K_{eff}=0.16 MJ/m^3 and $K = K_{eff} + \mu_0 M_s^2/2 = 0.34\,\text{MJ/m}^3$ by adjusting the out-of-plane

angular dependence of the R_{AHE}. Our main results are summarized in **Figure V.1** which correspond to the system //Pt(6)/[Co(0.2)/Ni(0.6)]3/Al(5). We can immediately identify that the magnetization is out-of-plane. And when we apply the assisted pulsed current with a field of +48.3 mT, we can see that we obtained the switching of the magnetization. If we reverse the sign of the applied field, -48.3 mT, the polarity of the cycle R(i) reverses its sign as well [225]. Something we overlooked then was the calculation of the spin hall angle, and the Hall angle. Using the equations described at the beginning of the chapter we obtain for $(Co/Ni)_3$ that $\theta_{AHE}^{Co/Ni} = 0.014$ which is relative large indicating the strong SOC origin at Co/Ni interfaces. The estimated current density, about 3×10^{11} A/m^2 in **Figure V.1c**, is in the typical range of SOT-switching in FM/HM systems.

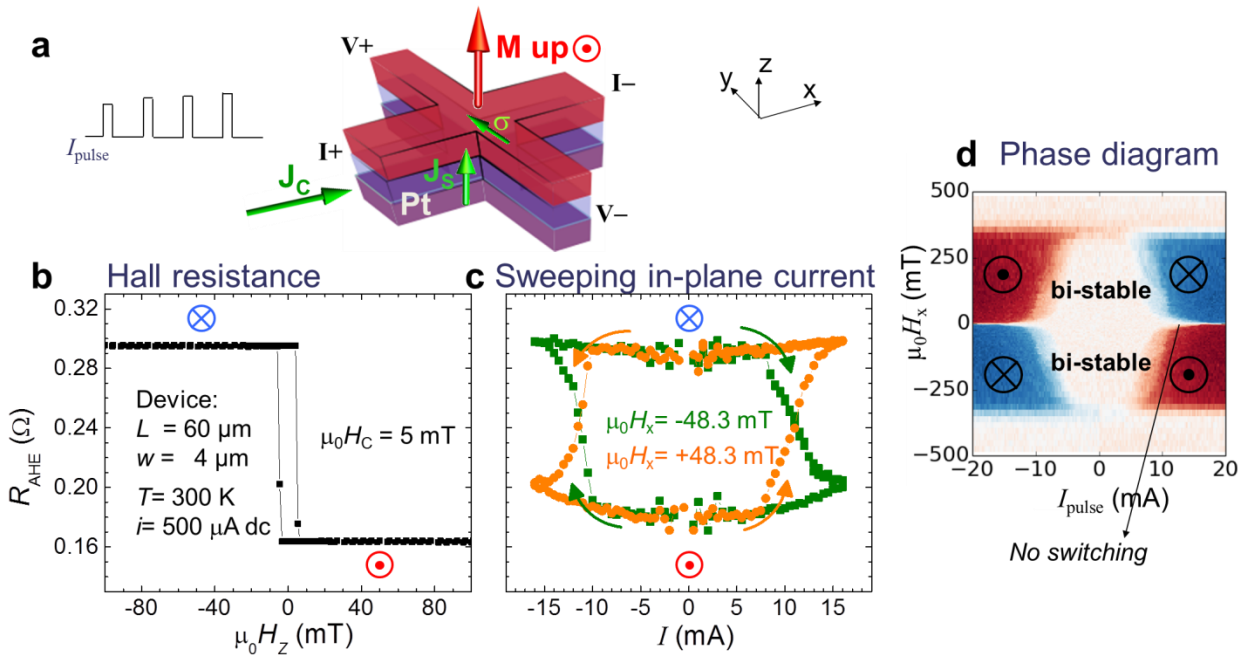

Figure V.1 Current-induced magnetization switching in Si-SiO_2//Pt(6)/[Co(0.2)/Ni(0.6)]$_3$/Al(5). (a) Schematic of the Hall cross bar patterned along with the labelled electrical connections for AHE measurement. (b-c) AHE resistance measured in a device with 4 um width at room temperature when sweeping magnetic field perpendicular to the film plane (b), and when sweeping amplitude of in-plane pulsed charge current (c). (d) Experimental H_x-I_{pulse} phase diagram of the current-induced magnetization switching obtained from different $R_{AHE}(I)$ curves as shown in (c). The minimum field to obtain the SOT-switching is 2.5 mT, and above 370 mT the magnetization lies in the plane. Adapted from [225].

Interfacial DMI and role of in-plane H_x

Now that we have been able to observe the current-induced magnetization switching, we wanted to address the role of the in-plane field H_x still necessary to assist such switching. For this, we consider the interfacial Dzyaloshinski-Moriya interaction (iDMI). This interaction has been widely reported in the Pt/Co interface.

To do this we carry out MOKE images with the same conditions of the switching obtained in **Figure V.1c**. The duration of the current pulse is 200 us. We present in **Figure V.2** three scenarios for different in-plane H_x field values. The first scenario is for zero field, where we observe only nucleation which occurs mainly on the sides of the bar where the Oersted field is anti-parallel to the initial state of magnetization. We can divide the formation of such nucleation into *horizontal* //x, and *vertical* //y domain walls as shown in **Figure V.2d**. We also observe that the nucleated DWS moves to the right, i.e. in the direction of the applied current and antiparallel to the flow of the electrons. This eliminates the spin transfer torque scenario and confirms the SOT scenario generated by the SHE of the Pt in Néel DW of a given chirality. The effective DL or SHE field is different from zero and //z on vertical DWs. Consequently, only the vertical domain walls will propagate along y but there is no switching of the magnetization.

On the other hand, in the geometry we use, having Néel DWs implies higher demagnetization energies than Bloch DWs. If we estimate the critical DMI value to favor such DWs, it results in $D_{crit} = (2/\pi)\mu_0 H_{NB} M_s \Delta = 0.10$ mJ/m^2, where $\mu_0 H_{NB} = 30$ mT is the necessary field to rotate the DW configuration from Bloch to Néel in the absence of DMI. The last value was obtained by micro-magnetic simulations. As the stiffness exchange constant is around A=15 pJ/m^3, the domain wall thickness is $\Delta = \sqrt{A/K_{eff}} = 9.8$ nm. Belmeguenai et *al*. experimentally measured the DMI value in Co/Pt using Brillouin Light Scattering [226]. If we normalize that value to the thickness of our magnetic layer, we get DMI≈0.7 mJ/m^2, which is higher than D_{crit}. The effective DMI field can then be estimated in our system and it results in $\mu_0 H_{DMI} = D/(M_s \Delta) = 133$ mT.

The second scenario is for an Hx field value less than the effective DMI field, **Figure V.2b**. We also see that there is first a nucleation mainly due to the Oersted field, but this time the horizontal DWs propagate and the magnetization switches in the strip. This is because the Hx field rotates the magnetic moments of the horizontal DW as illustrated in **Figure V.2d**. The rotation angle is determinated by the balance between H_x and H_{DMI} [227].

The last scenario is for a field value $H_x > H_{DMI}$, **Figure V.2c**. In this case the applied field overcomes the DMI field, and all DWs have their moments aligned along +x contributing to the expansion of the magnetization reversal.

There are other studies that also show that the switching of magnetization is due to a process of nucleation and propagation of domain walls. However, they report different origins of the nucleation, i.e., due to defects, a hotter electrode, and DMI.

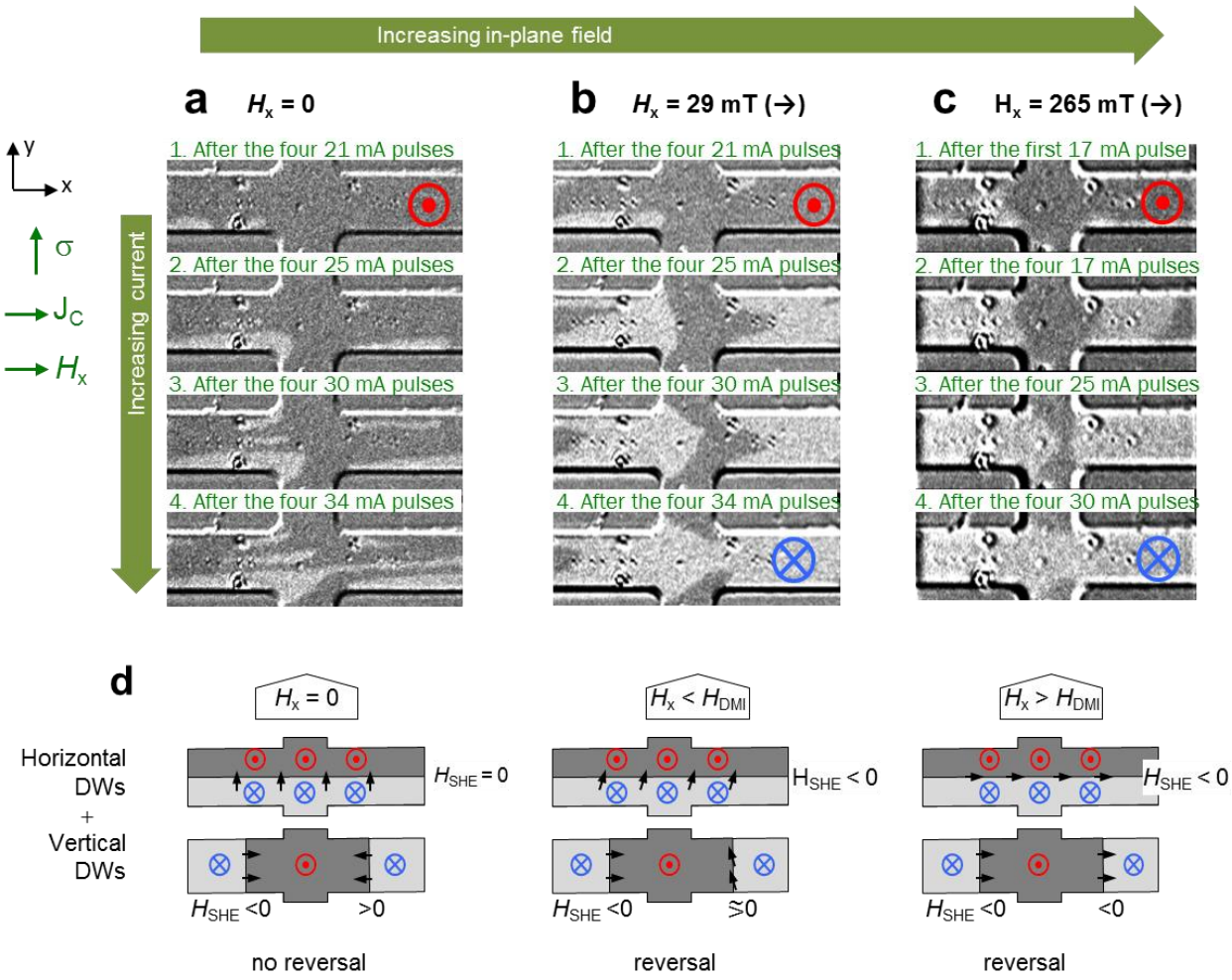

Figure V.2 The role of the in-plane H_x field in the SOT-switching. (a-c) Kerr images after application of current pulses for a given in-plane *Hx* field. The nucleation is mainly due to Oersted field where it is antiparallel to the initial state of the magnetization, +z. The charge current Jc flows rightwards as indicated so electrons flow leftwards. (d) Schematic of vertical and horizontal DWs where the black arrows stand for their local magnetization *m*. Magnetization reversal occurs only if DL or SHE effective field, H_{SHE} < 0, i.e //-z. The estimate DMI effective fields is H_{DMI}=133 mT.

V.3 W/CoTb/Al system

As soon as I arrived in Nancy in 2015 I started working on mounting the experimental setup to continue studying SOT-switching. I achieved this in particular with the help of Daniel Lacour. I got different results in typical FM/HM systems. In Nancy, my colleagues are specialists in the deposition of ferrimagnetic thin films. It was natural then to start these experiments with samples based on ferrimagnetic materials. I have obtained the results of this W/CoTb/Al system [228,229] together with Thai-Ha Pham, my Master student in 2016 and my PhD student between 10/2016 and 05/2020, I was the PhD co-director.

Ferrimagnetic materials (FiM)

A ferrimagnetic rare-earth - transition metal material TM_xRE_{1-x} is characterized by its two magnetic sublattices, one provided by the rare earth, M_{RE}, and the other one by the transition metal, M_{TM}, with antiferromagnetic coupling between them. As the magnetic moments are different, there is a net magnetization $M_s=M_{RE}-M_{TM}$ that changes with temperature T or composition x. At low temperature the M_{RE} magnetization is dominant and the net magnetization is then parallel to M_{RE}. This phase is called RE-rich. At high temperature and below the Curie temperature T_C, the transition metal magnetization M_{TM} is dominant and this phase is called TM-rich. The characteristic temperature where both magnetizations are compensated is called the magnetic compensation temperature, T_{MC}. There is another characteristic temperature, slightly higher than T_{MC}, where the angular moments are compensated, T_{AC}.

TM_xRE_{1-x} ferrimagnetic materials usually have strong bulk SOC which means that, even though they are amorphous, the net magnetization is perpendicular to the plane of the sample and the thicker the layer, the stronger the perpendicular anisotropy. This property presents an advantage for incorporating ferrimagnetic materials into various heterostructures and exploring SOT-switching. Additionally, as mentioned, its net magnetization can be tuned by varying temperature or composition. This represents a rich platform to perform a series of rich experiments.

Anomalous Hall Effect and SOT-switching in W/CoTb

The samples were grown by the magnetron sputtering technique by Michel Hehn. A series of $Si\text{-}SiO_2//W(3)/Co_xTb_{1-x}(3.5)/AlO_x(3)$ samples with x between 0.71 and 0.86 were studied. A first quick characterization to control that M is out of plane is carried out by means of Kerr curves. The polarity of the cycle changes when the sample is Co-rich or Tb-rich, **Figure V.3a**. This is because the Kerr rotation with the wavelength used, red, senses the Co only. Furthermore, the net saturation magnetization is characterized by the measurements using SQUID-VSM. Both results, Kerr and SQUID-VSM, show that the magnetic compensation at room temperature occurs at x=0.77. Another characteristic of ferrimagnetics is that the coercive field H_c diverges close to the compensation, **Figure V.3(a-b)**. The latter can be understood simple by the relationship $\mu_0 H_c \propto \mu_0 H_K = 2K/M_s$ and M_s tends to zero in the magnetic compensation point.

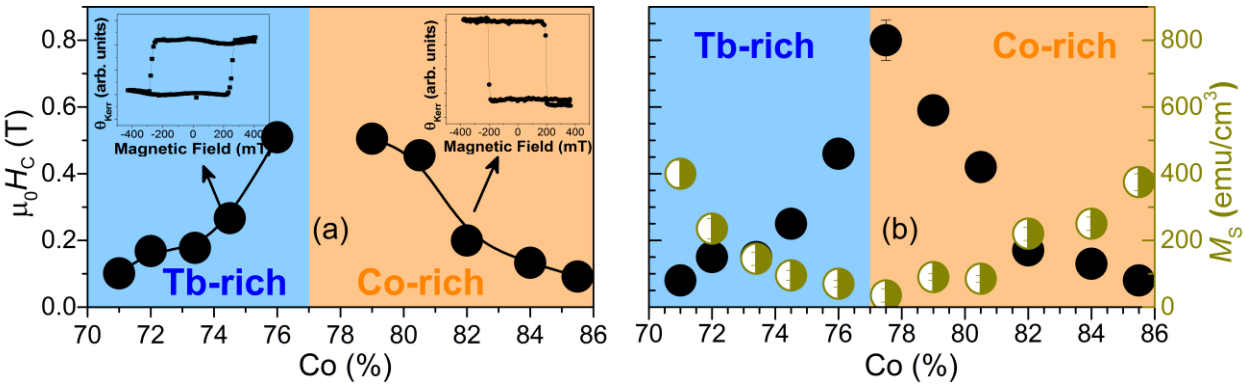

Figure V.3 Magnetic characterization of W/CoTb/Al systems at 300 K. Coercitive field (a-b) and net magnetic saturation (b) as function of Co concentration. H_c from Kerr cycles (a), and $M(H)$ cycles in SQUID-VSM (b). The insets in (a) are Kerr cycles for the indicated concentration. We see that H_c diverges and net M tends to zero at the magnetic compensation point. Adapted from [228].

The samples were micro-structured by standard optical lithography on Hall crosses with widths between 2 and 20 microns. Field-switching or $R_{AHE}(Hz)$ measurements show that the samples maintain their magnetization out of plane after the lithography process, **Figure V.4**. Furthermore, the compensation point is the same, 0.77. All this shows the robustness of the system. As mentioned, from the $R_{AHE}(Hz)$ curves the Hall angle can be obtained. This is shown in the **Figure V.5**. The Hall angle is also high, reaching 1.3% for Co0.78, close to the 1.4% estimated in Pt/Co/Ni)3/Al(5) seen in the previous section. This accounts for the bulk contribution of SOC in CoTb alloy.

In collaboration with colleagues at Spintec, particularly Olivier Boulle and a post-doc we share, Song-gun Je, the critical current equation for ferrimagnetics was derived [229]. For that we developed the LLG equation for each sublattice including the DL torque on each of them in the form $T_{RE(TM)} = \hbar\theta_{SHE}^{eff} J_c / (2eM_{RE(TM)}t_{FiM})$. In addition, it was considered that M_{TM} and M_{RE} always remain anti-parallel and that the angular momentum is totally transferred to the magnetic layer. After developing the modified LLG equation for ferrimagnetic relations, and solving the equation following the model of Lee et al. the critical current is reached. This expression is the same as given in equation(4.23).

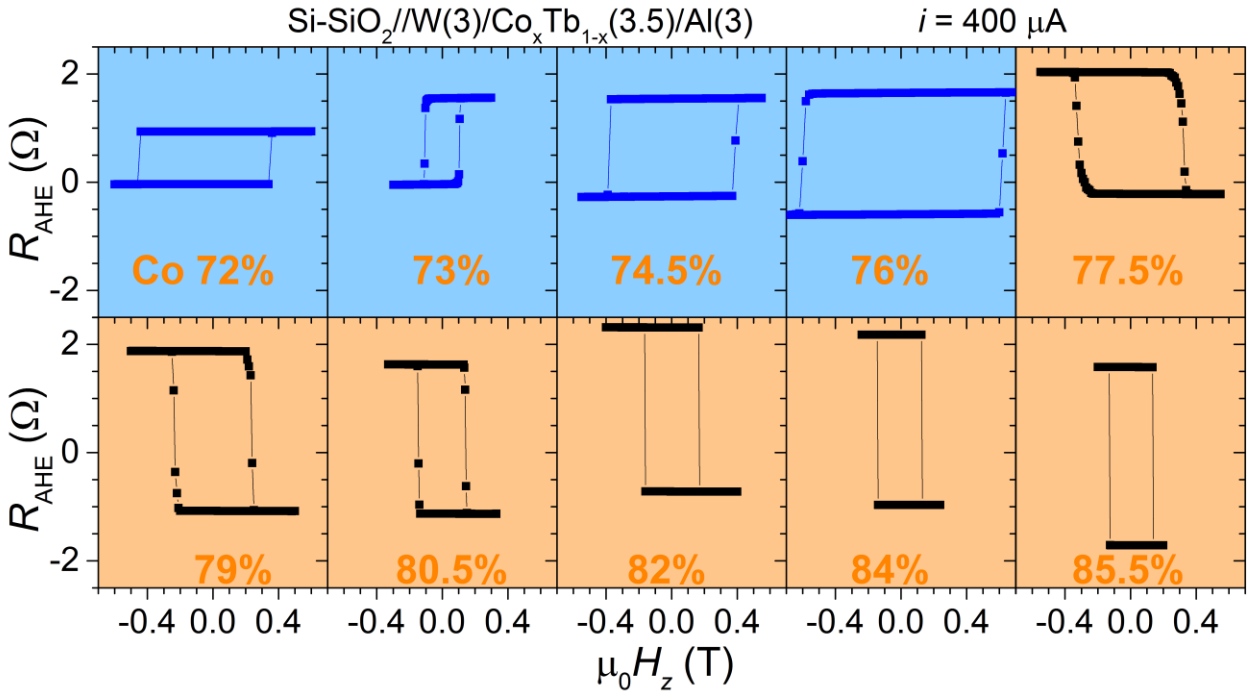

Figure V.4 Evolution of field-switching or $R_{AHE}(Hz)$ as function of Co concentration. Adapted from [228].

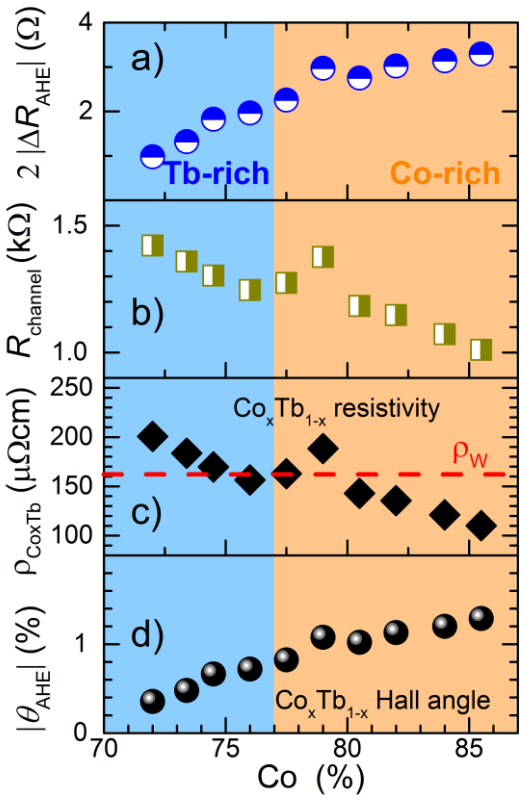

Figure V.5 W(3)/CoxTb1-x(3.5)/AlOx(3) composition dependence of AHE amplitude (a), longitudinal channel resistance in the Hall bar (b), CoTb resistivity (c), and Hall angle (d). Note that according to our convention, $\Delta R_{AHE} > 0$ (< 0) for Tb-rich (Co-rich). The dashed red line in (c) stands for the W resistivity.

The results of SOT-switching are presented below in the Figure V.6. This time we use 100 μs pulses. We can see that the jump is sharp at the critical or switching current, also that we have

the same amplitude, that is, we achieve 100% of the magnetization reversal. The H_x-I_{pulse} phase diagram was performed for the different samples (not shown). The minimum field to obtain the switching is as low as 5 mT.
Almost in parallel, in recent years, several groups have also reported SOT studies using FiM, especially GdFeCo and CoTb alloys or multilayers.

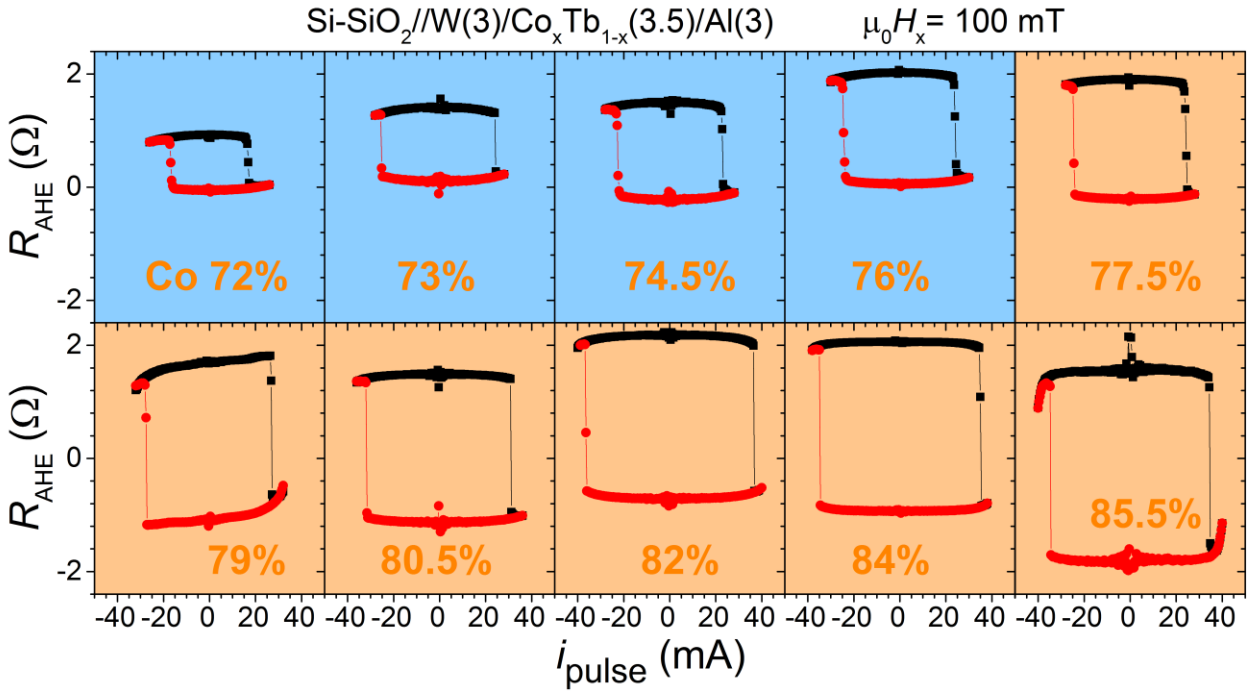

Figure V.6 Current-induced magnetization switching in W/Co_xTb_{1-x}/Al system. The amplitude are the same than for $R_{AHE}(H_z)$. If the in-plane field is reverse, the sign of the cycles are also reversed (not shown). However, the polarity or sign of the cycle in Tb-rich samples are opposite than it was expected.

Thermal contribution to the SOT-switching

All the characteristics presented above are consistent with SOT-switching except that in Tb-rich samples the polarity of the $R(i_{pulse})$ cycle is opposite to that expected and thus has the same polarity as the Co-rich samples. To elucidate this we measured $R(H_z)$ cycles with pulsed current of different intensities. The result can be seen in Figure V.7. We see that for i=19 mA the cycle starts to change sign, which means that the device was heated up to the magnetic compensation temperature. We see that even up to 34 mA the sample is still magnetic, that is, the temperature reached is lower than Tc. Finally, for this same sample, the critical switching current is 24 mA, i.e. above the magnetic compensation temperature. This explains the polarity observed in the samples Tb-rich. However, it also shows the robustness of these samples as all measurements are highly reproducible.

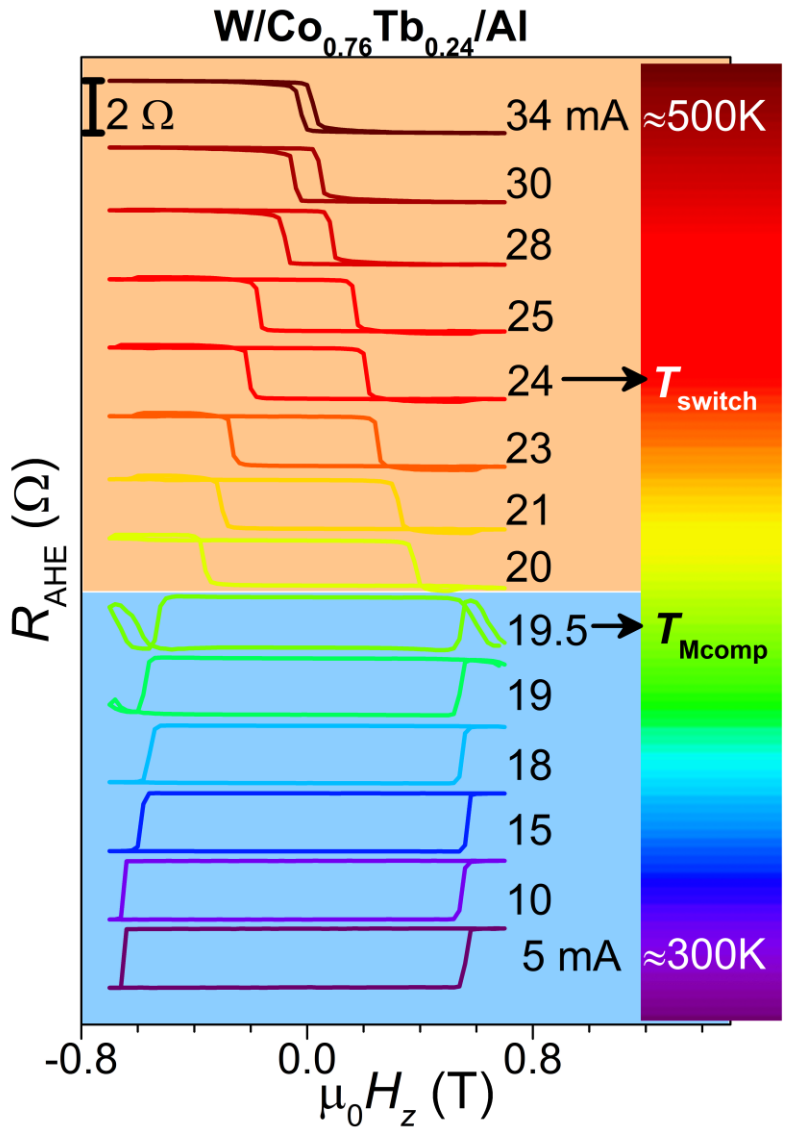

Figure V.7 $R_{AHE}(H_z)$ cycles with different pulse current intensities, instead of a small direct current of 0.4 mA. We can see that around 19.5 mA the cycle starts to change its sign. And already at 20 mA the cycle changed sign or polarity, that is, the device is above T_{MC}. In this sample, the switching current determined from the $R(i)$ cycles is about 24 mA.

Then, the temperature dependence of the whole series was systematically studied. The results are summarized in **Figure V.8** for $Co_{0.79}Tb_{0.21}$. We can see that the critical current increases linearly when the temperature decreases. In some samples there is saturation at lower temperatures, typically < 50 K or 20 K (not shown). This is explained by the increased anisotropy, requiring more H_x field, but anyway the H_k-H_x difference increases rapidly when the temperature is lowered, so this partially explains the increased switching current. The extrapolation of the linear dependence to "zero" current is called T^*. Although experimental limitations do not allow us to measure at temperatures higher than 350 K it would be very

interesting to see if the critical current is really reduced drastically near T^*. An alternative could be to change the system where the critical temperatures can be tuned to lower values.

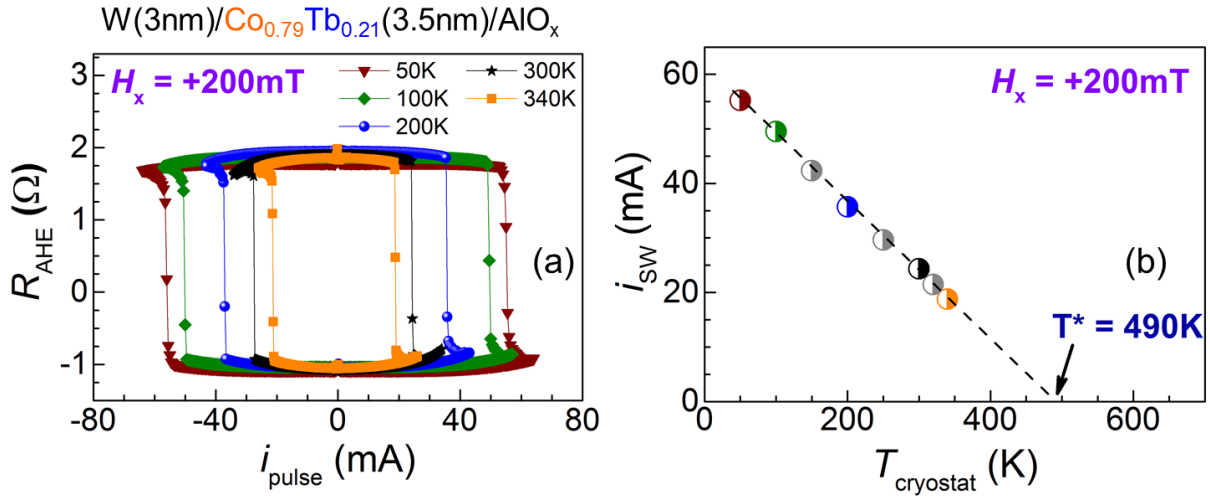

Figure V.8 SOT-switching temperature dependency. (a) Switching cycles with current at different cryostat temperatures. (b) Extraction of switching current as a function of $T_{cryostat}$. We see a linear dependence that extrapolated to i_{SW}=0 produces T*=490 K.

If we also perform longitudinal measurements with the same conditions in our W/CoTb/Al system, we notice that the switching current leads to the device to the same longitudinal resistance value irrespective of the initial temperature or cryostat temperature, which is the one that is experimentally set, **Figure V.9(a-b).** The same longitudinal resistance means the same temperature. We have called this temperature T_{switch} and it can be determined by measuring $R(T)$ with a small current, i.e. 400 uA << i_{sw}. The behavior is linear, in the highest range we can experimentally measure, which allows extrapolation to obtain this T_{switch} temperature as shown in **Figure V.9c**.

The phase diagram is presented in **Figure V.9d**. We can see that the $T_{MC,}$ and T_{AM} (not swhon), decrease linearly as the Co concentration increases. However, the new characteristic temperatures we report, T_{switch} and T^*, increase which would seem to indicate that they follow the Curie temperature.

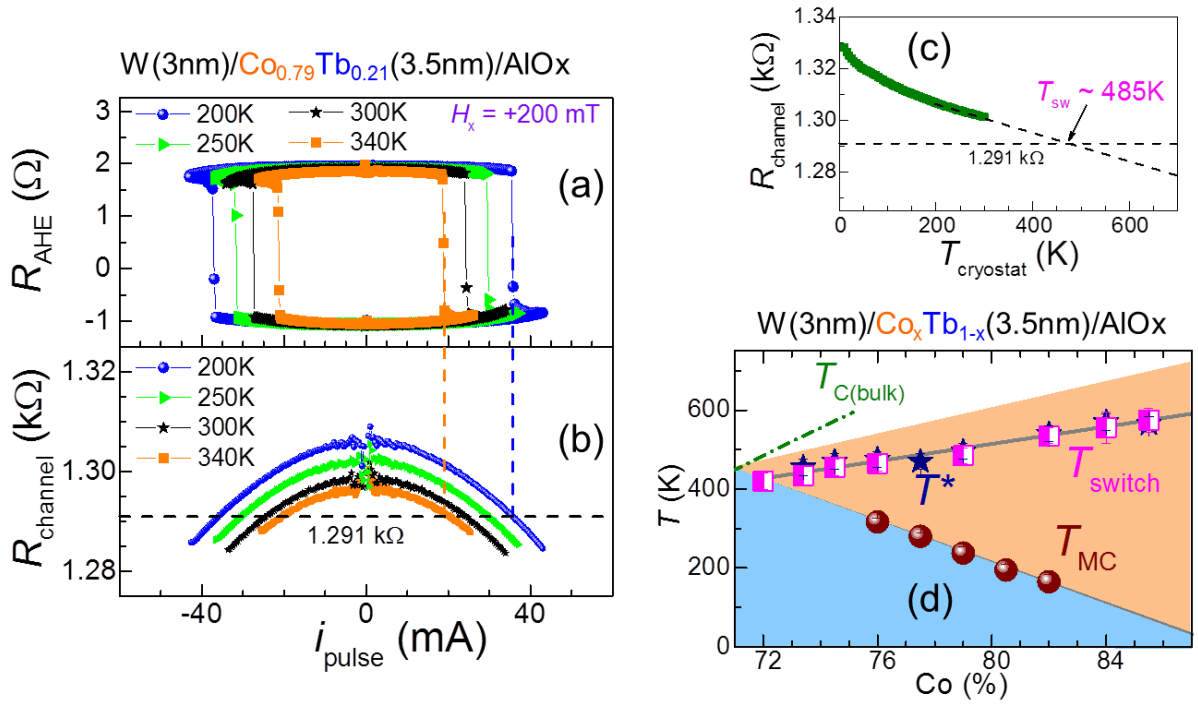

Figure V.9 Determination of switching temperature. (a) cycles R(i) at different crysotat temperaturas. (b) Longitudinal resistance of the current cannel measured with the same conditions as in (a). We can observe by following the vertical lines that at the switching current the channel has the same resistance independent of the temperature of the cryostat. This resistance is 1291 Ohm represented by the black dashed horizontal line. (c) The temperature associated with this resistance is determined according to the protocol shown. The current used is only 0.4 mA. (d) Phase diagram of the characteristic temperatures in our system. Adapted from [228]

The question that arises is what is the physical meaning of such a T_{switch} temperature? Recently, there is a theory that mentions a production of spin current driven by thermally excited magnons in the FiMs. This production is cancelled when $\partial M / \partial T = 0$ which happens between T_{MC} and T_C. Measuring the temperature dependence of the magnetization in FiM is complicated experimentally. Firstly, the FiM signal is low; secondly, as T increases the signal is further reduced (above T_{MC} increases a little but is weaker than below T_{MC}). In thin films, the signal is even weaker. Then, in order to achieve a good detection, the film must be placed in the SQUID in such a way that H is perpendicular to the plane of the sample. This is generally complicated in measurements at high temperatures. Finally, if it is measured at very high temperatures, the film properties may change irreversibly. Anyway, I will keep trying to measure that to know if both temperatures coincide. Maybe in thick enough samples like //W(3)/CoTb(100)/AlO_x(3). In parallel, a chemical study will be carried out using EDS-STEM.

Something that surprised me at first was the ease of achieving switching in this system, and with fairly low in-plane H_x fields despite CoTb's strong perpendicular anisotropy. Although we have not published, we have also studied systems with Pt such as //Pt/Co_xTb_{1-x}/AlOx. In

this case, we see that the compensation point moves to lower values of x, and that higher H_x fields are needed to achieve electrical switching. This is understood by the differences in electrical resistivity between Pt and W. In the system with Pt the heating of the CoTb layer by Joule effect is lower since more current flows through the Pt, keeping the perpendicular anisotropy high. However, as the W and CoTb have similar resistivities, the heating by Joule effect in CoTb is strong as we have shown. Nevertheless, that results in an advantage: when the device is heated, its perpendicular anisotropy is greatly reduced, facilitating electrical switching with a fairly low H_x field.

Ongoing research at IJL

My long-term research project when I joined the CNRS is related to the combination of two effects to manipulate magnetization: spin-obit torque and All optical switching (SOT + AOS). Although I have not done much, we advance little by little. It was complicated to find a good system. Usually AOS looks good on symmetrical HM/FM/HM systems, which cancel out the SOT for switching with current.

My other PhD student, Pierre Vallobra, had results manipulating the exchange bias (EB) with femto-second laser. The system was glass//Ta(3)/Pt(5)/IrMn/7)Co(0.6)/Pt(5) and has perpendicular EB [230]. With Soong-Geun Je we have also obtained the production of skyrmions in sputtered glass//Ta(3)/$Co_{72}Fe_8B_{20}$(wedge, 0.75-1.03)/TaOx(1.2) samples using fs laser [231].

Thai Pham and another post-doc tried to combine AOS and SOT in the W/CoTb/Al samples but the results are not systematic or exploitable as the laser pulse was not synchronized with the current pulse. An obvious shrinkage of the critical current is observed when having the fs laser. Currently, Boyu Zhang is working on it. Preliminary results would show that the combination depends on the polarity of the laser, circular right, left or linear.

Of course, there is mind the study of SOT in different types of systems, 3D and 2D. Some of them will be mentioned in the last chapter.

VI. Research Projets

Throughout the previous chapters, I have been discussing a little and giving shape to ideas of new systems or experiments to be carried out. Time is finite, and so are human resources. That is why funding for projects is crucial to carry out our ideas and the research we want. In this chapter, I summarize three ongoing projects that I am equally passionate about and that, I dream, they will give innovative results.

- The quantification of efficiency due to the spin anomalous Hall effect (SAHE), and the study of self-torque. The last one mainly with the second harmonic technique. This is a long-term project. We have resumed it more recently at the end of 2017. We're moving forward, slowly, but surely. Now we will be able to advance further as a thesis funded by the University of Lorraine will begin in October 2020 under my direction and co-direction of Sébastien Petit-Watelot.
- The study, characterization and exploration for spin-orbitronics applications of the magnetoelectric oxide $Ga_{2-x}Fe_xO_3$. An ANR PRC funds this project, which is in collaboration with colleagues at IPCMS in Strasbourg. I am the local PI.
- I recently got funding on another project, an ANR JCJC (young researcher) which I called TOPTRONICS. It is a project that I have been looking for a long time too. It is somehow the continuation of my work on Rashba interfaces and topological insulators. But this time also exploring the direct effects, and the switching of magnetization.

VI.1 SAHE and self-torque in ferro & ferrimagnetic materials

This study was recommenced at the end of 2017-begginig of 2018. The SHE or self-SHE had already been shown in FM materials experimentally by spin pumping for example [232]. However, new concepts were developed, such as the spin current produced in FM materials with different symmetry than the SHE. This concept, so-called spin anomalous Hall effect (SAHE) [233], accounts for the production of spin current in an FM material whose spin polarization is parallel to its magnetization as illustrated in the **Figure VI.1**. This effect has been quickly measured in NiFe [234] and CoFeB [235]. We have long wanted to study FiMs because of their strong SOC in bulk. This time we have chosen GdFeCo since 5d electrons of Gd provides SOC.

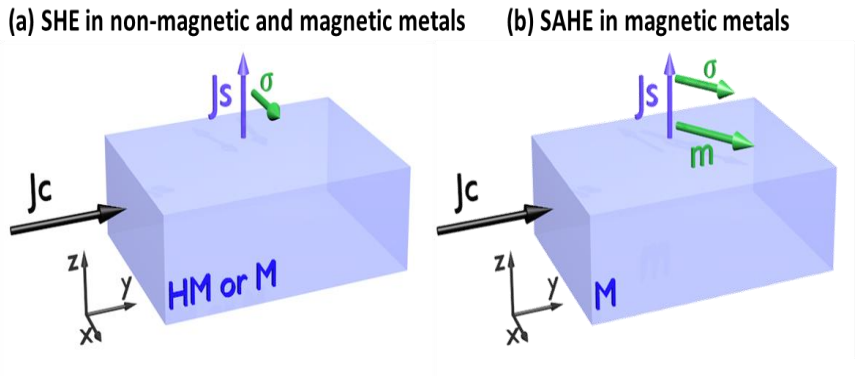

Figure VI.1 Schematic of SHE and SAHE. (a) In the SHE symmetry the spin current Js along z has a spin polarization σ perpendicular to both, Js and Jc, $\mathbf{J}_s \propto \theta_{\mathrm{SHE}}(\mathbf{J}_c \times \sigma)$. (b) In the SHE symmetry the spin current Js along z has a spin polarization σ parallel (or antiparallel) to magnetization m, $\mathbf{J}_s \propto \theta_{\mathrm{SAHE}}(\mathbf{J}_c \times \mathbf{m})$.

SAHE+SHE in ferrimagnets

We started with STFMR measurements and damping modulation as described in Chapter IV. We carried out these measures together with David Céspedes-Berrocal, an internship student from UNI in Lima, Peru, that spent 5 months with us in 2018, and then another 5 months in 2019. The main sample system is GdFeCo/Cu/NiFe grown by magnetron sputtering. The magnetization of NiFe is in the plane of the sample, and that of GdFeCo is naturally out of plane. This was verified independently by SQUID-VSM measurements and by broadband frequency dependence of the NiFe and GdFeCo resonance fields, respectively. In **Figure VI.2** we present some examples of the FMR spectrum, where we identify the NiFe and GdFeCo lines, and of the damping modulation of the NiFe line. At low frequencies, the resonance field of NiFe is low and the magnetization of GdFeCo is kept out of the plane. In this situation, we turn off the SAHE contribution of GdFeCo and leave only the SHE contribution. No modulation of the NiFe damping is observed with the added dc current. This was confirmed with other samples where the GdFeCo is much thicker, and in the whole frequency range measured m_{GdFeCo} are kept out of the plane. This indicates that the SHE contribution of GdFeCo would be weaker than the other contributions. However, returning to the main sample, at frequencies higher or equal than 10 GHz, the resonance field of NiFe is larger than the field needed to align m_{GdFeCo} within the plane. In this condition, a damping modulation of NiFe is observed, whose origin we have attributed to the SAHE effect plus SHE of GdFeCo.

We have checked with other systems to further validate our results. In samples where there is only Cu/NiFe we did not observe any damping modulation. We have compared with similar structures like Pt/Cu/NiFe where we also observe the damping modulation. If we quantify the conversion efficiency, as shown in Chapter IV eq. (4.26), we get $\theta_{\mathrm{Eff}}^{\mathrm{GdFeCo/Cu}} = +0.82 \pm 0.06$ for GdFeCo and $\theta_{\mathrm{SHE\text{-}Eff}}^{\mathrm{Pt/Cu}} = +0.032 \pm 0.002$ for Pt. Our results then show that the overall efficiency of GdFeCo/Cu is more than 20 times higher than the one in Pt/Cu. If we also quantify the

efficiency of the associated DL torque in these experiments, $\chi_{SOT}^{DL} = \frac{H_{DL}}{j_c} = \frac{\hbar}{2e}\frac{\theta_{SHE}^{eff}}{\mu_0 M_s t_F}$, we find that $\chi_{SOT(GdFeCo)}^{DL} = +9.9\times10^{-10}$ Oe/(A/m²) for GdFeCo/Cu and $\chi_{SOT(Pt)}^{DL} = +0.42\times10^{-10}$ Oe/(A/m²) for Pt. The value found for Pt is similar to other values already reported in that system [93]. However, the value for GdFeCo/Cu is very large, and it would be the highest reported so far at room temperature.

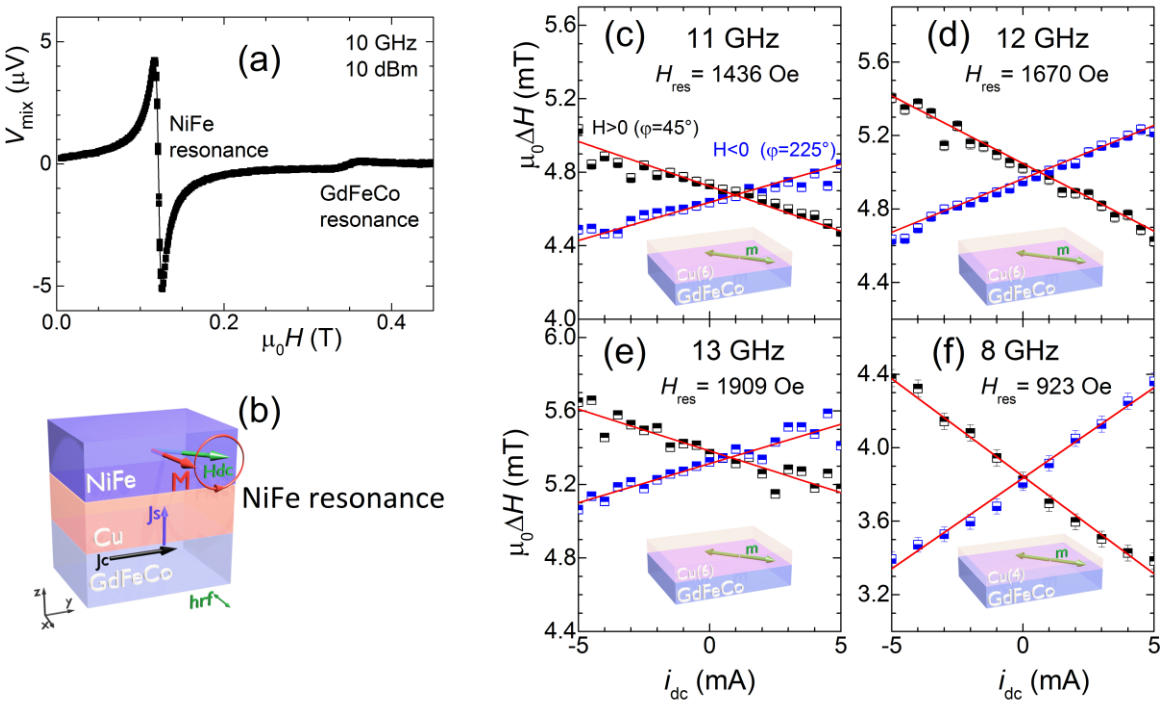

Figure VI.2 SAHE study in GdFeCo. (a) STFMR scan of GdFeCo/Cu(6)/NiFe three-layer coated with 3 nm Al. We can identify the FMR lines of each magnetic layer. (b) Sketch of the FMR condition of the NiFe and the conversion of charge current into spin current in the GdFeCo layer. (c-f) FMR linewidth modulation of NiFe with the dc bias current. In (f) the sample has a thinner Cu layer which allows the modulation to be observed at a lower frequency. Adapted from Céspedes-Berrocal *et al.* (*to be submitted*).

Self-torque in ferrimagnetic materials

Due to its symmetry, the SAHE cannot produce self-torque. However if you have a FM/NM Rashba interface, the FL component can produce self-torque, and the DL component also under certain conditions. We start then to study the FL and DL components in various GdFeCo based systems.

To advance with this study we carried out second harmonic measurements. We started this with David Céspedes-Berrocal during his second stay in the first half of 2019, and then

continued it with Aldo Arriola, also an internship student from UNI, and more recently with Heloïse Damas who is a master's student at the University of Lorraine.

Second harmonic

A technique that has spread rapidly to quantify the efficiency of inter-conversions between charge current and spin current and especially the DL and FL torques and fields is the technique so-called second harmonic. In this technique an ac current is applied and the transverse voltage of the first and second harmonic is measured in a Hall cross device. In a sample with the magnetization out of plane, i.e. M//z, when the field is applied in the plane parallel (perpendicular) to the current the coefficient h_{DL} (h_{FL}) can be extracted. As I will not show experimental results I will skip the formalism or measurement protocol, which is widely known [236–240]. I will only mention that during the M2 stage with Heloïse we have shown from the magnetic susceptibility and the LLG equation including the SOT terms the same equations that are used to determine the effective fields FL and DL [236–240].

In FiM materials, studies using bilayers with Pt or Ta have been reported. They show that DL torque efficiency seems to diverge around the magnetic compensation temperature or magnetic compensation concentration [241–243]. Although later it has been shown that the divergence would occur in the angular compensation [244]. Recently, DL and FL signals have been reported in isolated FiM, CoTb between Si_3N_4 [240]. Our results present different trends than those shown so far in the literature.

Zero-field switching

As I mentioned in the summary, we seek to explore and exploit the self-torque to achieve switching of magnetization without the use of heavy metals, and without any applied field. For now, I will only mention that we obtained the switching without a magnetic field, in a robust and reproducible way though still with heavy materials (measurements performed along with Heloïse Damas). *Note added in October 2020 after the first lockdown: it turned out that the zero-field switching could not be reproduced in other devices, so we believe that it was only the effect of a domain wall pinned in the very first device studied.*
Recently, it was shown that there is a concentration gradient in the GdFeCo layers and that this gives rise to DMI in the amorphous volume of the FiM [245]. If there is DMI, then there is also Rashba effect. This adds to our exploration of the self-torque in addition to exploiting the interfaces. There are very recent results showing electrical zero field switching on FM1/FM2 bilayers, or with wedges. We are also exploring and will explore other alternatives. There is much to be done. Dependence on thickness, concentration, and temperature should be studied as well as dependence in the selection of materials and interfaces, and so on.

VI.2 Exploring magneto-electric properties in $Ga_{2-x}Fe_xO_3$

A very attractive material used par excellence in magnonics is the ferromagnetic insulator YIG. It has the advantage of having low damping; it has also been used to study the longitudinal spin Seebeck effect, spin Nernst, spin Hall magnetoresistance and unidirectional magnetoresistance. On the other hand, the study of oxides is a very rich field itself. Even more if we add that it is magnetic, or AFM, and insulating. Recently, ISHE spin pumping has been reported in AFM/Pt and AFM/Ta bilayers [246,247]. This requires a special experimental facility where hundreds of GHz and multi-Tesla field can be reached. In our case we can only reach 40 or 65 GHz and 9T, soon up to 14 T but we do not have the facility to use higher frequencies.

What about $Ga_{2-x}Fe_xO_3$? $Ga_{2-x}Fe_xO_3$ is an oxide that is magnetic, insulator, and magneto-electric [248,249]. Although its magneto-electric properties have yet to be established or confirmed experimentally in thin films. The Curie temperature is about $T_C \approx 370$ K and M_s=100 kA/m^2 for x=1.4 in thin films and bulk [250–252]. Magnetic anisotropy constants of $Ga_{2-x}Fe_xO_3$ are high, which bring to FMR condition also in high frequencies range, between 90 and 130 GHz [253,254]. We have tried to measure it by applying a gate voltage, expecting to vary its magnetic anisotropy, but we have not yet observed FMR. We are then trying to study if they have a strong SAHE effect using a three-layer structure, $Ga_{0.6}Fe_{1.4}O$/Cu/NiFe as we have developed in the previous project. Also, we will perform the study of spin wave propagation in $Ga_{2-x}Fe_xO_3$ to estimate its spin diffusion length. To do this, we will use a simple geometry, of two bars or Pt strips parallel to each other. One bar will serve as a detector and the other as an injector. This has been widely used. Recently, using this geometry the SHE and SAHE study was reported in NiFe [234], and a high l_{sf} in epitaxial NiO [255].

We have been studying some magnetotransport properties using the $Ga_{0.4}Fe_{1.6}O_3(t)$/Pt(5) bilayer structured in Hall bars. Samples were grown by PLD on $SrTiO_3$ substrates at IPCMS in Strasbourg and the lithography and magnetotransport measurements performed in Nancy along with our post-doc Elodie Martin. **Figure VI.3** shows the $Ga_{2-x}Fe_xO_3$ crystalline structure and some results of longitudinal and transversal resistances. We observe that the sign of AHE changes between 40 K and 120 K (the AHE is better observed after taking off the linear contribution due to ordinary Hall effect). This is something observed in FMI/HM as YIG/Pt [256,257], YIG/Pd, etc. We are conducting more systematic and thorough measurements, and in control samples to discern whether the change in sign is due to some transition in Pt or $Ga_{2-x}Fe_xO_3$. Well understood, being the $Ga_{2-x}Fe_xO_3$ insulator, the magnetotransport is detected due to the interface and the induced moment in Pt. So far, we have no observed a sizable effect due to the gate voltage. The next step will be to use doped $SrTiO_3$:Nb substrate in order to have a more effective gating effect.

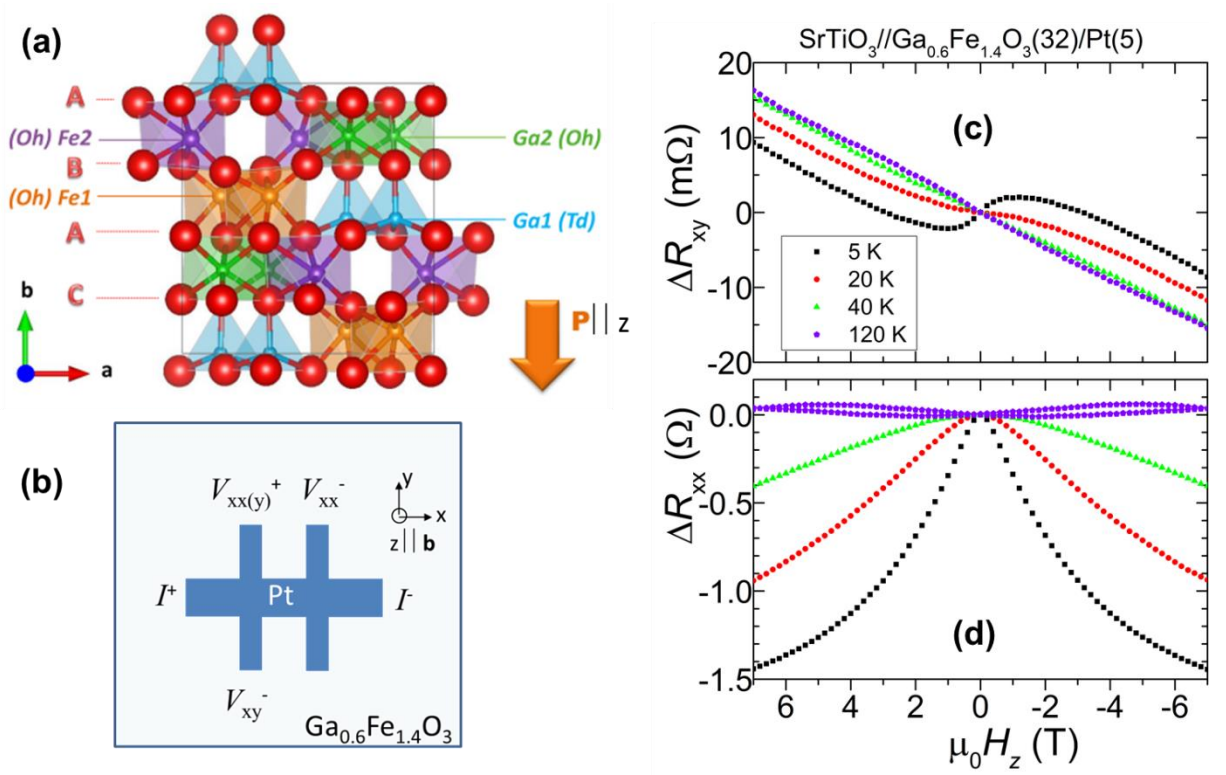

Figure VI.3 Towards confirmation of the magneto-electric effect in $Ga_{2-x}Fe_xO_3$. (a) The Pc21n orthorhombic structure of $Ga_{2-x}Fe_xO_3$ (GFO), showing the double hexagonal close-packed stacking of oxygens (ABAC), and the 3 octahedral and 1 tetrahedral cationic sites. The orange arrow stands for the electrical polarization P, which is perpendicular to the film plane. Adapted from [258]. (b) Schematic of a double-cross Hall bar of Pt patterned on top of GFO thin film. The connections for the longitudinal and transverse electrical measurements are shown together with the coordinate axis used. (c) Transversal and (d) longitudinal resistivities as function of perpendicular magnetic field. The variation of longitudinal resistance as function of *Hx* and *Hy* has the same behavior as for *Hz*. We can observe in both R_{xx} and R_{xy} that a transition occurs below 120 K

VI.3 Topological insulators and 2D systems for spin-orbitronic and spin-caloritronic

My most recent funded project is TOPTRONIC. I don't have much to say or present yet, as we are just getting started. I want to explore in this project new paradigms in this field using spin-charge current conversion by spin-momentum locking at interface states of novel topological insulators (TIs) such as α-Sn and half-Heusler alloys, i.e YPtBi,, GdPtBi, and so on, integrated with non-classical magnetic materials such as Heusler alloys (HA). This goal is strongly coupled to the objective of using the spin-charge current conversions in different types of devices including power generators for the transformation of heat flow into electrical

power thanks to new spin-thermal effects where a temperature gradient generates a spin current. The 3-Dimensional TIs are insulators in their bulk but hold metallic topological states in their surfaces which leads to a prediction of high efficiency for charge-spin current conversion by the phenomenon called Edelstein Effect (EE), and its reciprocal, the inverse EE as discussed in previous chapters. Linking materials growth, surface spectroscopies and spin-orbitronics studies, I intend to show that harnessing EE (IEE) in these new nanostructures is a very promising way for harvesting energy and magnetic memories applications. Two main goals of the project are schematized in **Figure VI.4**. Besides, fundamental questions open up such as: what is the interaction between a full spin polarized film and a TI film? I will study the role of the different parameters that govern the physics of these systems and the different time scales involved with the objective to tailor high efficiency devices. Achieving any of these aims will represent a major breakthrough towards topological spin-orbitronics and topological spin-caloritronics.

Stephane Andrieu, our MBE specialist, along with his PhD student, Victor Palin, have already succeeded in growing epitaxial YPdBi. We will soon see whether or not it is TI or Weyl semimetal by ARPES measurements.

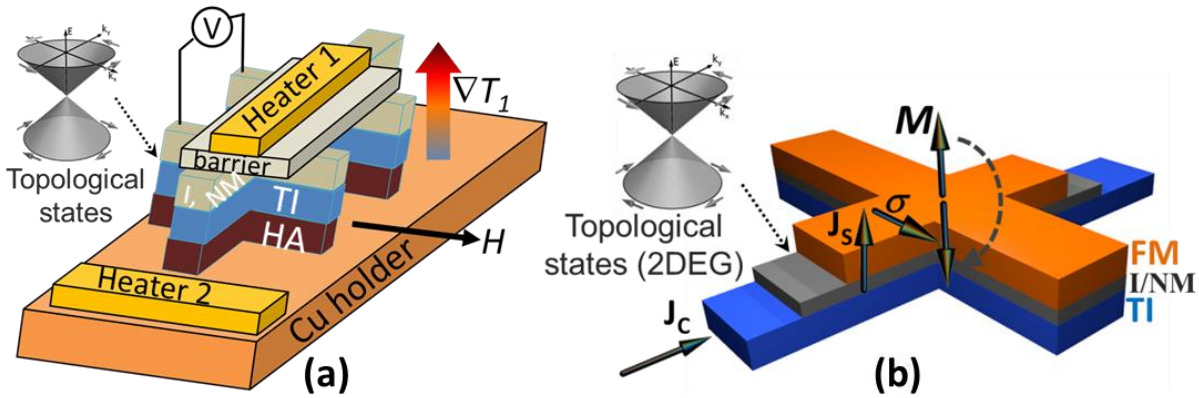

Figure VI.4 Two main goals of TOPTRONICS project. (a) A temperature gradient ∇T can generate a spin current in the ferromagnetic HA layer which in turn could be converted into an output voltage V, due to the expected high spin-charge conversion efficiency on the topological states. The combination of these effects can be used for harvesting energy. (b) Materials that have spin texture as in TI or two-dimensional systems (2DEG) can efficiently generate a Js spin current, which can then be used to manipulate the magnetization M of a ferromagnetic (FM) layer. These effects can be used in applications such as magnetic memory and logic circuits.

VI.4 Conclusions

I have described in this manuscript some of my main findings. All these results are related to spin current or spin accumulation as well as spin-charge current interconversion. I have described from the diffusion and absorption in nano-devices of lateral spin valves to the ferromagnetic resonance and dynamics of magnetization. Then I have moved to present and discuss results on spin pumping ferromagnetic resonance, spin-torque ferromagnetic resonance and spin-orbit torque switching. The first results are during my post-doc, then as a permanent researcher since October 2015. Since then, I have been enriched with the training or supervision of internship student, master students, doctoral students and post-doctoral fellows as well as collaborations with visiting researchers.

All the experiments I have described or mentioned will allow me to advance in the understanding of new effects and phenomena, as well as to face the current and future projects with more confidence since the study or realization of a research project will enrich the others projects as well.

References

[1] M. N. Baibich, J. M. Broto, A. Fert, F. N. Van Dau, F. Petroff, P. Etienne, G. Creuzet, A. Friederich, and J. Chazelas, "Giant Magnetoresistance of (001)Fe/(001)Cr Magnetic Superlattices" *Phys. Rev. Lett.* **61**, 2472 (1988).

[2] G. Binasch, P. Grünberg, F. Saurenbach, and W. Zinn, "Enhanced magnetoresistance in layered magnetic structures with antiferromagnetic interlayer exchange" *Phys. Rev. B* **39**, 4828 (1989).

[3] S. S. P. Parkin, N. More, and K. P. Roche, "Oscillations in exchange coupling and magnetoresistance in metallic superlattice structures: Co/Ru, Co/Cr, and Fe/Cr" *Phys. Rev. Lett.* (1990).

[4] B. Dieny, V. S. Speriosu, S. S. P. Parkin, B. A. Gurney, D. R. Wilhoit, and D. Mauri, "Giant magnetoresistive in soft ferromagnetic multilayers" *Phys. Rev. B* (1991).

[5] N. F. Mott, "The Electrical Conductivity of Transition Metals" *Proc. R. Soc. A Math. Phys. Eng. Sci.* **153**, 699 (1936).

[6] A. Fert and I. A. Campbell, "Two-current conduction in nickel" *Phys. Rev. Lett.* (1968).

[7] A. FERT and I. A. CAMPBELL, "TRANSPORT PROPERTIES OF FERROMAGNETIC TRANSITION METALS" *Le J. Phys. Colloq.* (1971).

[8] A. Fert and I. A. Campbell, "Electrical resistivity of ferromagnetic nickel and iron

based alloys" *J. Phys. F Met. Phys.* (1976).
[9] A. Fert and F. N. Van Dau, "Spintronics , from giant magnetoresistance to magnetic skyrmions and topological insulators" *Comptes Rendus Phys.* **20**, 817 (2019).
[10] S. Ikeda, J. Hayakawa, Y. Ashizawa, Y. M. Lee, K. Miura, H. Hasegawa, M. Tsunoda, F. Matsukura, and H. Ohno, "Tunnel magnetoresistance of 604% at 300 K by suppression of Ta diffusion in CoFeB/MgO/CoFeB pseudo-spin-valves annealed at high temperature" *Appl. Phys. Lett.* **93**, 082508 (2008).
[11] M. Julliere, "Tunneling between ferromagnetic films" *Phys. Lett. A* (1975).
[12] S. Maekawa and U. Gafvert, "Electron tunneling between ferromagnetic films" *IEEE Trans. Magn.* (1982).
[13] I. Oleinik, E. Y. Tsymbal, and D. Pettifor, "Structural and electronic properties of magnetic tunnel junction from first principles" *Phys. Rev. B - Condens. Matter Mater. Phys.* (2000).
[14] J. Mathon and A. Umerski, "Theory of tunneling magnetoresistance in a junction with a nonmagnetic metallic interlayer" *Phys. Rev. B - Condens. Matter Mater. Phys.* (1999).
[15] P. Mavropoulos, N. Papanikolaou, and P. H. Dederichs, "Complex band structure and tunneling through ferromagnet/insulator/ferromagnet junctions" *Phys. Rev. Lett.* (2000).
[16] X. G. Zhang and W. H. Butler, "Large magnetoresistance in bcc Co/MgO/Co and FeCo/MgO/FeCo tunnel junctions" *Phys. Rev. B - Condens. Matter Mater. Phys.* (2004).
[17] J. M. De Teresa, A. Barthélémy, A. Fert, J. P. Contour, F. Montaigne, and P. Seneor, "Role of metal-oxide interface in determining the spin polarization of magnetic tunnel junctions" *Science (80-.).* (1999).
[18] C. Chappert, A. Fert, and F. N. Van Dau, "The emergence of spin electronics in data storage" *Nat. Mater.* **6**, 813 (2007).
[19] Y. M. Lee, J. Hayakawa, S. Ikeda, F. Matsukura, and H. Ohno, "Effect of electrode composition on the tunnel magnetoresistance of pseudo-spin-valve magnetic tunnel junction with a MgO tunnel barrier" *Appl. Phys. Lett.* **90**, 23 (2007).
[20] A. Fert, "Origin, development, and future of spintronics (Nobel lecture)" *Rev. Mod. Phys.* **80**, 1517 (2008).
[21] J. C. Slonczewski, "Current-driven excitation of magnetic multilayers" *J. Magn. Magn. Mater.* **159**, L1 (1996).
[22] L. Berger, "Emission of spin waves by a magnetic multilayer traversed by a current" *Phys. Rev. B* **54**, 9353 (1996).
[23] M. Hosomi, H. Yamagishi, T. Yamamoto, K. Bessho, Y. Higo, K. Yamane, H. Yamada, M. Shoji, H. Hachino, C. Fukumoto, H. Nagao, and H. Kano, in *Tech. Dig. - Int. Electron Devices Meet. IEDM* (2005).
[24] "Everspin ships first ST-MRAM memory with 500 × performance of flash" *Comput. World* (n.d.).
[25] J. E. Hirsch, "Spin Hall Effect" *Phys. Rev. Lett.* **83**, 1834 (1999).
[26] S. Maekawa, S. O. Valenzuela, E. Saitoh, and T. Kimura, editors , *Spin Current* (Oxford University Press, 2012).
[27] K. Uchida, S. Takahashi, K. Harii, J. Ieda, W. Koshibae, K. Ando, S. Maekawa, and E. Saitoh, "Observation of the spin Seebeck effect" *Nature* **455**, 778 (2008).
[28] G. E. W. Bauer, E. Saitoh, and B. J. vanWees, "Spin caloritronics" *Nat. Mater.* **11**, 391 (2012).

[29] C. Zhou, Y. P. Liu, Z. Wang, S. J. Ma, M. W. Jia, R. Q. Wu, L. Zhou, W. Zhang, M. K. Liu, Y. Z. Wu, and J. Qi, "Broadband Terahertz Generation via the Interface Inverse Rashba-Edelstein Effect" *Phys. Rev. Lett.* **121**, 086801 (2018).
[30] Y. Tserkovnyak, A. Brataas, and G. E. W. Bauer, "Enhanced gilbert damping in thin ferromagnetic films." *Phys. Rev. Lett.* **88**, 117601 (2002).
[31] M. Weiler, H. Huebl, F. S. Goerg, F. D. Czeschka, R. Gross, and S. T. B. Goennenwein, "Spin Pumping with Coherent Elastic Waves" *Phys. Rev. Lett.* **108**, 176601 (2012).
[32] K. Uchida, H. Adachi, T. An, H. Nakayama, M. Toda, B. Hillebrands, S. Maekawa, and E. Saitoh, "Acoustic spin pumping: Direct generation of spin currents from sound waves in Pt/Y 3 Fe 5 O 12 hybrid structures" *J. Appl. Phys.* **111**, 053903 (2012).
[33] J. Puebla, M. Xu, B. Rana, K. Yamamoto, S. Maekawa, and Y. Otani, "Acoustic ferromagnetic resonance and spin pumping induced by surface acoustic waves" *J. Phys. D. Appl. Phys.* **53**, 264002 (2020).
[34] M. I. Dyakonov and V. I. Perel, "Current-induced spin orientation of electrons in semiconductors" *Phys. Lett. A* **35**, 459 (1971).
[35] Y. A. . Bychkov and E. I. Rashba, "Properties of a 2D electron gas with lifted spectral degeneracy" *JETP Lett.* **39**, 78 (1984).
[36] J. C. Rojas Sánchez, L. Vila, G. Desfonds, S. Gambarelli, J. P. Attané, J. M. De Teresa, C. Magén, and A. Fert, "Spin-to-charge conversion using Rashba coupling at the interface between non-magnetic materials" *Nat. Commun.* **4**, 2944 (2013).
[37] J. Sinova, S. O. Valenzuela, J. Wunderlich, C. H. Back, and T. Jungwirth, "Spin Hall effects" *Rev. Mod. Phys.* **87**, 1213 (2015).
[38] A. Hoffmann, "Spin Hall Effects in Metals" *IEEE Trans. Magn.* **49**, 5172 (2013).
[39] Y. Niimi and Y. Otani, "Reciprocal spin Hall effects in conductors with strong spin-orbit coupling: a review" *Reports Prog. Phys.* **78**, 124501 (2015).
[40] J. Sinova, D. Culcer, Q. Niu, N. A. Sinitsyn, T. Jungwirth, and A. H. MacDonald, "Universal intrinsic spin Hall effect" *Phys. Rev. Lett.* **92**, 126603 (2004).
[41] Y. K. Kato, R. C. Myers, A. C. Gossard, and D. D. Awschalom, "Observation of the spin hall effect in semiconductors" *Science (80-.).* (2004).
[42] K. Ando, S. Takahashi, J. Ieda, H. Kurebayashi, T. Trypiniotis, C. H. W. Barnes, S. Maekawa, and E. Saitoh, "Electrically tunable spin injector free from the impedance mismatch problem" *Nat. Mater.* **10**, 655 (2011).
[43] K. Ando and E. Saitoh, "Observation of the inverse spin Hall effect in silicon" *Nat. Commun.* **3**, 629 (2012).
[44] M. Koike, E. Shikoh, Y. Ando, T. Shinjo, S. Yamada, K. Hamaya, and M. Shiraishi, "Dynamical spin injection into p-type germanium at room temperature" *Appl. Phys. Express* **6**, 9 (2013).
[45] J.-C. Rojas-Sánchez, M. Cubukcu, A. Jain, C. Vergnaud, C. Portemont, C. Ducruet, A. Barski, A. Marty, L. Vila, and J.-P. Attané, "Spin pumping and inverse spin Hall effect in germanium" *Phys. Rev. B* **88**, 064403 (2013).
[46] A. Jain, J. C. Rojas-Sanchez, M. Cubukcu, J. Peiro, J. C. Le Breton, E. Prestat, C. Vergnaud, L. Louahadj, C. Portemont, C. Ducruet, V. Baltz, A. Barski, P. Bayle-Guillemaud, L. Vila, J. P. Attané, E. Augendre, G. Desfonds, S. Gambarelli, H. Jaffrès, J. M. George, and M. Jamet, "Crossover from spin accumulation into interface states to spin injection in the germanium conduction band" *Phys. Rev. Lett.* **109**, 1 (2012).
[47] A. Jain, J. C. Rojas-Sanchez, M. Cubukcu, J. Peiro, J. C. Le Breton, C. Vergnaud, E. Augendre, L. Vila, J. P. Attané, S. Gambarelli, H. Jaffrès, J. M. George, and M. Jamet,

"Transition from spin accumulation into interface states to spin injection in silicon and germanium conduction bands" *Eur. Phys. J. B* **86**, (2013).
[48] S. O. Valenzuela and M. Tinkham, "Direct electronic measurement of the spin Hall effect." *Nature* **442**, 176 (2006).
[49] L. Vila, T. Kimura, and Y. Otani, "Evolution of the Spin hall effect in Pt nanowires: Size and temperature effects" *Phys. Rev. Lett.* **99**, 1 (2007).
[50] K. Ando, S. Takahashi, J. Ieda, Y. Kajiwara, H. Nakayama, T. Yoshino, K. Harii, Y. Fujikawa, M. Matsuo, S. Maekawa, and E. Saitoh, "Inverse spin-Hall effect induced by spin pumping in metallic system" *J. Appl. Phys.* **109**, 103913 (2011).
[51] O. Mosendz, V. Vlaminck, J. E. Pearson, F. Y. Fradin, G. E. W. Bauer, S. D. Bader, and A. Hoffmann, "Detection and quantification of inverse spin Hall effect from spin pumping in permalloy/normal metal bilayers" *Phys. Rev. B* **82**, 214403 (2010).
[52] A. Azevedo, L. H. Vilela-Leão, R. L. Rodríguez-Suárez, A. F. Lacerda Santos, and S. M. Rezende, "Spin pumping and anisotropic magnetoresistance voltages in magnetic bilayers: Theory and experiment" *Phys. Rev. B - Condens. Matter Mater. Phys.* **83**, 1 (2011).
[53] K. Ando and E. Saitoh, "Inverse spin-Hall effect in palladium at room temperature" *J. Appl. Phys.* **108**, 113925 (2010).
[54] P. Gambardella and I. M. Miron, "Current-induced spin–orbit torques" *Phil. Trans. R. Soc. A* **369**, 3175 (2011).
[55] I. M. Miron, K. Garello, G. Gaudin, P.-J. Zermatten, M. V Costache, S. Auffret, S. Bandiera, B. Rodmacq, A. Schuhl, and P. Gambardella, "Perpendicular switching of a single ferromagnetic layer induced by in-plane current injection." *Nature* **476**, 189 (2011).
[56] L. Liu, O. J. Lee, T. J. Gudmundsen, D. C. Ralph, and R. a. Buhrman, "Current-induced switching of perpendicularly magnetized magnetic layers using spin torque from the spin hall effect" *Phys. Rev. Lett.* **109**, 096602 (2012).
[57] J. C. Rojas-Sánchez, N. Reyren, P. Laczkowski, W. Savero, J. P. Attané, C. Deranlot, M. Jamet, J. M. George, L. Vila, and H. Jaffrès, "Spin pumping and inverse spin hall effect in platinum and other 5d metals: The essential role of spin-memory loss and spin-current discontinuities at interfaces" *SPIE Proceding* (2014).
[58] V. Vlaminck, J. E. Pearson, S. D. Bader, and A. Hoffmann, "Dependence of spin pumping spin Hall effect measurements on layer thicknesses and stacking order" (2013).
[59] L. Liu, C.-F. Pai, Y. Li, H. W. Tseng, D. C. Ralph, and R. A. Buhrman, "Spin-Torque Switching with the Giant Spin Hall Effect of Tantalum" *Science* **336**, 555 (2012).
[60] C. Hahn, G. de Loubens, O. Klein, M. Viret, V. V Naletov, and J. Ben Youssef, "Comparative measurements of inverse spin Hall effects and magnetoresistance in YIG/Pt and YIG/Ta" *Phys. Rev. B* **87**, 174417 (2013).
[61] J. E. Gomez, B. Zerai Tedlla, N. R. Alvarez, G. Alejandro, E. Goovaerts, and A. Butera, "Spin transport parameters in Ni80Fe20/Ru and Ni80Fe20/Ta bilayers" *Phys. Rev. B* **90**, 184401 (2014).
[62] C.-F. Pai, L. Liu, Y. Li, H. W. Tseng, D. C. Ralph, and R. A. Buhrman, "Spin transfer torque devices utilizing the giant spin Hall effect of tungsten" *Appl. Phys. Lett.* **101**, 122404 (2012).
[63] Q. Hao, W. Chen, and G. Xiao, "Beta (b) tungsten thin films: Structure, electron transport, and giant spin Hall effect" *Appl. Phys. Lett.* **106**, 182403 (2015).
[64] K.-U. Demasius, T. Phung, W. Zhang, B. P. Hughes, S.-H. Yang, A. Kellock, W. Han,

A. Pushp, and S. S. P. Parkin, “Enhanced spin orbit torques by oxygen incorporation in tungsten films” *Nat. Commun.* **7**, 10644 (2015).
[65] J. Torrejon, J. Kim, J. Sinha, S. Mitani, M. Hayashi, M. Yamanouchi, and H. Ohno, “Interface control of the magnetic chirality in CoFeB/MgO heterostructures with heavy-metal underlayers.” *Nat. Commun.* **5**, 4655 (2014).
[66] Y. Lau and M. Hayashi, “Spin torque efficiency of Ta , W , and Pt in metallic bilayers evaluated by harmonic Hall and spin Hall magnetoresistance measurements” (2017).
[67] A. Fert, A. Friederich, and A. Hamzic, “Hall effect in dilute magnetic alloys” *J. Magn. Magn. Mater.* **24**, 231 (1981).
[68] A. Fert and P. M. Levy, “Spin hall effect induced by resonant scattering on impurities in metals” *Phys. Rev. Lett.* **106**, 1 (2011).
[69] M. Gradhand, D. V. Fedorov, P. Zahn, and I. Mertig, “Spin Hall angle versus spin diffusion length: Tailored by impurities” *Phys. Rev. B - Condens. Matter Mater. Phys.* **81**, 1 (2010).
[70] Y. Niimi, M. Morota, D. H. Wei, C. Deranlot, M. Basletic, A. Hamzic, A. Fert, and Y. Otani, “Extrinsic spin Hall effect induced by iridium impurities in copper” *Phys. Rev. Lett.* **106**, 1 (2011).
[71] Y. Niimi, Y. Kawanishi, D. H. Wei, C. Deranlot, H. X. Yang, M. Chshiev, T. Valet, A. Fert, and Y. Otani, “Giant spin hall effect induced by skew scattering from bismuth impurities inside thin film CuBi alloys” *Phys. Rev. Lett.* **109**, 1 (2012).
[72] Y. Niimi, H. Suzuki, Y. Kawanishi, Y. Omori, T. Valet, A. Fert, and Y. Otani, “Extrinsic spin Hall effects measured with lateral spin valve structures” *Phys. Rev. B - Condens. Matter Mater. Phys.* **89**, 1 (2014).
[73] P. Laczkowski, J. C. Rojas-Sánchez, W. Savero-Torres, H. Jaffrès, N. Reyren, C. Deranlot, L. Notin, C. Beigné, A. Marty, J. P. Attané, L. Vila, J. M. George, and A. Fert, “Experimental evidences of a large extrinsic spin Hall effect in AuW alloy” *Appl. Phys. Lett.* **104**, (2014).
[74] P. Laczkowski, H. Jaffrès, Y. Fu, N. Reyren, L. Notin, C. Beigné, J. Attané, L. Vila, J. George, and A. Marty, “Evaluation of the spin diffusion length of AuW alloy by spin absorption experiments in the limit of large spin-orbit interactions” 1 (2015).
[75] P. Laczkowski, Y. Fu, H. Yang, J.-C. Rojas-Sánchez, P. Noel, V. T. Pham, G. Zahnd, C. Deranlot, S. Collin, C. Bouard, P. Warin, V. Maurel, M. Chshiev, A. Marty, J.-P. Attané, A. Fert, H. Jaffrès, L. Vila, and J.-M. George, “Large enhancement of the spin Hall effect in Au by side-jump scattering on Ta impurities” *Phys. Rev. B* **96**, 140405(R) (2017).
[76] M. Gradhand, D. V. Fedorov, P. Zahn, and I. Mertig, “Extrinsic Spin Hall Effect from First Principles” *Phys. Rev. Lett.* **104**, 186403 (2010).
[77] N. Nagaosa, J. Sinova, S. Onoda, A. H. MacDonald, and N. P. Ong, “Anomalous Hall effect” *Rev. Mod. Phys.* **82**, 1539 (2010).
[78] J. Inoue and H. Ohno, “Taking the Hall effect for a spin” *Science (80-.).* (2005).
[79] J. Bass, W. P. Jr, W. P. P. Jr., W. P. Pratt, P. J. W. P. Bass J., W. P. P. Jr., and W. P. Pratt, “Spin-diffusion lengths in metals and alloys, and spin-flipping at metal/metal interfaces: an experimentalist’s critical review” *J. Phys. Condens. Matter* **19**, 183201 (2007).
[80] Y. Liu, Z. Yuan, R. J. H. Wesselink, A. A. Starikov, and P. J. Kelly, “Interface enhancement of gilbert damping from first principles” *Phys. Rev. Lett.* **113**, 207202 (2014).
[81] L. Wang, R. J. H. Wesselink, Y. Liu, Z. Yuan, K. Xia, and P. J. Kelly, “Giant Room

Temperature Interface Spin Hall and Inverse Spin Hall Effects" *Phys. Rev. Lett.* **116**, 196602 (2016).
[82] T. Okuda and A. Kimura, "Spin- and angle-resolved photoemission of strongly spin-orbit coupled systems" *J. Phys. Soc. Japan* **82**, 1 (2013).
[83] M. Z. Hasan and C. L. Kane, "*Colloquium* : Topological insulators" *Rev. Mod. Phys.* **82**, 3045 (2010).
[84] Y. Ando, "Topological Insulator Materials" *J. Phys. Soc. Japan* **82**, 1 (2013).
[85] A. Bansil, H. Lin, and T. Das, "*Colloquium* : Topological band theory" *Rev. Mod. Phys.* **88**, 021004 (2016).
[86] V. M. Edelstein, "Spin polarization of conduction electrons induced by electric current in two-dimensional asymmetric electron systems" *Solid State Commun.* **73**, 233 (1990).
[87] E. Ivchenko and G. Pikus, "New photogalvanic effect in gyrotropic crystals" *Sov. J. Exp. Theor. Phys. Lett.* (1978).
[88] A. Aronov and Y. Lyanda-Geller, "Nuclear electric resonance and orientation of carrier spins by an electric field" *Sov. J. Exp. Theor. Phys. Lett.* (1989).
[89] Y. V. N. L.S. Levitov, G.M. Eliashberg, "Magnetoelectric effects in conductors with mirror isomer symmetry" *Sov. Phys. JETP* (1985).
[90] K. Kondou, R. Yoshimi, A. Tsukazaki, Y. Fukuma, J. Matsuno, K. S. Takahashi, M. Kawasaki, Y. Tokura, and Y. Otani, "Fermi level dependent charge-to-spin current conversion by Dirac surface state of topological insulators" *Nat. Phys.* **1510**, 1510.03572 (2016).
[91] J. C. Rojas-Sánchez, S. Oyarzún, Y. Fu, A. Marty, C. Vergnaud, S. Gambarelli, L. Vila, M. Jamet, Y. Ohtsubo, A. Taleb-Ibrahimi, P. Le Fèvre, F. Bertran, N. Reyren, J. M. George, and A. Fert, "Spin to Charge Conversion at Room Temperature by Spin Pumping into a New Type of Topological Insulator: α -Sn Films" *Phys. Rev. Lett.* **116**, 096602 (2016).
[92] K. Shen, G. Vignale, and R. Raimondi, "Microscopic theory of the inverse Edelstein effect" *Phys. Rev. Lett.* **112**, 1 (2014).
[93] A. Manchon, J. Železný, I. M. Miron, T. Jungwirth, J. Sinova, A. Thiaville, K. Garello, and P. Gambardella, "Current-induced spin-orbit torques in ferromagnetic and antiferromagnetic systems" *Rev. Mod. Phys.* **91**, 035004 (2019).
[94] T. Jungwirth, J. Wunderlich, and K. Olejník, "Spin Hall effect devices" *Nat. Mater.* **11**, 382 (2012).
[95] M. Johnson and R. H. Silsbee, "Interfacial charge-spin coupling: Injection and detection of spin magnetization in metals" *Phys. Rev. Lett.* **55**, 1790 (1985).
[96] S. Takahashi and S. Maekawa, "Spin injection and transport in magnetic nanostructures" *Phys. C Supercond. Its Appl.* **437**–**438**, 309 (2006).
[97] F. J. Jedema, a T. Filip, and B. J. van Wees, "Electrical spin injection and accumulation at room temperature in an all-metal mesoscopic spin valve" *Nature* **410**, 345 (2001).
[98] F. J. Jedema, M. V. Costache, H. B. Heersche, J. J. A. Baselmans, and B. J. Van Wees, "Electrical detection of spin accumulation and spin precession at room temperature in metallic spin valves" *Appl. Phys. Lett.* **81**, 5162 (2002).
[99] F. J. Jedema, M. S. Nijboer, A. T. Filip, and B. J. van Wees, "Spin injection and spin accumulation in all-metal mesoscopic spin valves" *Phys. Rev. B - Condens. Matter Mater. Phys.* **67**, (2003).
[100] P. Łączkowski, L. Vila, S. Ferry, A. Marty, J. M. George, H. Jaffrès, A. Fert, T. Kimura, T. Yang, Y. Otani, and J. P. Attané, "Spin signal in metallic lateral spin valves

made by a multiple angle evaporation technique" *Appl. Phys. Express* **4**, 3 (2011).
[101] F. Casanova, A. Sharoni, M. Erekhinsky, and I. K. Schuller, "Control of spin injection by direct current in lateral spin valves" *Phys. Rev. B* **79**, 184415 (2009).
[102] M. Erekhinsky, A. Sharoni, F. Casanova, and I. K. Schuller, "Surface enhanced spin-flip scattering in lateral spin valves" *Appl. Phys. Lett.* **96**, 10 (2010).
[103] S. O. Valenzuela, "Nonlocal Electronic Spin Detection, Spin Accumulation and the Spin Hall Effect" *Int. J. Mod. Phys. B Condens. Matter Physics; Stat. Physics; Appl. Phys.* **23**, 2413 (2009).
[104] P. Laczkowski, H. Jaffrès, W. Savero-Torres, J. C. Rojas-Sánchez, Y. Fu, N. Reyren, C. Deranlot, L. Notin, C. Beigné, J. P. Attané, L. Vila, J. M. George, and A. Marty, "Evaluation of spin diffusion length of AuW alloys using spin absorption experiments in the limit of large spin-orbit interactions" *Phys. Rev. B - Condens. Matter Mater. Phys.* **92**, 1 (2015).
[105] P. Laczkowski, Y. Fu, H. Yang, J.-C. Rojas-Sánchez, P. Noel, V. T. Pham, G. Zahnd, C. Deranlot, S. Collin, C. Bouard, P. Warin, V. Maurel, M. Chshiev, A. Marty, J.-P. Attané, A. Fert, H. Jaffrès, L. Vila, and J.-M. George, "Large enhancement of the spin Hall effect in Au by scattering with side-jump on Ta impurities" 0 (2017).
[106] J. C. Rojas Sánchez, P. Laczkowski, W. F. Savero Torres, M. Cubukcu, V. D. Nguyen, L. Notin, C. Beigné, C. Vergnaud, A. Marty, M. Jamet, L. Vila, and J. P. Attané, "In-plane and out-of-plane spin precession in lateral spin-valves" *Appl. Phys. Lett.* **102**, (2013).
[107] S. O. Valenzuela and M. Tinkham, "Spin-polarized tunneling in room-temperature mesoscopic spin valves" *Appl. Phys. Lett.* **85**, 5914 (2004).
[108] W. Savero Torres, P. Laczkowski, V. D. Nguyen, J. C. Rojas Sánchez, L. Vila, A. Marty, M. Jamet, and J. P. Attané, "Switchable spin-current source controlled by magnetic domain walls" *Nano Lett.* **14**, 4016 (2014).
[109] L. LANDAU and E. LIFSHITZ, in *Perspect. Theor. Phys.* (1992), pp. 51–65.
[110] T. GILBERT, "A Lagrangian Formulation of the Gyromagnetic Equation of the Magnetization Field" *Phys. Rev.* **100**, 1243 (1955).
[111] B. Heinrich, R. Urban, and G. Woltersdorf, "Magnetic relaxation in metallic films: Single and multilayer structures" *J. Appl. Phys.* **91**, 7523 (2002).
[112] B. Heinrich, J. F. Cochran, and K. Myrtle, "The exchange splitting of phonon assisted microwave transmission at 9.5 GHz" *J. Appl. Phys.* **53**, 2092 (1982).
[113] B. Heinrich and Z. Frait, "Temperature Dependence of the FMR Linewidth of Iron Single-Crystal Platelets" *Phys. Status Solidi* **16**, K11 (1966).
[114] B. Heinrich, D. Fraitová, and V. Kamberský, "The Influence of s-d Exchange on Relaxation of Magnons in Metals" *Phys. Status Solidi* **23**, 501 (1967).
[115] S. Ingvarsson, L. Ritchie, X. Y. Liu, G. Xiao, J. C. Slonczewski, P. L. Trouilloud, and R. H. Koch, "Role of electron scattering in the magnetization relaxation of thin (formula presented) films" *Phys. Rev. B - Condens. Matter Mater. Phys.* (2002).
[116] S. Mankovsky, D. Ködderitzsch, G. Woltersdorf, and H. Ebert, "First-principles calculation of the Gilbert damping parameter via the linear response formalism with application to magnetic transition metals and alloys" *Phys. Rev. B* **87**, 014430 (2013).
[117] M. A. W. Schoen, D. Thonig, M. L. Schneider, T. J. Silva, H. T. Nembach, O. Eriksson, O. Karis, and J. M. Shaw, "Ultra-low magnetic damping of a metallic ferromagnet" *Nat. Phys.* **12**, 839 (2016).
[118] C. Guillemard, S. Petit-Watelot, L. Pasquier, D. Pierre, J. Ghanbaja, J.-C. Rojas-Sánchez, A. Bataille, J. Rault, P. Le Fèvre, F. Bertran, and S. Andrieu, "Ultralow

Magnetic Damping in Co 2 Mn-Based Heusler Compounds : Promising Materials for Spintronics" *Phys. Rev. Appl.* **11**, 064009 (2019).
[119] C. Guillemard, S. Petit-Watelot, J. C. Rojas-Sánchez, J. Hohlfeld, J. Ghanbaja, A. Bataille, P. Le Fèvre, F. Bertran, and S. Andrieu, "Polycrystalline Co2Mn-based Heusler thin films with high spin polarization and low magnetic damping" *Appl. Phys. Lett.* (2019).
[120] J. Smit and H. G. Beljers, "Ferromagnetic Resonance Absoprtion in BaFe12O19, a highly anisotropic crystal" *Philips Res. Rep.* **10**, 113 (1955).
[121] Y. Tserkovnyak, A. Brataas, and G. E. W. Bauer, "Spin pumping and magnetization dynamics in metallic multilayers" *Phys. Rev. B* **66**, 224403 (2002).
[122] R. H. Silsbee, a. Janossy, and P. Monod, "Coupling between ferromagnetic and conduction-spin-resonance modes at a ferromagnetic-normal-metal interface" *Phys. Rev. B* **19**, 4382 (1979).
[123] B. Heinrich, K. B. Urquhart, A. S. Arrott, J. F. Cochran, K. Myrtle, and S. T. Purcell, "Ferromagnetic-resonance study of ultrathin bcc Fe(100) films grown epitaxially on fcc Ag(100) substrates" *Phys. Rev. Lett.* **59**, 1756 (1987).
[124] S. Mizukami, Y. Ando, and T. Miyazaki, "Ferromagnetic resonance linewidth for NM/80NiFe/NM films (NM=Cu, Ta, Pd and Pt)" *J. Magn. Magn. Mater.* **226–230**, 1640 (2001).
[125] S. Mizukami, Y. Ando, and T. Miyazaki, "The Study on Ferromagnetic Resonance Linewidth for NM/80NiFe/NM (NM = Cu, Ta, Pd and Pt) Films" *Jpn. J. Appl. Phys.* **40**, 580 (2001).
[126] S. Mizukami, Y. Ando, and T. Miyazaki, "Effect of spin diffusion on Gilbert damping for a very thin permalloy layer in Cu/permalloy/Cu/Pt films" *Phys. Rev. B* **66**, 104413 (2002).
[127] K. Ando, T. Yoshino, and E. Saitoh, "Optimum condition for spin-current generation from magnetization precession in thin film systems" *Appl. Phys. Lett.* **94**, 2013 (2009).
[128] K. Ando and E. Saitoh, "Inverse spin-Hall effect in palladium at room temperature" *J. Appl. Phys.* **108**, 113925 (2010).
[129] Y. Tserkovnyak, A. Brataas, G. E. W. Bauer, and B. I. Halperin, "Nonlocal magnetization dynamics in ferromagnetic heterostructures" *Rev. Mod. Phys.* **77**, 1375 (2005).
[130] A. Azevedo, L. H. Vilela Leão, R. L. Rodriguez-Suarez, A. B. Oliveira, and S. M. Rezende, "Dc effect in ferromagnetic resonance: Evidence of the spin-pumping effect?" *J. Appl. Phys.* **97**, 1 (2005).
[131] E. Saitoh, M. Ueda, H. Miyajima, and G. Tatara, "Conversion of spin current into charge current at room temperature: Inverse spin-Hall effect" *Appl. Phys. Lett.* **88**, 182509 (2006).
[132] M. Harder, Y. Gui, and C.-M. Hu, "Electrical Detection of Magnetization Dynamics via Spin Rectification Eff ects" *Phys. Rep.* (2016).
[133] K. Gupta, R. J. H. Wesselink, R. Liu, Z. Yuan, and P. J. Kelly, "Disorder Dependence of Interface Spin Memory Loss" *Phys. Rev. Lett.* **124**, 87702 (2020).
[134] K. Eid, D. Portner, J. A. Borchers, R. Loloee, M. Al-Haj Darwish, M. Tsoi, R. D. Slater, K. V. O'Donovan, H. Kurt, W. P. Pratt, and J. Bass, "Absence of mean-free-path effects in the current-perpendicular-to-plane magnetoresistance of magnetic multilayers" *Phys. Rev. B - Condens. Matter Mater. Phys.* **65**, 054424 (2002).
[135] H. Kurt, R. Loloee, K. Eid, W. P. Pratt, and J. Bass, "Spin-memory loss at 4.2 K in sputtered Pd and Pt and at Pd/Cu and Pt/Cu interfaces" *Appl. Phys. Lett.* **81**, 4787

(2003).
[136] H. Y. T. Nguyen, W. P. Pratt, and J. Bass, “Spin-flipping in Pt and at Co/Pt interfaces” *J. Magn. Magn. Mater.* **361**, 30 (2014).
[137] W. Zhang, W. Han, X. Jiang, S.-H. Yang, and S. S. P. Parkin, “Role of transparency of platinum–ferromagnet interfaces in determining the intrinsic magnitude of the spin Hall effect” *Nat. Phys.* **11**, 496 (2015).
[138] X. Tao, Q. Liu, B. Miao, R. Yu, Z. Feng, L. Sun, B. You, J. Du, K. Chen, S. Zhang, L. Zhang, Z. Yuan, D. Wu, and H. Ding, “Self-consistent determination of spin hall angle and spin diffusion length in pt and pd: The role of the interface spin loss” *Sci. Adv.* (2018).
[139] Z. Feng, J. Hu, L. Sun, B. You, D. Wu, J. Du, W. Zhang, A. Hu, Y. Yang, D. M. Tang, B. S. Zhang, and H. F. Ding, “Spin Hall angle quantification from spin pumping and microwave photoresistance” *Phys. Rev. B* **85**, 214423 (2012).
[140] K. Chen and S. Zhang, “Spin Pumping in the Presence of Spin-Orbit Coupling” *Phys. Rev. Lett.* **114**, 126602 (2015).
[141] T. Nan, S. Emori, C. T. Boone, X. Wang, T. M. Oxholm, J. G. Jones, B. M. Howe, G. J. Brown, N. X. Sun, and A. Samples, “Comparison of spin-orbit torques and spin pumping across NiFe / Pt and NiFe / Cu / Pt interfaces” **214416**, 1 (2015).
[142] H. Nakayama, K. Ando, K. Harii, T. Yoshino, R. Takahashi, Y. Kajiwara, K. Uchida, Y. Fujikawa, and E. Saitoh, “Geometry dependence on inverse spin Hall effect induced by spin pumping in Ni81Fe19/Pt films” *Phys. Rev. B* **85**, 144408 (2012).
[143] Y. Niimi, Y. Kawanishi, D. H. Wei, C. Deranlot, H. X. Yang, M. Chshiev, T. Valet, A. Fert, and Y. Otani, “Giant spin hall effect induced by skew scattering from bismuth impurities inside thin film CuBi alloys” *Phys. Rev. Lett.* **109**, 1 (2012).
[144] M. Obstbaum, M. Decker, A. K. Greitner, M. Haertinger, T. N. G. Meier, M. Kronseder, K. Chadova, S. Wimmer, D. Ködderitzsch, H. Ebert, and C. H. Back, “Tuning Spin Hall Angles by Alloying” **167204**, 1 (2016).
[145] E. I. Rashba, “Theory of electrical spin injection: Tunnel contacts as a solution of the conductivity mismatch problem” *Phys. Rev. B* **62**, R16267 (2000).
[146] G. Schmidt, D. Ferrand, L. Molenkamp, A. Filip, and B. van Wees, “Fundamental obstacle for electrical spin injection from a ferromagnetic metal into a diffusive semiconductor” *Phys. Rev. B - Condens. Matter Mater. Phys.* R4790(R) (2000).
[147] A. Fert and H. Jaffrès, “Conditions for efficient spin injection from a ferromagnetic metal into a semiconductor” *Phys. Rev. B - Condens. Matter Mater. Phys.* **64**, 184420 (2001).
[148] M. Kanoun, R. Benabderrahmane, C. Duluard, C. Baraduc, N. Bruyant, A. Bsiesy, and H. Achard, “Electrical study of ferromagnet-oxide-semiconductor diode for a magnetic memory device integrated on silicon” *Appl. Phys. Lett.* **90**, 192508 (2007).
[149] M. Tran, H. Jaffrès, C. Deranlot, J. M. George, A. Fert, A. Miard, and A. Lemaître, “Enhancement of the spin accumulation at the interface between a spin-polarized tunnel junction and a semiconductor” *Phys. Rev. Lett.* **102**, 036601 (2009).
[150] S. P. Dash, S. Sharma, J. C. Le Breton, J. Peiro, H. Jaffrès, J. M. George, A. Lemaître, and R. Jansen, “Spin precession and inverted Hanle effect in a semiconductor near a finite-roughness ferromagnetic interface” *Phys. Rev. B - Condens. Matter Mater. Phys.* **84**, 054410 (2011).
[151] B. T. Jonker, G. Kioseoglou, A. T. Hanbicki, C. H. Li, and P. E. Thompson, “Electrical spin-injection into silicon from a ferromagnetic metal/tunnel barrier contact” *Nat. Phys.* **3**, 542 (2007).

[152] I. Appelbaum, B. Huang, and D. J. Monsma, “Electronic measurement and control of spin transport in silicon” *Nature* **447**, 295 (2007).
[153] Y. Zhou, W. Han, L. Te Chang, F. Xiu, M. Wang, M. Oehme, I. A. Fischer, J. Schulze, R. K. Kawakami, and K. L. Wang, “Electrical spin injection and transport in germanium” *Phys. Rev. B - Condens. Matter Mater. Phys.* **84**, 125323 (2011).
[154] K. Ando, S. Takahashi, J. Ieda, H. Kurebayashi, T. Trypiniotis, C. H. W. Barnes, S. Maekawa, and E. Saitoh, “Electrically tunable spin injector free from the impedance mismatch problem” *Nat. Mater.* **10**, 655 (2011).
[155] K. Ando and E. Saitoh, “Observation of the inverse spin Hall effect in silicon” *Nat. Commun.* **3**, 629 (2012).
[156] J.-C. Rojas-Sánchez, M. Cubukcu, A. Jain, C. Vergnaud, C. Portemont, C. Ducruet, A. Barski, A. Marty, L. Vila, J. P. Attané, E. Augendre, G. Desfonds, S. Gambarelli, H. Jaffrès, J. M. George, and M. Jamet, “Spin pumping and inverse spin Hall effect in germanium” *Phys. Rev. B* **88**, 064403 (2013).
[157] S. P. Dash, S. Sharma, R. S. Patel, M. P. De Jong, and R. Jansen, “Electrical creation of spin polarization in silicon at room temperature” *Nature* **462**, 491 (2009).
[158] R. Iguchi, K. Ando, R. Takahashi, T. An, E. Saitoh, and T. Sato, “Spin Pumping without Three-Magnon Splitting in Polycrystalline Bi1Y2Fe5O12/Pt Bilayer Structure” *Jpn. J. Appl. Phys.* **51**, 1 (2012).
[159] N. Mecking, Y. S. Gui, and C. M. Hu, “Microwave photovoltage and photoresistance effects in ferromagnetic microstrips” *Phys. Rev. B - Condens. Matter Mater. Phys.* **76**, 1 (2007).
[160] S. Gupta, R. Medwal, D. Kodama, K. Kondou, Y. Otani, and Y. Fukuma, “Important role of magnetization precession angle measurement in inverse spin Hall effect induced by spin pumping” *Appl. Phys. Lett.* **110**, 022404 (2017).
[161] S. M. Rezende, R. L. Rodr, R. O. Cunha, A. R. Rodrigues, F. L. A. Machado, G. A. F. Guerra, J. C. L. Ortiz, and A. Azevedo, “Magnon spin-current theory for the longitudinal spin-Seebeck effect” *Phys. Rev. B* **89**, 014416 (2014).
[162] G. E. W. Bauer, A. H. MacDonald, and S. Maekawa, “‘Spin Caloritronics’” *Solid State Commun.* **150**, 459 (2010).
[163] K. ichi Uchida, H. Adachi, T. Kikkawa, A. Kirihara, M. Ishida, S. Yorozu, S. Maekawa, and E. Saitoh, “Thermoelectric Generation Based on Spin Seebeck Effects” *Proc. IEEE* **104**, 1946 (2016).
[164] S. Meyer, Y. Chen, S. Wimmer, M. Althammer, T. Wimmer, R. Schlitz, S. Geprägs, H. Huebl, D. Ködderitzsch, H. Ebert, G. E. W. Bauer, R. Gross, and S. T. B. Goennenwein, “Observation of the spin Nernst e ect” *Nat. Mater.* **16**, 977 (2017).
[165] P. Sheng, Y. Sakuraba, Y. Lau, S. Takahashi, S. Mitani, and M. Hayashi, “The spin Nernst effect in tungsten” *Sci. Adv.* **3**, e1701503 (2017).
[166] G. Vignale and I. V. Tokatly, “Theory of the nonlinear Rashba-Edelstein effect” 1 (2015).
[167] S. Zhang and A. Fert, “Conversion between spin and charge currents with topological insulators” *Phys. Rev. B* **94**, 184423 (2016).
[168] E. Lesne, Y. Fu, S. Oyarzun, J. C. Rojas-Sánchez, D. C. Vaz, H. Naganuma, G. Sicoli, J.-P. Attané, M. Jamet, E. Jacquet, J.-M. George, A. Barthélémy, H. Jaffrès, A. Fert, M. Bibes, and L. Vila, “Highly efficient and tunable spin-to-charge conversion through Rashba coupling at oxide interfaces” *Nat. Mater.* **15**, 1261 (2016).
[169] S. Oyarzún, A. K. Nandy, F. Rortais, J.-C. Rojas-Sánchez, M. T. Dau, and P. Noël, “Evidence for spin-to-charge conversion by Rashba coupling in metallic states at the

Fe/Ge(111) interface" *Nat. Commun.* **7**, 13857 (2016).
[170] C. Rinaldi, J. C. Rojas-Sánchez, R. N. Wang, Y. Fu, S. Oyarzun, L. Vila, S. Bertoli, M. Asa, L. Baldrati, M. Cantoni, J. M. George, R. Calarco, A. Fert, and R. Bertacco, "Evidence for spin to charge conversion in GeTe(111)" *APL Mater.* **4**, (2016).
[171] C. R. Ast, J. Henk, A. Ernst, L. Moreschini, M. C. Falub, D. Pacilé, P. Bruno, K. Kern, and M. Grioni, "Giant Spin Splitting through Surface Alloying" *Phys. Rev. Lett.* **98**, 186807 (2007).
[172] Y. M. Koroteev, G. Bihlmayer, J. E. Gayone, E. V. Chulkov, S. Bl??gel, P. M. Echenique, and P. Hofmann, "Strong spin-orbit splitting on Bi surfaces" *Phys. Rev. Lett.* **93**, 046403 (2004).
[173] D. Hou, Z. Qiu, K. Harii, Y. Kajiwara, K. Uchida, Y. Fujikawa, H. Nakayama, T. Yoshino, T. An, K. Ando, X. Jin, and E. Saitoh, "Interface induced inverse spin Hall effect in bismuth/permalloy bilayer" *Appl. Phys. Lett.* **101**, (2012).
[174] S. D. Ganichev, E. L. Ivchenko, V. V. Bel'kov, S. A. Tarasenko, M. Sollinger, D. Weiss, W. Wegscheider, and W. Prettl, "Spin-galvanic effect" *Nature* **417**, 153 (2002).
[175] W. Zhang, M. B. Jungfleisch, W. Jiang, J. E. Pearson, and A. Hoffmann, "Spin pumping and inverse Rashba-Edelstein effect in NiFe/Ag/Bi and NiFe/Ag/Sb" *J. Appl. Phys.* **117**, 17C727 (2015).
[176] H. Bentmann, T. Kuzumaki, G. Bihlmayer, S. Blügel, E. V. Chulkov, F. Reinert, and K. Sakamoto, "Spin orientation and sign of the Rashba splitting in Bi/Cu(111)" *Phys. Rev. B* **84**, 115426 (2011).
[177] S. Karube, K. Kondou, and Y. C. Otani, "Experimental observation of spin-to-charge current conversion at non-magnetic metal/Bi2O3 interfaces" *Appl. Phys. Express* **9**, (2016).
[178] H. J. Zhang, S. Yamamoto, B. Gu, H. Li, M. Maekawa, Y. Fukaya, and a. Kawasuso, "Charge-to-Spin Conversion and Spin Diffusion in Bi/Ag Bilayers Observed by Spin-Polarized Positron Beam" *Phys. Rev. Lett.* **114**, 1 (2015).
[179] S. Sangiao, J. M. De Teresa, L. Morellon, I. Lucas, M. C. Martinez-Velarte, and M. Viret, "Control of the spin to charge conversion using the inverse Rashba-Edelstein effect" *Appl. Phys. Lett.* **106**, 172403 (2015).
[180] A. Ohtomo and H. Y. Hwang, "A high-mobility electron gas at the LAO/STO heterointerface." *Nature* **427**, 423 (2004).
[181] A. F. Santander-Syro, O. Copie, T. Kondo, F. Fortuna, S. Pailhès, R. Weht, X. G. Qiu, F. Bertran, A. Nicolaou, A. Taleb-Ibrahimi, P. Le Fèvre, G. Herranz, M. Bibes, N. Reyren, Y. Apertet, P. Lecoeur, A. Barthélémy, and M. J. Rozenberg, "Two-dimensional electron gas with universal subbands at the surface of SrTiO(3)." *Nature* **469**, 189 (2011).
[182] M. Basletic, J. L. Maurice, C. Carrétéro, G. Herranz, O. Copie, M. Bibes, É. Jacquet, K. Bouzehouane, S. Fusil, and A. Barthélémy, "Mapping the spatial distribution of charge carriers in LaAlO 3/SrTiO3 heterostructures" *Nat. Mater.* (2008).
[183] O. Copie, V. Garcia, C. Bödefeld, C. Carrétéro, M. Bibes, G. Herranz, E. Jacquet, J. L. Maurice, B. Vinter, S. Fusil, K. Bouzehouane, H. Jaffrès, and A. Barthélémy, "Towards two-dimensional metallic behavior at LaAlO3/SrTiO3 interfaces" *Phys. Rev. Lett.* (2009).
[184] E. Lesne, N. Reyren, D. Doennig, R. Mattana, H. Jaffrès, V. Cros, F. Petroff, F. Choueikani, P. Ohresser, R. Pentcheva, A. Barthélémy, and M. Bibes, "Suppression of the critical thickness threshold for conductivity at the LaAlO3 /SrTiO3 interface" *Nat. Commun.* (2014).

[185] N. Reyren, M. Bibes, E. Lesne, J.-M. George, C. Deranlot, S. Collin, A. Barthélémy, and H. Jaffrès, "Gate-Controlled Spin Injection at LaAlO3/SrTiO3 Interfaces" *Phys. Rev. Lett.* **108**, 186802 (2012).
[186] Q. Song, H. Zhang, T. Su, W. Yuan, Y. Chen, W. Xing, J. Shi, J. R. Sun, and W. Han, "Observation of Inverse Edelstein Effect in Rashba-Split 2DEG between SrTiO3 and LaAlO3 at Room Temperature" *Sci. Adv.* **3**, e1602312 (2017).
[187] Y. Wang, R. Ramaswamy, M. Motapothula, K. Narayanapillai, D. Zhu, J. Yu, T. Venkatesan, and H. Yang, "Room-Temperature Giant Charge-to-Spin Conversion at the SrTiO3 − LaAlO3 Oxide Interface" *Nano Lett.* **17**, 7659 (2017).
[188] J. Y. Chauleau, M. Boselli, S. Gariglio, R. Weil, G. De Loubens, J. M. Triscone, and M. Viret, "Efficient spin-to-charge conversion in the 2D electron liquid at the LAO/STO interface" *EPL* (2016).
[189] Y. Ohtsubo, S. Hatta, N. Kawai, A. Mori, Y. Takeichi, K. Yaji, H. Okuyama, and T. Aruga, "Spin-polarized surface states on Br/Ge(111)-(1×1): Surface spin polarization without heavy elements" *Phys. Rev. B - Condens. Matter Mater. Phys.* (2012).
[190] Y. Ohtsubo, K. Yaji, S. Hatta, H. Okuyama, and T. Aruga, "Two-dimensional states localized in subsurface layers of Ge(111)" *Phys. Rev. B - Condens. Matter Mater. Phys.* **88**, 1 (2013).
[191] L. Chen, M. Decker, M. Kronseder, R. Islinger, M. Gmitra, D. Schuh, D. Bougeard, J. Fabian, D. Weiss, and C. H. Back, "Robust spin-orbit torque and spin-galvanic effect at the Fe/GaAs (001) interface at room temperature" *Nat. Commun.* (2016).
[192] Y. Shiomi, K. Nomura, Y. Kajiwara, K. Eto, M. Novak, K. Segawa, Y. Ando, and E. Saitoh, "Spin-Electricity Conversion Induced by Spin Injection into Topological Insulators" *Phys. Rev. Lett.* **113**, 196601 (2014).
[193] Q. Song, J. Mi, D. Zhao, T. Su, W. Yuan, W. Xing, Y. Chen, T. Wang, T. Wu, X. H. Chen, X. C. Xie, C. Zhang, J. Shi, and W. Han, "Spin injection and inverse Edelstein effect in the surface states of topological Kondo insulator SmB6" *Nat. Commun.* (2016).
[194] T. Liu, Y. Li, L. Gu, J. Ding, H. Chang, P. A. P. Janantha, B. Kalinikos, V. Novosad, A. Hoffmann, R. Wu, C. L. Chien, and M. Wu, "Nontrivial Nature and Penetration Depth of Topological Surface States in SmB6 Thin Films" *Phys. Rev. Lett.* (2018).
[195] P. Deorani, J. Son, K. Banerjee, N. Koirala, M. Brahlek, S. Oh, and H. Yang, "Observation of inverse spin Hall effect in bismuth selenide" *Phys. Rev. B* **90**, 094403 (2014).
[196] M. Jamali, J. S. Lee, J. S. Jeong, F. Mahfouzi, Y. Lv, Z. Zhao, B. K. Nikolic, K. A. Mkhoyan, N. Samarth, and J. P. Wang, "Giant Spin Pumping and Inverse Spin Hall Effect in the Presence of Surface and Bulk Spin-Orbit Coupling of Topological Insulator Bi2Se3" *Nano Lett.* **15**, 7126 (2015).
[197] J. Zhang, J. P. Velev, X. Dang, and E. Y. Tsymbal, "Band structure and spin texture of Bi2Se3 3d ferromagnetic metal interface" *Phys. Rev. B* **94**, 014435 (2016).
[198] H. Wang, J. Kally, J. S. Lee, T. Liu, H. Chang, D. R. Hickey, K. A. Mkhoyan, M. Wu, A. Richardella, and N. Samarth, "Surface-State-Dominated Spin-Charge Current Conversion in Topological-Insulator–Ferromagnetic-Insulator Heterostructures" *Phys. Rev. Lett.* **117**, 076601 (2016).
[199] L. Fu and C. L. Kane, "Topological insulators with inversion symmetry" *Phys. Rev. B* **76**, 45302 (2007).
[200] Y. Ohtsubo, P. Le Fèvre, F. Bertran, and A. Taleb-Ibrahimi, "Dirac cone with helical spin polarization in ultrathin -Sn(001) films" *Phys. Rev. Lett.* **111**, 216401 (2013).

[201] Y. Xu, B. Yan, H. J. Zhang, J. Wang, G. Xu, P. Tang, W. Duan, and S. C. Zhang, "Large-gap quantum spin hall insulators in tin films" *Phys. Rev. Lett.* **111**, 1 (2013).
[202] A. Barfuss, L. Dudy, M. R. Scholz, H. Roth, P. Höpfner, C. Blumenstein, G. Landolt, J. H. Dil, N. C. Plumb, M. Radovic, A. Bostwick, E. Rotenberg, A. Fleszar, G. Bihlmayer, D. Wortmann, G. Li, W. Hanke, R. Claessen, and J. Schäfer, "Elemental Topological Insulator with Tunable Fermi Level: Strained a-Sn on InSb(001)" *Phys. Rev. Lett.* **111**, 1 (2013).
[203] S. Küfner, M. Fitzner, and F. Bechstedt, "Topological α-Sn surface states versus film thickness and strain" *Phys. Rev. B* **90**, 125312 (2014).
[204] V. A. Rogalev, T. Rauch, M. R. Scholz, F. Reis, L. Dudy, A. Fleszar, M. Husanu, V. N. Strocov, J. Henk, I. Mertig, J. Schäfer, and R. Claessen, "Double band inversion in α -Sn : Appearance of topological surface states and the role of orbital composition" *Phys. Rev. B* **95**, 161117(R) (2017).
[205] S. I. Kiselev, J. C. Sankey, I. N. Krivorotov, N. C. Emley, R. J. Schoelkopf, R. A. Buhrman, and D. C. Ralph, "Microwave oscillations of a nanomagnet driven by a spin-polarized current" *Nature* **425**, 380 (2003).
[206] S. Petit, C. Baraduc, C. Thirion, U. Ebels, Y. Liu, M. Li, P. Wang, and B. Dieny, "Spin-Torque Influence on the High-Frequency Magnetization Fluctuations in Magnetic Tunnel Junctions" *Phys. Rev. Lett.* **98**, 077203 (2007).
[207] J. C. Sankey, Y.-T. Cui, J. Z. Sun, J. C. Slonczewski, R. A. Buhrman, and D. C. Ralph, "Measurement of the spin-transfer-torque vector in magnetic tunnel junctions" *Nat. Phys.* **4**, 67 (2008).
[208] H. Kubota, A. Fukushima, K. Yakushiji, T. Nagahama, S. Yuasa, K. Ando, H. Maehara, Y. Nagamine, K. Tsunekawa, D. D. Djayaprawira, N. Watanabe, and Y. Suzuki, "Quantitative measurement of voltage dependence of spin-transfer torque in MgO-based magnetic tunnel junctions" *Nat. Phys.* **4**, 37 (2008).
[209] L. Liu, T. Moriyama, D. C. Ralph, and R. A. Buhrman, "Spin-torque ferromagnetic resonance induced by the spin Hall effect" *Phys. Rev. Lett.* **106**, 036601 (2011).
[210] D. Fang, H. Kurebayashi, J. Wunderlich, K. Vyborny, R. P. Zarbo, R. P. Campion, A. Casiraghi, B. L. Gallagher, T. Jungwirth, and A. J. Ferguson, "Spin – orbit-driven ferromagnetic resonance" **6**, 413 (2011).
[211] K. Kondou, H. Sukegawa, S. Mitani, K. Tsukagoshi, and S. Kasai, "Evaluation of Spin Hall Angle and Spin Diffusion Length by Using Spin Current-Induced Ferromagnetic Resonance" *Appl. Phys. Express* **5**, 073002 (2012).
[212] A. Ganguly, K. Kondou, H. Sukegawa, S. Mitani, S. Kasai, Y. Niimi, Y. Otani, and A. Barman, "Thickness dependence of spin torque ferromagnetic resonance in Co75Fe25/Pt bilayer films" *Appl. Phys. Lett.* **104**, 072405 (2014).
[213] V. Tshitoyan, C. Ciccarelli, A. P. Mihai, M. Ali, A. C. Irvine, T. A. Moore, T. Jungwirth, and A. J. Ferguson, "Electrical manipulation of ferromagnetic NiFe by antiferromagnetic IrMn" **214406**, 1 (2015).
[214] C. Guillemard, S. Petit-Watelot, S. Andrieu, and J.-C. Rojas-Sánchez, "Charge-spin current conversion in high quality epitaxial Fe/Pt systems : Isotropic spin Hall angle along different in-plane crystalline directions" *Appl. Phys. Lett.* **113**, 262404 (2018).
[215] W. Skowroński, Ł. Karwacki, S. Ziętek, J. Kanak, S. Łazarski, K. Grochot, T. Stobiecki, P. Kuświk, F. Stobiecki, and J. Barnaś, "Determination of Spin Hall Angle in Heavy-Metal/Co-Fe-B-Based Heterostructures with Interfacial Spin-Orbit Fields" *Phys. Rev. Appl.* **11**, 024039 (2019).
[216] E. Liu, T. Fache, D. Cespedes-Berrocal, Z. Zhang, S. Petit-Watelot, S. Mangin, F. Xu,

and J.-C. Rojas-Sánchez, “Strain-Enhanced Charge-to-Spin Conversion in Ta / Fe / Pt Multilayers Grown on Flexible Mica Substrate” *Phys. Rev. Appl.* **12**, 044074 (2019).
[217] J.-W. Xu and A. D. Kent, “Charge-To-Spin Conversion Efficiency in Ferromagnetic Nanowires by Spin Torque Ferromagnetic Resonance: Reconciling Lineshape and Linewidth Analysis Methods” *Phys. Rev. Appl.* **14**, 014012 (2020).
[218] T. Jungwirth, X. Marti, P. Wadley, and J. Wunderlich, “Antiferromagnetic spintronics” *Nat. Nanotechnol.* (2016).
[219] V. Baltz, A. Manchon, M. Tsoi, T. Moriyama, T. Ono, and Y. Tserkovnyak, “Antiferromagnetic spintronics” *Rev. Mod. Phys.* **90**, 015005 (2018).
[220] H. Saglam, J. C. Rojas-sanchez, S. Petit, M. Hehn, W. Zhang, J. E. Pearson, S. Mangin, and A. Hoffmann, “Independence of spin-orbit torques from the exchange bias direction in Ni 81 Fe 19 / IrMn bilayers” *Phys. Rev. B* **98**, 094407 (2018).
[221] K. Gilmore, M. D. Stiles, J. Seib, D. Steiauf, and M. Fähnle, “Anisotropic damping of the magnetization dynamics in Ni , Co , and Fe” *Phys. Rev. B* **81**, 174414 (2010).
[222] L. Chen, S. Mankovsky, S. Wimmer, M. A. W. Schoen, H. S. Körner, M. Kronseder, D. Schuh, D. Bougeard, H. Ebert, D. Weiss, and C. H. Back, “Emergence of anisotropic Gilbert damping in ultrathin Fe layers on GaAs (001)” *Nat. Phys.* **14**, 490 (2018).
[223] J. C. Rojas-Sánchez and A. Fert, “Compared Efficiencies of Conversions between Charge and Spin Current by Spin-Orbit Interactions in Two- and Three-Dimensional Systems” *Phys. Rev. Appl.* **11**, 054049 (2019).
[224] K.-S. K.-J. Lee, S.-W. Lee, B.-C. Min, and K.-S. K.-J. Lee, “Threshold current for switching of a perpendicular magnetic layer induced by spin Hall effect” *Appl. Phys. Lett.* **102**, 112410 (2013).
[225] J. C. Rojas-Sánchez, P. Laczkowski, J. Sampaio, S. Collin, K. Bouzehouane, N. Reyren, H. Jaffrès, A. Mougin, and J. M. George, “Perpendicular magnetization reversal in Pt/[Co/Ni]3/Al multilayers via the spin Hall effect of Pt” *Appl. Phys. Lett.* **108**, 082406 (2016).
[226] M. Belmeguenai, J.-P. Adam, Y. Roussigné, S. Eimer, T. Devolder, J.-V. Kim, S. M. Cherif, A. Stashkevich, and A. Thiaville, “Interfacial Dzyaloshinskii-Moriya interaction in perpendicularly magnetized Pt/Co/AlO x ultrathin films measured by Brillouin light spectroscopy” *Phys. Rev. B* **91**, 180405 (2015).
[227] O. Boulle, S. Rohart, L. D. Buda-Prejbeanu, E. Jué, I. M. Miron, S. Pizzini, J. Vogel, G. Gaudin, and a. Thiaville, “Domain wall tilting in the presence of the Dzyaloshinskii-Moriya interaction in out-of-plane magnetized magnetic nanotracks” *Phys. Rev. Lett.* **111**, 1 (2013).
[228] T. H. Pham, S.-G. Je, P. Vallobra, T. Fache, D. Lacour, G. Malinowski, M. C. Cyrille, G. Gaudin, O. Boulle, M. Hehn, J.-C. Rojas-Sánchez, and S. Mangin, “Thermal Contribution to the Spin-Orbit Torque in Metallic-Ferrimagnetic Systems” *Phys. Rev. Appl.* **9**, 064032 (2018).
[229] S. Je, J. C. Rojas-Sanchez, T. H. Pham, P. Vallobra, G. Malinowski, D. Lacour, T. Fache, M. Cyrille, D. Kim, S.-B. Choe, M. Belmeguenai, M. Hehn, S. Mangin, G. Gaudin, and O. Boulle, “Spin-orbit torque-induced switching in ferrimagnetic alloys : Experiments and modeling” *Appl. Phys. Lett.* **112**, 062401 (2018).
[230] P. Vallobra, T. Fache, Y. Xu, L. Zhang, G. Malinowski, M. Hehn, J.-C. Rojas-Sánchez, E. E. Fullerton, and S. Mangin, “Manipulating exchange bias using all-optical helicity-dependent switching” *Phys. Rev. B* **96**, 144403 (2017).
[231] S.-G. Je, P. Vallobra, T. Srivastava, J.-C. Rojas-Sánchez, T. H. Pham, M. Hehn, G.

Malinowski, C. Baraduc, S. Auffret, G. Gaudin, S. Mangin, H. Béa, and O. Boulle, "Creation of Magnetic Skyrmion Bubble Lattices by Ultrafast Laser in Ultrathin Films" *Nano Lett.* **18**, 7362 (2018).
[232] A. Tsukahara, Y. Ando, Y. Kitamura, H. Emoto, E. Shikoh, M. P. Delmo, T. Shinjo, and M. Shiraishi, "Self-induced inverse spin Hall effect in permalloy at room temperature" *Phys. Rev. B* **89**, 235317 (2014).
[233] T. Taniguchi, J. Grollier, and M. D. Stiles, "Spin-Transfer Torques Generated by the Anomalous Hall Effect and Anisotropic Magnetoresistance" *Phys. Rev. Appl.* **3**, 044001 (2015).
[234] K. S. Das, W. Y. Schoemaker, B. J. Van Wees, and I. J. Vera-Marun, "Spin injection and detection via the anomalous spin Hall effect of a ferromagnetic metal" *Phys. Rev. B* **96**, 1 (2017).
[235] S. Iihama, T. Taniguchi, K. Yakushiji, A. Fukushima, Y. Shiota, S. Tsunegi, R. Hiramatsu, S. Yuasa, Y. Suzuki, and H. Kubota, "Spin-transfer torque induced by the spin anomalous Hall effect" *Nat. Electron.* **1**, 120 (2018).
[236] M. Hayashi, J. Kim, M. Yamanouchi, and H. Ohno, "Quantitative characterization of the spin-orbit torque using harmonic Hall voltage measurements" *Phys. Rev. B* **89**, 144425 (2014).
[237] K. Garello, I. M. Miron, C. O. Avci, F. Freimuth, Y. Mokrousov, S. Blügel, S. Auffret, O. Boulle, G. Gaudin, and P. Gambardella, "Symmetry and magnitude of spin–orbit torques in ferromagnetic heterostructures" *Nat. Nanotechnol.* **8**, 587 (2013).
[238] C. O. Avci, K. Garello, C. Nistor, S. Godey, B. Ballesteros, A. Mugarza, A. Barla, M. Valvidares, E. Pellegrin, A. Ghosh, I. M. Miron, O. Boulle, S. Auffret, G. Gaudin, and P. Gambardella, "Fieldlike and antidamping spin-orbit torques in as-grown and annealed Ta/CoFeB/MgO layers" *Phys. Rev. B* **89**, 214419 (2014).
[239] A. Ghosh, K. Garello, C. O. Avci, M. Gabureac, and P. Gambardella, "Interface-Enhanced Spin-Orbit Torques and Current-Induced Magnetization Switching of Pd/Co/AlOx Layers" *Phys. Rev. Appl.* **7**, 014004 (2017).
[240] J. W. Lee, J. Y. Park, J. M. Yuk, and B. Park, "Spin-Orbit Torque in a Perpendicularly Magnetized Ferrimagnetic TbCo Single Layer" *Phys. Rev. Appl.* **13**, 044030 (2020).
[241] J. Finley and L. Liu, "Spin-Orbit Torque Efficiency in Compensated Ferrimagnetic Cobalt-Terbium Alloys" *Phys. Rev. Appl.* **054001**, 1 (2016).
[242] R. Mishra, J. Yu, X. Qiu, M. Motapothula, T. Venkatesan, and H. Yang, "Anomalous Current-Induced Spin Torques in Ferrimagnets near Compensation" *Phys. Rev. Lett.* **118**, 167201 (2017).
[243] N. Roschewsky, C. Lambert, and S. Salahuddin, "Spin-orbit torque switching of ultralarge-thickness ferrimagnetic GdFeCo" *Phys. Rev. B* **96**, 064406 (2017).
[244] K.-J. Kim, S. K. Kim, Y. Hirata, S. Oh, T. Tono, D.-H. Kim, T. Okuno, W. S. Ham, S. Kim, G. Go, Y. Tserkovnyak, A. Tsukamoto, T. Moriyama, K. Lee, and T. Ono, "Fast domain wall motion in the vicinity of the angular momentum compensation temperature of ferrimagnets" *Nat. Mater.* **16**, 1187 (2017).
[245] D. Kim, M. Haruta, H. Ko, G. Go, H. Park, T. Nishimura, D. Kim, T. Okuno, Y. Hirata, Y. Futakawa, H. Yoshikawa, W. Ham, S. Kim, H. Kurata, A. Tsukamoto, Y. Shiota, T. Moriyama, S. Choe, K. Lee, and T. Ono, "Bulk Dzyaloshinskii – Moriya interaction in amorphous ferrimagnetic alloys" *Nat. Mater.* **18**, 685 (2019).
[246] J. Li, C. B. Wilson, R. Cheng, M. Lohmann, M. Kavand, W. Yuan, M. Aldosary, N. Agladze, P. Wei, M. S. Sherwin, and J. Shi, "Spin current from sub-terahertz-generated antiferromagnetic magnons" *Nature* **578**, 70 (2020).

[247] P. Vaidya, S. A. Morley, J. van Tol, Y. Liu, R. Cheng, A. Brataas, D. Lederman, and E. del Barco, "Subterahertz spin pumping from an insulating antiferromagnet" *Science (80-.).* **368**, 160 (2020).
[248] G. T. Rado, "Observation and Possible Mechanisms of Magnetoelectric Effects in a Ferromagnet" *Phys. Rev. Lett.* **13**, 335 (1964).
[249] D. Stoeffler, "First principles study of the electric polarization and of its switching in the multiferroic GaFeO 3 system" *J. Phys. Condens. Matter* **24**, 185502 (2012).
[250] T. Arima, D. Higashiyama, Y. Kaneko, J. P. He, T. Goto, S. Miyasaka, T. Kimura, K. Oikawa, T. Kamiyama, R. Kumai, and Y. Tokura, "Structural and magnetoelectric properties of Ga2-xFexO3 single crystals grown by a floating-zone method" *Phys. Rev. B* **70**, 064426 (2004).
[251] A. Thomasson, S. Cherifi, C. Lefevre, F. Roulland, B. Gautier, D. Albertini, C. Meny, and N. Viart, "Room temperature multiferroicity in $Ga_{0.6}Fe_{1.4}O_3$:Mg thin films" *J. Appl. Phys.* **113**, 214101 (2013).
[252] M. Trassin, N. Viart, G. Versini, S. Barre, G. Pourroy, J. Lee, W. Jo, K. Dumesnil, C. Dufour, and S. Robert, "Room temperature ferrimagnetic thin films of the magnetoelectric $Ga_{2-x}Fe_xO_3$" *J. Mater. Chem.* **19**, 8876 (2009).
[253] J. Dweck, "Ferromagnetic Resonance in the Highly Anisotropic Ferrimagnet Gallium Iron Oxide" *Phys. Rev.* **168**, 602 (1968).
[254] L. Chao, M. N. Afsar, and S. Ohkoshi, "Microwave and millimeter wave dielectric permittivity and magnetic permeability of epsilon-gallium-iron-oxide nano-powders" *J. Appl. Phys.* **117**, 17B324 (2015).
[255] R. Lebrun, A. Ross, S. A. Bender, A. Qaiumzadeh, L. Baldrati, J. Cramer, A. Brataas, R. A. Duine, and M. Kläui, "Tunable long-distance spin transport in a crystalline antiferromagnetic iron oxide" *Nature* **561**, 222 (2018).
[256] Y. Shiomi, T. Ohtani, S. Iguchi, T. Sasaki, Z. Qiu, H. Nakayama, K. Uchida, and E. Saitoh, "Interface-dependent magnetotransport properties for thin Pt films on ferrimagnetic Y 3 Fe 5 O 12" *Appl. Phys. Lett.* **104**, 242406 (2014).
[257] S. Meyer, R. Schlitz, S. Geprägs, M. Opel, H. Huebl, R. Gross, and S. T. B. Goennenwein, "Anomalous Hall effect in YIG|Pt bilayers" *Appl. Phys. Lett.* **106**, 132402 (2015).
[258] B. Kundys, F. Roulland, C. Lefèvre, C. Mény, A. Thomasson, and N. Viart, "Room temperature polarization in the ferrimagnetic Ga2−xFexO3 ceramics" *J. Eur. Ceram. Soc.* **35**, 2277 (2015).

Annexe A: Curriculum Vitae

ROJAS SANCHEZ Juan Carlos, CNRS Researcher Scientist

Institute Jean Lamour UMR 7198 CNRS
Université de Lorraine
2 allée André Guinier BP 50840
54011 Nancy Cedex, FRANCE

Date of birth: 10/28/1976
Place of birth: Chepén, La Libertad, Peru
Nationality: French - Peruvian
Two children (born in 2000 and 2009)
Marital status: married

Mail: juan-carlos.rojas-sanchez@univ-lorraine.fr
ResearcherID: N-9963-2015 (http://www.researcherid.com/rid/N-9963-2015)

EDUCATION

- Apr. 2005 – Feb. 2011 **PhD in Physics**. Balseiro Institute (National University of Cuyo) – Bariloche Atomic Center, Bariloche, Argentina. Awarded on February 15th, 2011. Interrupted all 2010, back in Peru.
- Aug. 2003 – Dec. 2004 **Master in Physics**. Balseiro Institute - Bariloche, Argentina.
- Jan. 2000 – Jul. 2003 Interruption (teaching position in Peru).
- Apr. 1994 – Dec. 1999 **Bachelor in Physics**. Science Faculty, National University of Engineering, Lima, Peru.

CURRENT POISTION

Since October 2015: **CNRS permanent researcher** position at Institute Jean Lamour (IJL), Nancy, France**.** "Chargé de recherché" (1st rank in this national concourse with 4 CNRS positions and 90 admitted applicants).

INSTITUTIONAL RESPONSABILITIES

- January 2018- Present **Head of the Micro and nanotechnology platform of Lorraine** IJL's CC-MINALOR (250 m^2 cleanroom facilities including three permanent staff). Institute Jean Lamour.

FELLOWSHIPS AND PREVIOUS POSITIONS

- Oct. 2013-Sept. 2015 Unité Mixte de Physique CNRS/Thales, Palaiseau, France Postdctoral fellow in the group of Prof. A. Fert.
- Aug. 2013 – Sept. 2013 *Institut Néel*, Grenoble. France. Postdoctoral fellow
- Jan. 2013 – Jul. 2013 SPINTEC, INAC/CEA-Grenoble. France. ANR SpinHall postdoctoral fellow

- Jul. 2011 – Jan. 2013 *Laboratoire de Nanostructures et Magnetisme* INAC/CEA-Grenoble, France. Eurotalents-CEA (FP7 Marie Curie Actions). Postdoctoral fellow.

FUNDING as principal investigator:

- TOPTRONICS Topological Spin-orbitronics. ANR- France. Grant: 256 k€. 01/2020-09/2023. https://spin.ijl.cnrs.fr/projects/toptronic/
- *MISSION* (MagnetoelectrIc oxideS for SpIn-OrbitroNics). ANR- France. Grant: 202 k€. 10/2018-03/2022. https://spin.ijl.cnrs.fr/projects/mission/
- *RECENT* (RECycling Energy with New Thermoelectric effects). Cellule Energie-CNRS. Grant: 15 k€. 2017.
- *Chercheur de l'avenir*. FEDER-FSE Lorraine. Grant: 50 k€. 2016-2018.
- *CEA*-Eurotalents. PEOPLE Marie Curie Actions. Post-doctoral fellowship. Grant: 102 k€. 2011-2013

AWARDS

CNRS Bronze medal 2020

MAIN TOPICS OF RESEARCH: SPINTRONICS / SPIN-ORBITRONICS

- Spintronic, spin-orbitronics and spin caloritronics: Study of spin-orbit torque, spin pumping ferromagnetic resonance, spin-torque ferromagnetic resonance, spin Hall magnetoresistance, spin Hall effect, Edelstein effect and Spin Seebeck effect, second harmonic, unidirectional magnetoresistance. Recently, discovery of huge spin anomalous Hall effect in GdFeCo ferrimagnetic films and self-induced spin-orbit torque
- October 2013 – September 2015:
  - ❖ Inverse Edelstein Effect by spin pumping ferromagnetic resonance: Spin-charge current conversion in topological insulators and oxides Rashba interfaces.
  - ❖ Spin-orbit torque switching in Pt/(Co/Ni)3/Al.
- August 2013 – September 2013:
  - ❖ Magnetic Domain Wall propagation in Pt/Co/GdOx.
- July 2011 – July 2013:
  - ❖ Inverse spin Hall Effect and spin pumping ferromagnetic resonance: Spin memory loss at Co/Pt, and Co/Cu/Pt interfaces. Determination of spin Hall angle and spin diffusion length of Pt.
  - ❖ Inverse Edelstein Effect by spin pumping ferromagnetic resonance: Spin-charge current conversion at Ag/Bi Rashba interface.
  - ❖ ISHE and spin pumping ferromagnetic resonance in semiconductors: Spin injection in Ge.
  - ❖ Spin Hall Effect, Inverse Spin Hall effect and spin absorption in lateral spin valves.
  - ❖ Hanle effect in lateral spin valves: in-plane and out-of-plane spin precession.
- April 2005 – February 2011: Ph.D. in Physics at Balseiro Institute, Bariloche, Argentina.
  - ❖ Growth and characterization of oxides perovskites: multilayers and super-lattices.
  - ❖ Exchange bias at oxides La0.25Sr0.75MnO3/LaNiO3 interfaces.
  - ❖ Ferromagnetic resonance study: determination of magnetic anisotropies
  - ❖ Microfabrication of magnetic tunnel junction based on oxides perovskites.

SUPERVISION since October 2015 at Institut Jean Lamour, Nancy:

- **2 Ph.D.** students:
  Pierre VALLOBRA ended 05/02/2019
  Thai Ha PHAM ended 05/05/2020
- **3 Master** students:
  Thai Ha PHAM (2016)
  Jean-Loüis BELLO (2018)
  Heloïse DAMAS (2020)
- **Mentoring of 10 internships** students from USA (2), Peru (2), China (3), Mexico (1) and Argentine(1)
  Heisemberg TARAZONA: 2 months in 2017, PhD student at *Universidad Nacional Mayor de San Marcos*, Peru.
  Hilal SAGLAM: 6 months in 2017, PhD student at Argonne National Laboratory, Illinois, USA.
  Jianying QIN: 15 months 2017-2018, PhD student at State Key Laboratory of Magnetism, Institute of Physics, Chinese Academy of Sciences, Chine.
  Sheena PATEL: 9 months started 2017, PhD student at California University, San Diego, USA.
  Jinhui SHEN: 1 month July 2018, PhD student at Fudan University, Shanghai, Chine.
  David Luciano CESPEDES-BERROCAL: 5 months started March 2018, B.S. Physics Engineering student at *Universidad Nacional de Ingeniería*, Peru. 6 more months in 2019
  Aldo ARRIOLA-CORDOVA: 4 months started September 15th 2019, B.S. Physics Engineering student at *Universidad Nacional de Ingeniería*, Peru.
  Yunhan CAI: 12 months started March 2019, PhD student at Fudan University, Shanghai, Chine.
  Silvestre NOVOA: 6 months started March 2020, Master student at UNAM, Mexico.
  María-José BURGOS: 6 months started March 2020, PhD student at Balseiro Institute-CAB, Argentina.

TEACHING ACTIVITIES

- Mar. 2011 – Jul. 2011 Contractual assistant professor at National University of Engineering, Peru. Total 84 hours. I was in charge of Tutorials (seminars and work labs) of several modules for undergraduate students of Electric and Electronic engineering.
- Aug. 2010 – Dec. 2010 Contractual Professor at National University of Engineering, Peru. Total 132 hours. Lecturer in «Material characterization». Master in Physics: 28 hours of lectures and 56h of work lab. 48h of lecturers in «Experimental Physics» for graduated students.
- Mar. 2001 – Jul. 2003 Contractual assistant professor at National University of Engineering, Peru. Total 588 hours, an average of 196h/year . I was in charge of Tutorials (seminars and work labs) of several modules to physics undergraduate students.
- Jul. 2000 – Dec. 2002 Contractual assistant professor at Cayetano Héredia University

(medicine undergraduate student, 168h), and *Universidad de Ciencias Aplicadas* (engineering undergraduate student, 96h). tutorials, seminar and work lab of General Physics.

- Mar. 2000 – Jul. 2000 Math teacher at elementary school, Lima, Peru.

ORGANISATION OF SCIENTIFIC MEETINGS

- **2019:** Co-chair of **SPIN PERU**, International Workshop Spintronics 2019, Ollantaytambo, Peru. http://spinphys.riken.jp/workshop/spinperu/
- **2018:** Chair of the last **focus session in spin-orbitronic MA.57 at the Joint DPG/EPS** in Berlin, Germany.
- **2017:** Scientific committee and local organizing committee member at the **IEEE Frontiers in Magnetism: Topological Insulator and Outreach for applications** in Nancy, France.
- **2016:** Scientific committee member and chair in one session at the International **IWST**, Nancy, France.
- **2016:** Local committee member at the **Colloque Louis Néel**, Saint-Dié-des-Vosges, France.
- **2015:** Chair of the **FR.G.3_Domain Wall Motion session in the 20th ICM**, Barcelona, Spain.

REVIEWING AND EVALUATION ACTIVITIES since October 2015

- **Referee for** international peer-reviewed major scientific journals: Nat. group (Nat Phys., Nat. Mater. Nat Asia Mater., Sc. Reports), APS (PRL, PRB, PRAppl, PRX, Rev. Mod. Phys.), AIP (APL, JAP), Wiley (Advance Materials Lett., Adv. Materials, PSS RRL), ACS (Nano Letter)
- **Reviewer of research project** for UNMSM, Peru (2017); FONDECYT, Chile (2017); US Department of Energy, USA (2018, 2019); AENAS, Spain (2018); ANR, France (2019,2020); EU.
- **Expert for the French Micro and nanotechnology Obervatory** (OMNT), 2016-2017.
- **Board member** of Ph. D. Thesis Defense, June 2017, SPINTEC, Grenoble, France.

RESEARCH RECORD (ISI Web of Science, July 2020)

- **40 publications** in international peer-reviewed journal including 1 Nat. Mater., 2 Nat. Comm., 3 Nano Lett., 3 Phys. Rev. Lett, 4 Phys. Rev. Appl., 8 Phys. Rev. B and 6 Appl. Phys. Lett. I am the first author in 9 of my publications and second author in other 9 publications.
- **1479 citations** (36.9 citations per article).
- **4 highly cited paper** (top 1% for the field and publication year). First author in three of them and corresponding author in the fourth one. Nat Comm. 2013, PRL 2014, PRL 2016 and Nat. Materials 2016
- **h-index: 16**

CONFERENCES AND SEMINARS

- **17 invited presentations** including APS March meeting 2017, Young researcher leaders group - Spice, Mainz 2017, Intermag 2018, DPG/EPS 2018, EMRS Fall 2018.
- **8 contributed talks** at international conferences such as Intermag 2018 (2)
- **14 seminars** at Universities and research laboratory including SPINTEC in 2016, ETH Zurich in 2017, Nanogune-Spain, UCLA-USA, NJUST-Nanjing-China and Southeast Univ-Nanjing-China in 2018.

Some selected personal invited conferences

1. *Topological insulators and Rashba interfaces as efficient converters of spin to charge current: towards low power consumption and energy harvesting*. **EMRS Fall Meeting** in Warsaw, Poland, September 17th-20th, 2018. **Invited**
2. *Highly and tunable spin-to-charge conversion in 2D electron gas at $LaAlO_3/SrTiO_3$ interfaces*. **Intermag 2018** in Singapore, April 23th-27th, 2018. **Invited**
3. *Interfacial spin-orbitronic: spin-charge conversion in topological insulators and Rashba interfaces*. **65th AVS Symposium** in Long Beach, CA, October 21-26, 2018. **Invited**
4. *Topological insulators and Rashba interfaces as efficient spin-charge current converters*. **JMC** 2018 in Grenoble, August 27th-31st. **Invited**
5. Interfacial spin-orbitronic: Rashba interfaces and topological insulators as efficient spin-charge current converters. **DPG/EPS Meeting** 2018 in Berlin, March 11th-18th. **Invited**
6. *Interfacial spin-orbitronics: large spin-charge current conversion in α-Sn topological insulator and potential for giant Spin Seebeck effect in YIG/α-Sn*. **Young Research Leaders Group Workshop**: **Insulator spintronics-strong-coupling, coherence and entanglement** (Mainz, Germany, July 31st - August 4th 2017). **Invited**
7. *Efficient spin-orbitronic systems: Rashba interfaces and topological*, **New Trends in Topological Insulators, NTTI2017**, (Locarno, Switzerland, July 16th-21st 2017). **Invited**
8. *Spin-to-charge conversion at interfaces: spin pumping, Rashba coupling, and topological insulators*. **APS March Meeting 2017** (New Orleans, USA, March 2017). **Invited**
9. *Tuning the Spin Orbit Torque-critical current density to reverse perpendicular magnetization in CoTb ferrimagnetic based alloys*. **14th RIEC International Workshop on Spintronics** (Sendai, Japan, November 2016). **Invited**.
10. *Rashba interfaces and Topological Insulators for efficient spin-to-charge current conversion at room temperature*, **International Workshop on nano-Spin Conversion and Quantum Spin Dynamics, NSCS-QSD**, (Tokyo, Japan, October 2016). **Invited**.

Early achievements track-record

11 SELECTED PUBLICATIONS. *Citations numbers from ISI Web of Science and google scholar (GS)*

- **Spin-charge current conversion in metals and semiconductors**

1. *Spin Pumping and Inverse Spin Hall Effect in Germanium*. **J. -C. Rojas-Sánchez**, M. Cubukcu, A. Jain, C. Vergnaud, C. Portemont, C. Ducruet, A. Barski, A. Marty, L. Vila, J.-P. Attané, E. Augendre, G. Desfonds, S. Gambarelli, H. Jaffrès, J. -M. George and M. Jamet. Phys. Rev. B 88, 064403 (2013). **Cited 58, 80 in GS**. **First author.**

2. *Spin pumping and inverse spin Hall effect in platinum: the essential role of spin-memory loss at metallic interfaces.* **J-C. Rojas-Sánchez**, N. Reyren, P. Laczkowski, W. Savero, J-P. Attané, C. Deranlot, M. Jamet, J-M. George, L. Vila and H. Jaffrès:. Phys. Rev. Lett. 112, 106602 (2014). **Highly cited (301, 417 in GS). First author.**
3. *Experimental evidences of a large extrinsic spin Hall effect in AuW alloy.* P Laczkowski, **J-C Rojas-Sánchez**, W Savero-Torres, H Jaffrès, N Reyren, C Deranlot, L Notin, C Beigné, A Marty, J-P Attané, L Vila, J-M George and A Fert. Appl. Phys. Lett. 104, 142403 (2014). **Cited 40, 66 in GS.**

- **Inverse Edelstein Effect: Spin-charge current conversion in Rashba interfaces and topological insulators:**

4. *Spin-to-charge conversion using Rashba coupling at the interface between non-magnetic materials*.
   J C Rojas Sánchez, L. Vila, G. Desfonds, S. Gambarelli, J.P. Attané, J. M. De Teresa, C. Magén and A. Fert: Nature Comm. 4:2944 doi: 10.1038/ncomms3944 (2013).
   Highly cited (315, 456 in GS). First author. Opened a new research line.
5. *Spin to charge conversion at room temperature by spin pumping into a new type of topological insulator: α-Sn films.*
   J.-C. Rojas-Sánchez, S. Oyarzun, Y. Fu, A. Marty, C. Vergnaud, S. Gambarelli, L. Vila, M. Jamet, Y. Ohtsubo, A. Taleb-Ibrahimi, P. Le Fèvre, F. Bertran, N. Reyren, J.-M. George and A. Fert: Phys. Rev. Lett. 116, 096602 (2016).
   Highly cited (120, 194 in GS). First author and corresponding author. So far the only study where the existence of topological states was evidenced by ARPES prior to the spintronics experiments in the very same sample. The largest spin/charge current conversion efficiency measured at room temperature.
6. *Highly efficient and tunable spin-to-charge conversion through Rashba coupling at oxide interfaces.*
   E. Lesne, Y. Fu, S. Oyarzun, J.C. Rojas-Sánchez, D.C. Vaz, H. Naganuma, G. Sicoli, J.-P. Attané, M. Jamet, E. Jacquet, J-M. George, A. Barthélémy, H. Jaffres, A. Fert, M. Bibes and L. Vila. Nat. Mater. 15, 1261 (2016).
   Highly cited (178 citations, 231 in GS). Corresponding author. The largest spin/charge current conversion efficiency measured (at 7 K).

- **Spin-orbit torque magnetization switching**

7. *Perpendicular magnetization reversal in Pt/[Co/Ni]$_3$/Al multilayers via the Spin Hall Effect of Pt.*
   J.-C. Rojas-Sánchez, P. Laczkowski , J. Sampaio, S. Collin, K. Bouzehouane, N. Reyren, H. Jaffres, A. Mougin and J.-M. George. Appl. Phys. Lett. 108, 082406 (2016).
   Cited 39, 45 in GS. First author and corresponding author.
8. *Thermal Contribution to the Spin-Orbit Torque in Metallic-Ferrimagnetic Systems*. Thai Ha Pham, S-G Je, Pierre Vallobra, Thibaud Fache, Daniel Lacour, Gregory Malinowski, Marie-Claire Cyrille, Gilles Gaudin, Olivier Boulle, Michel Hehn, **J-C Rojas-Sánchez** and Stéphane Mangin. Phys. Rev. Appl. 9, 064032 (2018).
   Corresponding author. **Cited 12, 16 in GS**. Discovery of a new characteristic temperature, T_{switch}, above the magnetic and angular compensation temperatures and below Curie temperature. **First author is my PhD student**.

- **Exchange bias, optical switching and skyrmions**

9. Manipulating exchange bias using all-optical helicity-dependent switching.

P. Vallobra, T. Fache, Y. Xu, L. Zhang, G. Malinowski, M. Hehn, J.-C. Rojas-Sánchez, E. E. Fullerton, and S. Mangin. Phys. Rev. B 96, 144403 (2017). Corresponding author. Cited 5, 8 in GS. First author is my PhD student.

10. *Creation of Magnetic Skyrmion Bubble Lattices by Ultrafast Laser in Ultrathin Films*. Soong-Geun Je, Pierre Vallobra, Titiksha Srivastava, Juan-Carlos Rojas-Sánchez, Thai Ha Pham, Michel Hehn, Gregory Malinowski, Claire Baraduc, Stéphane Auffret, Gilles Gaudin, Stéphane Mangin, Hélène Béa, Olivier Boulle. Nano letters 18, 7362-7371 (2018). (14 citations, 26 in GS). Fist author is a post-doc and the second author is my Ph. D. student.

- **Spin-orbit driven ferromagnetic resonance or spin-torque ferromagnetic resonance**

11. *Charge-spin current conversion in high quality epitaxial Fe/Pt systems: Isotropic spin Hall angle along different in-plane crystalline directions.* C.Guillemard,S. Petit-Watelot, S. Andrieu and J-C Rojas-Sánchez. Appl. Phys. Lett. 113, 262404 (2018). Last author and corresponding author. Cited 5, 5 in GS.

Annexe B: Publication list

The publications list is ranked by citations number according to ISI Web of Science (July 2020).

1. Spin-to-charge conversion using Rashba coupling at the interface between non-magnetic materials.
   Rojas Sanchez, J. C.; Vila, L.; Desfonds, G.; Gambarelli, S.; Attane, J. P.; De Teresa, J. M.; Magen, C.; Fert, A.
   Nature communications 4, 2944 (2013). DOI : https://doi.org/10.1038/ncomms3944
   315 citations
2. Spin Pumping and Inverse Spin Hall Effect in Platinum: The Essential Role of Spin-Memory Loss at Metallic Interfaces
   Rojas-Sanchez, J. -C.; Reyren, N.; Laczkowski, P.; Savero, W.; Attane, J. -P.; Deranlot, C.; Jamet, M.; George, J. -M.; Vila, L.; Jaffres, H.
   Physical Review Letters **112**, 106602 (2014). DOI: https://doi.org/10.1103/PhysRevLett.112.106602
   301 citations
3. Highly efficient and tunable spin-to-charge conversion through Rashba coupling at oxide interfaces
   Lesne, E.; Fu, Yu; Oyarzun, S.; Rojas-Sanchez, J. C.; Vaz, D. C.; Naganuma, H.; Sicoli, G.; Attane, J. -P.; Jamet, M.; Jacquet, E.; George, J. -M.; Barthelemy, A.; Jaffres, H.; Fert, A.; Bibes, M.; Vila, L.
   Nature materials 15, 1261 (2016). DOI: https://doi.org/10.1038/NMAT4726
   178 citations
4. Spin to Charge Conversion at Room Temperature by Spin Pumping into a New Type of Topological Insulator: alpha-Sn Films
   Rojas-Sanchez, J. -C.; Oyarzun, S.; Fu, Y.; Marty, A.; Vergnaud, C.; Gambarelli, S.; Vila, L.; Jamet, M.; Ohtsubo, Y.; Taleb-Ibrahimi, A.; Le Fevre, P.; Bertran, F.; Reyren, N.; George, J. -M.; Fert, A.
   Physical Review Letters **116**, 096602 (2016).
   DOI: https://doi.org/10.1103/PhysRevLett.116.096602
   120 citations
5. Crossover from Spin Accumulation into Interface States to Spin Injection in the Germanium Conduction Band
   Jain, A.; Rojas-Sanchez, J. -C.; Cubukcu, M.; Peiro, J.; Le Breton, J. C.; Prestat, E.; Vergnaud, C.; Louahadj, L.; Portemont, C.; Ducruet, C.; Baltz, V.; Barski, A.; Bayle-Guillemaud, P.; Vila, L.; Attane, J. -P.; Augendre, E.; Desfonds, G.; Gambarelli, S.; Jaffres, H.; George, J. -M.; Jamet, M.
   Physical Review Letters **109**, 106603 (2012).
   DOI: https://doi.org/10.1103/PhysRevLett.109.106603
   67 citations
6. Exchange-bias effect at $La_{0.75}Sr_{0.25}MnO_3/LaNiO_3$ interfaces
   Rojas Sanchez, J. C.; Nelson-Cheeseman, B.; Granada, M.; Arenholz, E.; Steren, L. B.
   Physical Review B **85**, 094427 (2012). DOI: https://doi.org/10.1103/PhysRevB.85.094427
   59 citations

7. Spin pumping and inverse spin Hall effect in germanium
   Rojas-Sanchez, J. -C.; Cubukcu, M.; Jain, A.; Vergnaud, C.; Portemont, C.; Ducruet, C.; Barski, A.; Marty, A.; Vila, L.; Attane, J. -P.; Augendre, E.; Desfonds, G.; Gambarelli, S.; Jaffres, H.; George, J. -M.; Jamet, M.
   Physical Review B **88**, 064403 (2013). DOI: https://doi.org/10.1103/PhysRevB.88.064403
   58 citations
8. Experimental evidences of a large extrinsic spin Hall effect in AuW alloy
   Laczkowski, P.; Rojas-Sanchez, J-C; Savero-Torres, W.; Jaffres, H.; Reyren, N.; Deranlot, C.; Notin, L.; Beigne, C.; Marty, A.; Attane, J-P; Vila, L.; George, J-M; Fert, A.
   Applied Physics Letters **104**, 142403 (2014). DOI: https://doi.org/10.1063/1.4870835
   52 citations
9. Perpendicular magnetization reversal in Pt/[Co/Ni](3)/Al multilayers via the spin Hall effect of Pt
   Rojas-Sanchez, J-C.; Laczkowski, P.; Sampaio, J.; Collin, S.; Bouzehouane, K.; Reyren, N.; Jaffres, H.; Mougin, A.; George, J-M.
   Applied Physics Letters **108**, 082406 (2016). DOI: https://doi.org/10.1063/1.4942672
   39 citations
10. Velocity asymmetry of Dzyaloshinskii domain walls in the creep and flow regimes
    Vanatka, M.; Rojas-Sanchez, J-C; Vogel, J.; Bonfim, M.; Belmeguenai, M.; Roussigne, Y.; Stashkevich, A.; Thiaville, A.; Pizzini, S.
    Journal of Physics: Condensed Matter **27**, 326002 (2015). DOI: https://doi.org/10.1088/0953-8984/27/32/326002
    32 citations
11. Very large domain wall velocities in Pt/Co/GdOx and Pt/Co/Gd trilayers with Dzyaloshinskii-Moriya interaction
    Thai Ha Pham; Vogel, J.; Sampaio, J.; Vanatka, M.; Rojas-Sanchez, J-C; Bonfim, M.; Chaves, D. S.; Choueikani, F.; Ohresser, P.; Otero, E.; Thiaville, A.; Pizzini, S.
    EPL (Europhysics Letters) **113**, 67001 (2016). DOI: https://doi.org/10.1209/0295-5075/113/67001
    32 citations
12. Spin-orbit torque-induced switching in ferrimagnetic alloys: Experiments and modeling
    Je, Soong-Geun; Rojas-Sanchez, Juan-Carlos; Thai Ha Pham; Vallobra, Pierre; Malinowski, Gregory; Lacour, Daniel; Fache, Thibaud; Cyrille, Marie-Claire; Kim, Dae-Yun; Choe, Sug-Bong; Belmeguenai, Mohamed; Hehn, Michel; Mangin, Stephane; Gaudin, Gilles; Boulle, Olivier
    Applied Physics Letters **112**, 062401 (2018). DOI: https://doi.org/10.1063/1.5017738
    20 citations
13. Large enhancement of the spin Hall effect in Au by side-jump scattering on Ta impurities
    Laczkowski, P.; Fu, Y.; Yang, H.; Rojas-Sanchez, J. -C.; Noel, P.; Pham, V. T.; Zahnd, G.; Deranlot, C.; Collin, S.; Bouard, C.; Warin, P.; Maurel, V.; Chshiev, M.; Marty, A.; Attane, J. -P.; Fert, A.; Jaffres, H.; Vila, L.; George, J. -M.
    Physical Review B **96**, 140405 (2017). DOI: https://doi.org/10.1103/PhysRevB.96.140405
    19 citations

14. Evidence for spin-to-charge conversion by Rashba coupling in metallic states at the Fe/Ge(111) interface
    Oyarzun, S.; Nandy, A. K.; Rortais, F.; Rojas-Sanchez, J.-C.; Dau, M. -T.; Noel, P.; Laczkowski, P.; Pouget, S.; Okuno, H.; Vila, L.; Vergnaud, C.; Beigne, C.; Marty, A.; Attane, J. -P.; Gambarelli, S.; George, J. -M.; Jaffres, H.; Bluegel, S.; Jamet, M.
    Nature communications **7**, 13857 (2016). DOI: https://doi.org/10.1038/ncomms13857
    19 citations
15. Spin transport in p-type germanium
    Rortais, F.; Oyarzun, S.; Bottegoni, F.; Rojas-Sanchez, J-C; Laczkowski, P.; Ferrari, A.; Vergnaud, C.; Ducruet, C.; Beigne, C.; Reyren, N.; Marty, A.; Attane, J-P; Vila, L.; Gambarelli, S.; Widiez, J.; Ciccacci, F.; Jaffres, H.; George, J-M; Jamet, M.
    Journal of Physics: Condensed Matter **28**, 165801 (2016).
    DOI: https://doi.org/10.1088/0953-8984/28/16/165801
    17 citations
16. Evidence for spin to charge conversion in GeTe(111)
    Rinaldi, C.; Rojas-Sanchez, J. C.; Wang, R. N.; Fu, Y.; Oyarzun, S.; Vila, L.; Bertoli, S.; Asa, M.; Baldrati, L.; Cantoni, M.; George, J.-M.; Calarco, R.; Fert, A.; Bertacco, R.
    APL Materials 4, 032501 (2016). DOI: https://doi.org/10.1063/1.4941276
    16 citations
17. Independence of spin-orbit torques from the exchange bias direction in Ni81Fe19/IrMn bilayers
    Saglam, Hilal; Rojas-Sanchez, J. Carlos; Petit, Sebastien; Hehn, Michel; Zhang, Wei; Pearson, John E.; Mangin, Stephane; Hoffmann, Axel
    Physical Review B **98**, 094407 (2018). DOI:
    https://doi.org/10.1103/PhysRevB.98.094407
    16 citations
18. Creation of Magnetic Skyrmion Bubble Lattices by Ultrafast Laser in Ultrathin Films
    Je, Soong-Geun; Vallobra, Pierre; Srivastava, Titiksha; Rojas-Sanchez, Juan-Carlos; Thai Ha Pham; Hehn, Michel; Malinowski, Gregory; Baraduc, Claire; Auffret, Stephane; Gaudin, Gilles; Mangin, Stephane; Bea, Helene; Boulle, Olivier
    Nano letters **18**, 7362 (2018). DOI: https://doi.org/10.1021/acs.nanolett.8b03653
    14 citations
19. Switchable Spin-Current Source Controlled by Magnetic Domain Walls
    Torres, W. Savero; Laczkowski, P.; Nguyen, V. D.; Sanchez, J. C. Rojas; Vila, L.; Marty, A.; Jamet, M.; Attane, J. P.
    Nano letters **14**, 4016 (2014). DOI: https://doi.org/10.1021/nl501453p
    13 citations
20. Thermal Contribution to the Spin-Orbit Torque in Metallic-Ferrimagnetic Systems
    Thai Ha Pham; Je, S. -G.; Vallobra, P.; Fache, T.; Lacour, D.; Malinowski, G.; Cyrille, M. C.; Gaudin, G.; Boulle, O.; Hehn, M.; Rojas-Sanchez, J. -C.; Mangin, S.
    Physical Review Applied **9**, 064032 (2018).
    DOI: https://doi.org/10.1103/PhysRevApplied.9.064032
    12 citations
21. Ultralow Magnetic Damping in Co_2Mn-Based Hensler Compounds: Promising Materials for Spintronics
    C Guillemard, S Petit-Watelot, L Pasquier, D Pierre, J Ghanbaja, JC Rojas-Sánchez, A Bataille, J Rault, P Le Fèvre, F Bertran, Stephane Andrieu
    Physical Review Applied **11**, 064009 (2019).

DOI: https://doi.org/10.1103/PhysRevApplied.11.064009
8 citation

22. Evaluation of spin diffusion length of AuW alloys using spin absorption experiments in the limit of large spin-orbit interactions
Laczkowski, P.; Jaffres, H.; Savero-Torres, W.; Rojas-Sanchez, J.-C.; Fu, Y.; Reyren, N.; Deranlot, C.; Notin, L.; Beigne, C.; Attane, J. -P.; Vila, L.; George, J.-M.; Marty, A.
Physical Review B **92**, 214405 (2015). DOI: https://doi.org/10.1103/PhysRevB.92.214405
7 citations
23. In-plane and out-of-plane spin precession in lateral spin-valves
Sanchez, J. -C. Rojas; Laczkowski, P.; Torres, W. F. Savero; Cubukcu, M.; Nguyen, V. D.; Notin, L.; Beigne, C.; Vergnaud, C.; Marty, A.; Jamet, M.; Vila, L.; Attane, J. P.
Applied Physics Letters **102**, 132408 (2013). DOI: https://doi.org/10.1063/1.4800537
7 citations
24. Nonmonotonic aftereffect measurements in perpendicular synthetic ferrimagnets
Fache, T.; Tarazona, H. S.; Liu, J.; L'vova, G.; Applegate, M. J.; Rojas-Sanchez, J. C.; Petit-Watelot, S.; Landauro, C., V; Quispe-Marcatoma, J.; Morgunov, R.; Barnes, C. H. W.; Mangin, S.
Physical Review B **98**, 064410 (2018). DOI: https://doi.org/10.1103/PhysRevB.98.064410
6 citation
25. Magnetoresistance effect in (La, Sr)MnO3 bicrystalline films
Alejandro, G.; Steren, L. B.; Pastoriza, H.; Vega, D.; Granada, M.; Rojas Sanchez, J. C.; Sirena, M.; Alascio, B.
Journal of Physics: Condensed Matter **22**, 346007 (2010).
DOI: https://doi.org/10.1088/0953-8984/22/34/346007
6 citations
26. Magnetic study of La0.75Sr0.25MnO3/LaNiO3 multilayers
Granada, Mara; Sanchez, J. Carlos Rojas; Steren, Laura B.; Leyva, A. Gabriela
Physica B: Condensed Matter **384**, 68 (2006).
DOI: https://doi.org/10.1016/j.physb.2006.05.074
6 citations
27. Charge-spin current conversion in high quality epitaxial Fe/Pt systems: Isotropic spin Hall angle along different in-plane crystalline directions
Guillemard, C.; Petit-Watelot, S.; Andrieu, S.; Rojas-Sanchez, J. -C.
Applied Physics Letters **113** , 262404 (2018). DOI: https://doi.org/10.1063/1.5079236
5 citations
28. Roughness in manganite-based superlattices
Rojas Sanchez, J. C.; Granada, M.; Steren, L. B.; Mazzaro, I.; Mosca, D. H.
Applied Surface Science **254**, 219 (2007).
DOI: https://doi.org/10.1016/j.apsusc.2007.07.036
5 citations
29. Manipulating exchange bias using all-optical helicity-dependent switching
Vallobra, P.; Fache, T.; Xu, Y.; Zhang, L.; Malinowski, G.; Hehn, M.; Rojas-Sanchez, J. -C.; Fullerton, E. E.; Mangin, S.
Physical Review B **96**, 144403 (2017). DOI: https://doi.org/10.1103/PhysRevB.96.144403
5 citations

30. Giant magnetoresistance in oxide-based metallic multilayers
    Granada, Mara; Sanchez, J. Carlos Rojas; Steren, Laura B.
    Applied Physics Letters **91**, 072110 (2007). DOI: https://doi.org/10.1063/1.2772237
    5 citations
31. Transition from spin accumulation into interface states to spin injection in silicon and germanium conduction bands
    Jain, Abhinav; Rojas-Sanchez, Juan-Carlos; Cubukcu, Murat; Peiro, Julian; Le Breton, Jean-Christophe; Vergnaud, Celine; Augendre, Emmanuel; Vila, Laurent; Attane, Jean-Philippe; Gambarelli, Serge; Jaffres, Henri; George, Jean-Marie; Jamet, Matthieu
    The European Physical Journal B **86**, 140 (2013).
    DOI: https://doi.org/10.1140/epjb/e2013-31067-7
    4 citations
32. Spin-Orbit Torque Switching of a Nearly Compensated Ferrimagnet by Topological Surface States
    Hao Wu, Yong Xu, Peng Deng, Quanjun Pan, Seyed Armin Razavi, Kin Wong, Li Huang, Bingqian Dai, Qiming Shao, Guoqiang Yu, Xiufeng Han, Juan-Carlos Rojas-Sánchez, Stéphane Mangin, Kang L Wang
    Advanced Materials **31**, 1901681 (2019). DOI:
    https://doi.org/10.1002/adma.201901681
    3 citation
33. Polycrystalline Co2Mn-based Heusler thin films with high spin polarization and low magnetic damping
    C Guillemard, S Petit-Watelot, J-C Rojas-Sánchez, J Hohlfeld, J Ghanbaja, A Bataille, P Le Fèvre, F Bertran, S Andrieu
    Applied Physics Letters **115** , 172401 (2019). DOI: https://doi.org/10.1063/1.5121614
    2 citations
34. Evidence of Pure Spin-Current Generated by Spin Pumping in Interface-Localized States in Hybrid Metal-Silicon-Metal Vertical Structures
    Cerqueira, Carolina; Qin, Jian Yin; Dang, Huong; Djeffal, Abdelhak; Le Breton, Jean-Christophe; Hehn, Michel; Rojas-Sanchez, Juan-Carlos; Devaux, Xavier; Suire, Stephane; Migot, Sylvie; Schieffer, Philippe; Mussot, Jean-Georges; Laczkowski, Piotr; Anane, Abdelmadjid; Petit-Watelot, Sebastien; Stoffel, Mathieu; Mangin, Stephane; Liu, Zhi; Cheng, Bu Wen; Han, Xiu Feng; Jaffres, Henri; George, Jean-Marie; Lu, Yuan
    Nano letters **19**, 90 (2018). DOI: https://doi.org/10.1021/acs.nanolett.8b03386
    2 citation
35. Strain-Enhanced Charge-to-Spin Conversion in Ta/Fe/Pt Multilayers Grown on Flexible Mica Substrate.
    Er Liu, T Fache, D Cespedes-Berrocal, Zhi Zhang, S Petit-Watelot, Stéphane Mangin, Feng Xu, J-C Rojas-Sánchez
    Physical Review Applied **11**, 054049 (2019).
    DOI: https://doi.org/10.1103/PhysRevApplied.12.044074
    2 citation
36. Compared Efficiencies of Conversions between Charge and Spin Current by Spin-Orbit Interactions in Two-and Three-Dimensional Systems.
    JC Rojas-Sánchez and A. Fert
    Physical Review Applied **11**, 054049 (2019).
    DOI: https://doi.org/10.1103/PhysRevApplied.11.054049

2 citation

37. Excess velocity of magnetic domain walls close to the depinning field
    Caballero, Nirvana B.; Fernandez Aguirre, Ivan; Albornoz, Lucas J.; Kolton, Alejandro B.; Carlos Rojas-Sanchez, Juan; Collin, Sophie; Marie George, Jean; Diaz Pardo, Rebeca; Jeudy, Vincent; Bustingorry, Sebastian; Curiale, Javier
    Physical Review B **96**, 224422 (2017). DOI: https://doi.org/10.1103/PhysRevB.96.224422
    2 citation
38. Spin-Charge Conversion Phenomena in Germanium
    Oyarzun, Simon; Rortais, Fabien; Rojas-Sanchez, Juan-Carlos; Bottegoni, Federico; Laczkowski, Piotr; Vergnaud, Celine; Pouget, Stephanie; Okuno, Hanako; Vila, Laurent; Attane, Jean-Philippe; Beigne, Cyrille; Marty, Alain; Gambarelli, Serge; Ducruet, Clarisse; Widiez, Julie; George, Jean-Marie; Jaffres, Henri; Jamet, Matthieu
    Journal of the Physical Society of Japan **86**, 011002 (2016).
    DOI: https://doi.org/10.7566/JPSJ.86.011002
    2 citation
39. Spin pumping and inverse spin Hall effect in Platinum and other 5d metals: The essential role of spin-memory loss and spin-current discontinuities at interfaces
    Rojas-Sanchez, J. -C.; Reyren, N.; Laczkowski, P.; Savero, W.; Attane, J. -P.; Deranlot, C.; Gambarelli, S.; Jamet, M.; George, J. -M.; Vila, L.; Jaffres, H.
    Spintronics VII 9167, 916729 (2014). DOI: https://doi.org/10.1117/12.2059646
    1 citation
40. Spin-dependent transport characterization in metallic lateral spin valves using one-dimensional and three-dimensional modeling
    P. Laczkowski, M. Cosset-Cheneau, W. Savero-Torres, V. T. Pham, G. Zahnd, H. Jaffrès, N. Reyren, J.-C. Rojas-Sànchez, A. Marty, L. Vila, J.-M. George, and J.-P. Attané
    Physical Review B **99**, 134436 (2019). DOI: https://doi.org/10.1103/PhysRevB.99.134436
    0 citation